DCT 185

Moment Redistribution and the Service II Limit State

by

JENNIFER RIGHMAN O'CONNELL
MICHAEL J. ZETTLEMOYER

Department of Civil and Environmental Engineering
College of Engineering
University of Delaware

August 2007

Delaware Center for Transportation
University of Delaware
355 DuPont Hall
Newark, Delaware 19716
(302) 831-1446

Moment Redistribution and the Service II Limit State

By

Jennifer Righman McConnell
Michael J. Zettlemoyer

Department of Civil and Environmental Engineering
College of Engineering
University of Delaware
Newark, Delaware 19716

DELAWARE CENTER FOR TRANSPORTATION
University of Delaware
Newark, Delaware 19716

This work was sponsored by the Delaware Center for Transportation and was prepared in cooperation with the Delaware Department of Transportation. The contents of this report reflect the views of the authors who are responsible for the facts and accuracy of the data presented herein. The contents do not necessarily reflect the official views of the Delaware Center for Transportation or the Delaware Department of Transportation at the time of publication. This report does not constitute a standard, specification, or regulation.

The Delaware Center for Transportation is a university-wide multi-disciplinary research unit reporting to the Chair of the Department of Civil and Environmental Engineering, and is co-sponsored by the University of Delaware and the Delaware Department of Transportation.

DCT Staff

Ardeshir Faghri
Director

Jerome Lewis
Associate Director

Wanda L. Taylor
Assistant to the Director

Lawrence H. Klepner
T^2 Program Coordinator

Sandi Wolfe
Secretary

DCT Policy Council

Robert Taylor, Co-Chair
Chief Engineer, Delaware Department of Transportation

Eric Kaler, Co-Chair
Dean, College of Engineering

The Honorable Tony DeLuca
Chair, Delaware Senate Transportation Committee

The Honorable Richard Cathcart
Chair, Delaware House of Representatives Transportation Committee

Timothy K. Barnekov
Dean, College of Human Resources, Education and Public Policy

Michael J. Chajes
Chair, Civil and Environmental Engineering

Ralph A. Reeb
Director of Planning, Delaware Department of Transportation

Stephen Kingsberry
Director, Delaware Transit Corporation

Shannon Marchman
Representative of the Director of the Delaware Development Office

Roger Roy
Representative, Transportation Management Association

Jim Johnson
Executive Director, Delaware River & Bay Authority

Delaware Center for Transportation
University of Delaware
Newark, DE 19716
(302) 831-1446

Moment Redistribution and the Service II Limit State

by Jennifer Righman McConnell and Michael J. Zettlemoyer

DEPARTMENT OF
CIVIL & ENVIRONMENTAL ENGINEERING
UNIVERSITY OF DELAWARE

The Center For
INNOVATIVE
BRIDGE ENGINEERING

August 2007

Executive Summary

A concern regarding the use of design procedures that allow steel girder stresses to exceed the yield strength of the steel is the effect on permanent deformations, which are intended to be controlled by the requirements of the Service II limit state. In many situations, particularly for compact girders, the Service II limit state of the AASHTO *LRFD Bridge Design Specifications* governs the design. This limit state is calibrated to yield similar proportions as the overload check of the AASHTO *Standard Specifications for Highway Bridges*. The research reported here was carried out in the belief that the Service II limit state should be re-evaluated in light of the calibration of the strength limit states of the *LRFD Specifications*. The objective of the work was to evaluate the current stress limits for steel I-girders at the Service II limit state. AASHTO Specifications (2004) limit the maximum allowable stress to 95% of the yield stress for composite girders and 80% of the yield stress for non-composite girders. These limits were originally intended to prevent objectionable levels of deformation. However, the basis for these limits is not well founded. Because these stress limits frequently control the design of compact sections in positive bending, a more thorough evaluation of these limits is warranted. Such an evaluation was a primary objective of this work, which was expected to result in alternative design requirements for the Service II limit state.

The report is organized as follows:

Chapter 1 presents introductory information, including brief background information on the AASHTO Limit States, the Service II Limit State, and moment redistribution. Additionally, Chapter 1 discusses the need for the research, objectives of the research, scope of the research, and the organization of this thesis. The objectives of this research were to provide experimental data on service stresses versus deflection and to provide experimental data on service stresses at various levels of moment redistribution.

Chapter 2 provides a detailed background review of topics critical to this research. Topics included the AASHTO Limit States, the Service II Limit State, and moment redistribution. The AASHO Road Test was found to be the origin of the Service II Limit State flange stress limits, and a detailed discussion of this study is also included in Chapter 2. Finally, criteria for the basis of the flange stress limits of the Service II Limit State were investigated and are discussed to provide guidance on future rational design criteria. Existing research in this area is presented and future recommendations for research are provided.

Chapter 3 discusses details for the design of the experimental test set-up and test specimen, including the scope of the design, test specimen characteristics, lateral bracing, and instrumentation for the experimental testing. Here, the decision process used to determine the test set-up geometry and specific test specimen characteristics is detailed.

Chapter 4 presents aspects regarding the experimental testing of the research through a discussion of the construction process and testing procedures. The

discussion of the construction process provides an overall sense for the steps needed to build the test set-up and test specimen, while the discussion of the testing procedure provides details of load application during the experimental testing.

The experimental strain and deflection data is graphically displayed and discussed in **Chapter 5** through load versus deflection and load versus strain graphs. Analysis of the experimental data resulted in determination of the experimental stresses and moments, which are also graphically displayed and discussed in Chapter 5. Figures of applied load versus service stress, service stress versus deflection, and applied load versus moment provide a detailed method for the evaluation of experimental testing results and formulation of conclusions.

Chapter 6 provides a summary and conclusions of the work and then makes recommendations for future work. Although the final outcome of the experimental results did not satisfy the stated objectives for the research due to loading circumstances beyond the control of the research team, the methods and procedures presented will prove useful. The construction methods, testing procedures, numeric data analysis, and graphical display of data/results presented in this report are an adequate and efficient method for achieving the research objectives. Additional experimental research will need to be conducted and data gathered regarding the Service II Limit State and moment redistribution procedures for further investigation into the efficiency of these design criteria. This thesis has provided a systematic approach to acquire the experimental data necessary; therefore, this report should be utilized as a guide for future testing.

It is recommended that future testing of continuous-span specimens include High Performance Steel (HPS), grade 50 steel, non-composite girders, composite girders, plate girders, and variations in span length. Future experimental testing must apply enough incremental loading to reach the eventual ultimate capacity of the test specimen and thus enable achievement of both objectives regarding high levels of stress and moment redistribution. The data analysis files and methods for graphical display used for this research thesis may be used for rapid experimental interpretation and conclusion. One potential minor area of experimental improvement is the application of strain gages at all locations of recorded deflection. This would be beneficial because it would have provided more locations for further analysis of stress versus deflection data at the locations of theoretical maximum deflection in the spans.

EVALUATION OF THE SERVICE II LIMIT STATE FOR

AASHTO ELASTIC AND MOMENT REDISTRIBUTION PROCEDURES

by

Michael Joseph Zettlemoyer

A thesis submitted to the Faculty of the University of Delaware in partial fulfillment of the requirements for the degree of Master of Civil Engineering

Spring 2007

EVALUATION OF THE SERVICE II LIMIT STATE FOR

AASHTO ELASTIC AND MOMENT REDISTRIBUTION PROCEDURES

by

Michael Joseph Zettlemoyer

Approved: _____
Jennifer Righman McConnell, Ph.D.
Professor in charge of thesis on behalf of the Advisory Committee

Approved: _____
Michael J. Chajes, Ph.D.
Chair of the Department of Civil & Environmental Engineering

Approved: _____
Eric W. Kaler, Ph.D.
Dean of the College of Engineering

Approved: _____
Carolyn A. Thoroughgood, Ph.D.
Vice Provost for Research and Graduate Studies

TABLE OF CONTENTS

List of Tables

List of Figures

Abstract

Typically, for compact girders, the Service II Limit State of the AASHTO Load and Resistance Factor Design (LRFD) Specifications (2005) governs the design by limiting the stress in the girder flanges to a fraction of the yield strength of the steel. This limit state corresponds to the overload check in the 1992 AASHTO Standard Specifications and is intended to prevent objectionable permanent deformations due to unexpected severe traffic loadings, which would impair rideablilty. Because the Service II Limit State: (1) is not calibrated based on LRFD methodology, (2) has an ambiguous objective of preventing "objectionable deformations" and, (3) has a profound governing impact on the design of steel girders, further investigation into the Service II Limit State is needed. Furthermore, there is a concern regarding the implications of the Service II Limit State and the effect on permanent deformations as a result of optional moment redistribution design procedures, which allow steel girder stresses to exceed the yield strength of the steel.

The intention of this thesis is to provide experimental data to further investigate the objectives of the Service II Limit State, the effects of moment redistribution design, and how they relate to one another. Therefore, the objectives of this research are to provide experimental data on service stresses versus deflection/permanent set and to provide experimental data on service stresses at various levels of moment redistribution. In an effort to realize these research objectives background research was done regarding the origin of the Service II Limit State and other integral aspects of the design criteria. Additionally, an experiment was designed and performed on a composite continuous-span test specimen to collect the experimental data on strains and deflections needed.

The experimental research for this thesis did not provide the data necessary to facilitate further investigation into the objectives of this research due to circumstances beyond the control of the research team. However, a systematic approach was developed for the experimental test specimen design, the construction, the testing procedure, the numeric data analysis, and the graphical display of data/results. These developments will be valuable in future experimental testing of continuous-span specimens.

Chapter 1

1. Introduction

1.1 Background

1.1.1 AASHTO Limit States

The current AASHTO specifications (AASHTO 2005) are based on the latest design methodology, identified as Load and Resistance Factor Design (LRFD). LRFD rationalizes and modernizes previous design methods, such as Allowable Stress Design (ASD) and Load Factor Design (LFD). It is described as "rational" because LRFD is a statistical based design method that accounts for the unknown properties of materials and the uncertainty of design loads. LRFD is characterized as "modernized" because it better accounts for the continuing design trend towards indeterminate structures due to their design advantages. There are two underylying limit state design criteria within the LRFD Specifications; the Serviceability Limit States (SLS) and the Ultimate Limit States (ULS). The SLS are concerned with issues of maintenance costs, user comfort, crack widths, and gradual deterioration. The ULS are ultimately concerned with the responses of the structure under peak loading conditions, such as bending capacity, shear capacity, and stability. LRFD methodology was first incorporated into the design criteria for select ULS of the AASHTO specifications (AASHTO 1994).

The LRFD Specifications define varying load combinations for four sets of design criteria: service limit states, fatigue and fracture limit states, strength limit states, and the extreme event limit states. The service limit states and fatigue and fracture limit states are considered SLS, while the strength limit states and the

extreme event limit states are considered ULS. The limit states applicable to steel structures include Service Limit State I, Service Limit State II, Strength Limit State I, Stength Limit State II, Strength Limit State III, Strength Limit State IV, Strength Limit State V, Fatigue Limit State, Extreme Event Limit State I, and Extreme Event Limit State II. Chapter 2, Section 2.1.1 of this thesis further details these limit states applicable to steel stuctures. The Service II Limit State is the primary focus of this thesis because of the integral role it plays in the design of compact steel girders and moment redistribution design specifications.

1.1.2 Service II Limit State

The design criteria of the service limit states are intended to insure the desired functionality of the structure is maintained with routine everyday loadings. For steel girders, the applicable service limit state is the Service II limit state, which places limits on flange stresses in an effort to avoid unacceptable deformations. The current Service II Limit State provisions, found in the AASHTO Specifications (AASHTO 2005), correspond to the overload check in the 1992 AASHTO Standard Specifications. The overload check in the Standard Specifications was based on successful past practice and the experimental results of the AASHO "Road Test". No calibration of this limit state according to LRFD methodology has yet to be performed. Furthermore, it is the basis of the original overload check that raises several concerns with regard to the Service II flange stress limits.

1.1.3 Moment Redistribution

Moment redistribution is an optional design methodology in the AASHTO Specifications (AASHTO 2005) that utilizes concepts of inelastic behavior and is applicable to indeterminate structures (continuous-span structures). To give an overview of this design philosophy, consider a typical continuous-span structure.

The structure experiences large negative bending moments at the interior pier support compared to the lesser positive bending moments at mid-span locations. These negative bending moments govern a conventional elastic design. However, because the structure initially yields at the interior pier support, a plastic hinge is formed. Once the plastic hinge is developed at the interior pier support, additional moment is redistributed to the positive moment regions near mid-span. Moment redistribution design allows the designer to account for this behavior and thus provides a more economic and efficient design by resulting in lower applied moments in negative bending regions.

In addition to resulting in smaller cross-section requirements in negative bending, the advantages also include a reduced need for cover plates and flange transitions. This can result in savings in both material and fabrication costs, along with a design with more favorable fatigue characteristics. Additionally, moment redistribution design better predicts the strength of existing structures, and as a result eliminates unnecessary rehabilitation or replacement.

The moment redistribution process is based on the assumption that the section has sufficient ductility and inelastic rotation capacity at a plastic moment level greater than or equal to the redistribution moment at the interior pier support. This is assumed satisfied in current design procedures by limiting the design procedure to relatively compact members and limiting the allowable moment redistribution to 20% of the elastic moment at the interior pier supports. These assumptions are often criticized for their conservatism. Additionally, moment redistribution design procedures under the service limit state load combinations rarely provides an improved and more efficient design compared with elastic design procedures.

1.2 Need for Research

1.2.1 Intent of the Service II Limit State

The intentions of the service II limit state are unclear and not well established. As previously mentioned, the service II load combination is applied to steel bridges to limit yielding, which is an attempt to eliminate "objectionable" kinking of members/connections, and to prevent repeated slipping of bolted connections. Furthermore, the commentary of the LRFD Specifications states, "This limit state check is intended to prevent objectionable permanent deformations due to expected severe traffic loadings which would impair rideability. It corresponds to the overload check in the 1992 AASHTO Standard Specifications and is merely an indicator of successful past practice…". To prevent "objectionable" deflections, the specifications simply limit the flange stress to 95% and 80% of the yield stress for composite and non-composite girders, respectively. These stress values were subjectively chosen for the introduction of the original Load Factor Design stress provisions (Vincent 1969). The limiting criteria of "objectionable deflections" and "impaired rideability" are ambiguous and are not quantified or established anywhere in the specifications. This raises several concerns and leaves room for varying interpretations of the intention of the code. Mertz and Kulicki present the following questions regarding this issue:

1. What degree of kinking of the vertical alignment is "objectionable", in terms of rideability?
2. Can this kinking be quantified in terms of percentage of flange yielding?
3. What degree of flange yielding corresponds to the "objectionable" degree of kinking?

1.2.2 Consequences of the Service II Limit State

Since the inception of the LRFD Specifications, extensive knowledge and experience has been gained through research and practice regarding the effects of the specifications on the design of steel bridges. In general terms, there are governing trends of the LRFD Specifications on the design of steel bridges that have been noted by design engineers. Some of these trends directly relate to the effect that the Service II Limit State has on the overall design. For example, steel plate girders and rolled beams are typically compact in the positive moment region. These beams, particularly rolled beams, often have the capability to reach the plastic moment capacity of the beam, but are often limited by the moment that initiates crushing of the slab. Under the strength limit state, they generally retain a reserve flexural capacity 30% greater than the yield strength. However, these sections are usually governed by the 95% flange yield stress provision incorporated into the flexural check of the service II limit state, which may unnecessarily limit the capacity of these members.

1.2.3 Moment Redistribution Design

As previously mentioned, the moment redistribution design process is based on the assumption that the section has sufficient ductility. These assumptions are not guaranteed under the current LRFD Specifications, but instead rely on conservative assumptions in an attempt to achieve the needed ductility, and as a result are often criticized for their conservatism. Redistribution moments are calculated for moment redistribution design at the service and/or strength limit states. Rarely is it the case that a more efficient design results from the service limit state load combinations. Therefore, the question is raised regarding the inclusion of the service limit state for moment redistribution design. Particularly because moment redistribution design is based on principles of allowing permanent

deflections, while the service limit state is intended to prevent objectionable permanent deflections. These conflicting objectives suggest that perhaps moment redistribution should not be permitted at the service limit state.

1.3 Problem Description

Load and Resistance Factor Design (LRFD) methodology is a statistical reliability theory based approach to engineering design. However, only the strength limit states have been calibrated based on reliability theory. The other limit states were calibrated to past practice (Nowak 1992). As a result, there has been substantial criticism of this raised by academia and other circles. Because the LRFD Specifications have been accepted by industry and academia, the service and fatigue-and-fracture limit states should also be calibrated on reliability theory in an effort to further develop the design of highway bridges. It is unclear what calibration criteria are applicable and if the available information is sufficient (Mertz and Kulicki 1997).

1.4 Objectives of the Research

1.4.1 Service Stress versus Deflection

The first objective of this research is to provide experimental data on service stresses versus deflection and permanent set. As previously mentioned, the flange stress limits of the service limit state regularly govern the design of the section for compact girders. This experimental data will provide more information related to what live load deflections and permanent set deformations can be expected for high levels of service stress. This is important because it is unclear how to quantify what deflections and deformations make the section "objectionable". Additionally, to be discussed in Chapter 2, the flange stress limits

of the Service II Limit State are founded on the experimental testing of a limited number of simple-span bridges for stress versus permanent set data. In addition to adding another experimental data point related to the foundation of this design criterion, data from this research will be the result of a continuous-span specimen. The prominent use of continuous-span structures in modern bridge design makes this update essential.

1.4.2 Service Stress versus Moment Redistribution

The second objective of this research is to provide experimental data on service stresses at various levels of moment redistribution. This will allow for the comparison to the existing service stress limits included in the service limit state for moment redistribution design. It is felt that compact composite sections can experience larger service stresses at larger amounts of moment redistribution than the current LRFD Specifications permit, without resulting in "objectionable" deformations. The eventual goal of acquiring this data is the future evaluation of service requirements for varying moment redistribution designs.

1.5 Scope of the Research

1.5.1 Background Review

The first task of the research project is a background review of literature corresponding to the objectives of this research thesis. The main goal of the background review is to evaluate and gather all relevant information from currently available literature. This is done in an attempt to provide background information necessary to fully understand the concepts of the AASHTO limit states, the Service II Limit State, and moment redistribution design procedures. An additional purpose of the background review is to investigate the basis for the current flange stress

limits of the Service II Limit State and to discuss any information providing guidance on future rational design criteria for this limit state.

1.5.2 Experimental Design/Testing

The experimental design for this research thesis includes a discussion of the laboratory geometric constraints for the experimental set-up. Once established, a discussion of the decision process is presented for issues of test specimen scaling, material selection, and instrumentation for experimental data collection. The experimental data to be recorded includes strain and deflection, which is essential for satisfying the objectives of the research. The experimental testing for this research thesis provides a discussion and a display of figures revealing the steps taken to construct the experimental set-up and test specimen. Additionally, the testing procedures for the application of the actuator load and collection of the experimental data is presented.

1.5.3 Evaluation of Girder Stress and Deformation

The purpose for the evaluation of the girder stresses and deformations is related to first objectives of providing experimental stress versus deflection/permanent set data related to the first objective. In the absence of stress-strain data, the strains recorded from the experimental testing are converted to stress via the modulus of elasticity. Again, this will provide additional information on actual live load deflection and permanent deformation for a compact composite section at high magnitudes of stress relative to the yield strength. This evaluation will hopefully provide further useful information regarding the current governing and ambiguous design criteria of the Service II Limit State.

1.5.4 Evaluation of Girder Stress and Strain

The purpose for the evaluation of the girder strains and stresses is related to the second objective of providing experimental data on stress at various levels of moment redistribution. Strain is converted to stress via the modulus of elasticity. The stresses are then used to calculate moment via theoretical moment of inertia values and experimental neutral axis locations. The goal of this evaluation is to show that much larger amounts of moment redistribution may be obtained without compromising the function of the beam.

1.6 Thesis Organization

This thesis will be organized in the following format:

Chapter 1 – Introduction provides brief background information on key concepts needed to understand the contents of this thesis, which include the AASHTO Limit States, Service II Limit State, and Moment Redistribution. The introduction also provides statements/questions regarding the problem description and need for this research. Such issues involve the intent and limitations of the Service II Limit State and current moment redistribution design procedures. In addition, objectives of the research and a detailed explanation of the research steps taken to complete this thesis are provided.

Chapter 2 – Background Review provides a detailed discussion of the background literature on the AASHTO Limit States, the Service II Limit State, and moment redistribution design procedures. Details of the AASHO Road Test are thoroughly discussed because the experimental results were identified as the basis for the flange stress limits of the Service II Limit State. Additionally, a background discussion providing future guidance on rational design criteria for the Service II Limit State is presented.

Chapter 3 – Experimental Design includes a description of the goals of the experimental design, design procedures, specimen geometries, and other general information. This chapter also includes details regarding the bracing design and instrumentation application for data collection during the experiment.

Chapter 4 – Experimental Testing provides details of the steps taken for the construction of the test specimen and experimental test set-up. This chapter also includes details regarding the testing procedures used for application of the applied loads and data collection.

Chapter 5 – Experimental Results graphically displays and discusses the experimental data collected during testing. Figures and discussion regarding the analysis of the experimental data is also presented. Conclusions are based on the behavior of the experimental test specimen and how the collected experimental data relates to the research objectives.

Chapter 6 – Summary and Conclusions present reiteration of the objectives and presents a summary of key findings. Additionally, final conclusions regarding the results of this research and a discussion of recommendations for an improvement and/or addition of future work needed in this research area is included.

Chapter 2

2. Background

The subsequent sections of this chapter provide a detailed background discussion of literature on the AASHTO Limit States, the Service II Limit State, and moment redistribution design procedures. This information is necessary to fully understand these concepts and topics that are essential to the objectives and problem description for this research thesis. Details of the AASHO Road Test are thoroughly discussed because the experimental results were identified as the basis for the flange stress limits of the Service II Limit State. Additionally, a background discussion providing future guidance on rational design criteria for the Service II Limit State is presented.

2.1 Detailed Review of AASHTO Design Criteria

2.1.1 AASHTO Limit States

Bridge systems and bridge components are designed to serve desired functions. When a desired function is no longer satisfied then that condition is defined as a limit state (Barker and Puckett 1997). The failure of a bridge can come in many forms, such as cracking, excessive deformations, exceeding of the bending moment capacity, et cetera. The limit states fall into one of two categories: Ultimate Limit States (ULS) and Serviceability Limit States (SLS). The ULS coincide with bending capacity, shear capacity, and stability, while the SLS coincide with gradual deterioration, user comfort, and maintenance costs (Nowak 1999).

Initially, the American Association of State Highway Officials (AASHO) Standard Specifications for Highway Bridges based the limit states on Allowable

Stress Design (ASD). ASD methodology places limits on the stresses caused by loads to a fraction of the yield stress of the material. This design method was developed for statically determinate metal structures and has several shortcomings when applied to the design of modern structures, most notably the reliance on deterministic loads and the subjective selection of safety factors.

Beginning in the early 1970's, revisions to ASD were made to represent the variable predictability of certain load types, such as vehicular and wind by adjusting design factors. This design philosophy became known as Load Factor Design (LFD). In 1988, NCHRP Project 12-33, "Development of a Comprehensive Bridge Specification and Commentary", was established in an effort to replace the AASHTO Standard Specifications for Highway Bridges with a new design code. The Standard Specifications were thought to be disjointed, fragmented, and not state of the art (Nowak 1999). As a result, Load and Resistance Factor Design (LRFD) was developed to account for the ASD and LFD shortcomings. LRFD utilizes both resistance factors and load factors to account for variability in material characteristics and loads that a bridge will endure over its lifetime (Nowak 1999). LRFD design methodology also achieves a uniform level of safety for the calibrated limit states, which excludes the service limit states. Calibration of the limit states is based on a statistical probability of failure approach (Barker and Puckett 1997).

The AASHTO LRFD Limit States were first introduced in 1994 through the inception of the first edition of the AASHTO LRFD Bridge Design Specifications. A bridge designer must account for four sets of limit state design criteria, as specified by Article 1.3.2 of the LRFD Specifications. These design criteria include the service limit states, fatigue and fracture limit states, strength limit states, and the extreme event limit states (Mertz and Kulicki 1997). Articles 1.3.2.2, 1.3.2.3, 1.3.2.4, and 1.3.2.5 of the most current edition of the specifications, the AASHTO LRFD Bridge Design Specifications, Third Edition (AASHTO 2005), characterizes the service limit

state, fatigue and fracture limit state, strength limit state, and extreme event limit state respectively.

As stated by these articles, the service limit states place restrictions on stress, deformation, and crack width. The fatigue limit states place restrictions on stress range resulting from the cyclical loading and unloading of vehicular traffic and other dynamic responses. Fatigue limit states also specify material toughness requirements of the AASHTO Material Specifications. The strength limit states ensure the strength and stability, both locally and globally, to resist specified statistically significant load combinations that a bridge is expected to experience during its design life. The extreme event limit states ensure the structural survival of a bridge during a major earthquake, flood, or collision with a vehicle, vessel, or ice flow (AASHTO 2005).

Article 3.4.1 of the LRFD Specifications, presents the load combinations for the four limit state sets. The limit state load combinations applicable to steel bridges include: Strength Limit States I through V, Extreme Event Limit States I and II, Service Limit States I and II, and the Fatigue Limit State. These load combinations are defined as follows:

- Strength I – Basic load combination relating to the normal vehicular use of the bridge without wind.
- Strength II – Load combination relating to the use of the bridge by owner-specified special design vehicles, evaluation permit vehicles, or both without wind.
- Strength III – Load combination relating to the bridge exposed to wind velocity exceeding 55 mph.
- Strength IV – Load combination relating to very high dead load to live load force effect ratios.
- Strength V – Load combination relating to normal vehicular use of the bridge with wind of 55 mph velocity.
- Extreme Event I – Load combination including earthquake.

- Extreme Event II – Load combination relating to ice load, collision by vessels and vehicles, and certain hydraulic events with a reduced live load other than that which is part of the vehicular collision load.

- Service I – Load combination relating to the normal operational use of the bridge with a 55 mph wind and all loads taken at their nominal values. Also related to deflection control in buried metal structures, tunnel liner plate, and thermoplastic pipe and to control crack width in reinforced concrete structures. This load combination should also be used for the investigation of slope stability.

- Service II – Load combination intended to control yielding of steel structures and slip of slip-critical connections due to vehicular live load.

- Fatigue – Fatigue and fracture load combination relating to repetitive gravitational vehicular live load and dynamic responses under a single design truck having specified axle spacing.

Table 2.1 displays these load combinations applicable to steel structures and their corresponding load factors as specified in the LRFD Specifications (AASHTO 2005). Tables 2.2 and 2.3 provide a key for the permanent design loads and transient design loads respectively, as found in Table 2.1.

Table 2.1 Load Combinations and Load Factors (AASHTO 2005)

Load Combination Limit State	*DC* *DD* *DW* *EH* *EV* *ES* *EL*	*LL* *IM* *CE* *BR* *PL* *LS*	*WA*	*WS*	*WL*	*FR*	*TU* *CR* *SH*	*TG*	*SE*	Use One of These at a Time			
										EQ	*IC*	*CT*	*CV*
STRENGTH I (unless noted)	γ_p	1.75	1.00	—	—	1.00	0.50/1.20	γ_{TG}	γ_{SE}	—	—	—	—
STRENGTH II	γ_p	1.35	1.00	—	—	1.00	0.50/1.20	γ_{TG}	γ_{SE}	—	—	—	—
STRENGTH III	γ_p	—	1.00	1.40	—	1.00	0.50/1.20	γ_{TG}	γ_{SE}	—	—	—	—
STRENGTH IV *EH, EV, ES, DW DC* ONLY	γ_p 1.5	—	1.00	—	—	1.00	0.50/1.20	—	—	—	—	—	—
STRENGTH V	γ_p	1.35	1.00	0.40	1.0	1.00	0.50/1.20	γ_{TG}	γ_{SE}	—	—	—	—
EXTREME EVENT I	γ_p	γ_{EQ}	1.00	—	—	1.00	—	—	—	1.00	—	—	—
EXTREME EVENT II	γ_p	0.50	1.00	—	—	1.00	—	—	—	—	1.00	1.00	1.00
SERVICE I	1.00	1.00	1.00	0.30	1.0	1.00	1.00/1.20	γ_{TG}	γ_{SE}	—	—	—	—
SERVICE II	1.00	1.30	1.00	—	—	1.00	1.00/1.20	—	—	—	—	—	—
FATIGUE—*LL, IM* & *CE* ONLY	—	0.75	—	—	—	—	—	—	—	—	—	—	—

Table 2.2 Permanent Load Definition Key

Permanent Loads	Description
DD =	downdrag
DC =	dead load of structural components and nonstructural attachments
DW =	dead load of wearing surfaces and utilities
EH =	horizontal earth pressure load
EL =	accumulated locked-in force effects resulting from the construction process, including the secondary forces from post-tensioning
ES =	earth surcharge load
EV =	vertical pressure from dead load of earth fill

Table 2.3 Transient Load Definition Key

Transient Loads	Description
BR =	vehicular braking force
CE =	vehicular centrifugal force
CR =	creep
CT =	vehicular collision force
CV =	vessel collision force
EQ =	earthquake
FR =	friction
IC =	ice load
IM =	vehicular dynamic load allowance
LL =	vehicular live load
LS =	live load surcharge
PL =	pedestrian live load
SE =	settlement
SH =	shrinkage
TG =	temperature gradient
TU =	uniform temperature
WA =	water load and steam pressure
WL =	wind on live load
WS =	wind load on structure

Equation 2-1 is the general equation for LRFD methodology found in the LRFD Specifications (AASHTO 2005) that must be satisfied for all bridge components and connections at each applicable limit state.

$$\sum \eta_i \gamma_i Q_i \leq \phi R_n = R_r \qquad (2\text{-}1)$$

Where,

η = load modifier: a factor relating to ductility, redundancy, and operational importance.

γ = load factor: a statistically based multiplier applied to force effects.

Q = force effect.

R_n = nominal resistance.

R_r = factored resistance: ϕR_n.

This section provided an overview of the limit states and load combinations applicable to steel structures. In a typical bridge design, all of these

design criteria would be evaluated and applied as necessary. As mentioned in Chapter 1, the need for this research, problem description, and objectives of the research thesis surround criteria issues of the Service II Limit State. The following section will present a detailed overview to provide sufficient background information on the Service II Limit State.

2.1.2 Service II Limit State

The AASHTO LRFD Bridge Design Specifications, Third Edition states that the intent of the Service II limit state is to control yielding of steel structures and slip of slip-critical connections due to vehicular live load. The Service Limit State originates from the overload check of the 1992 AASHTO Standard Specifications and is based on successful past practice. Article 6.10.4 of the LRFD Specifications details the design of steel structures for the service limit state.

Elastic deformations are stress/strain linear in nature and relate to stress in the material below the yield stress. As specified by the LRFD Specifications (AASHTO 2005), the design of steel structures for elastic deformations is to be limited to avoid "undesirable structural and humanistic psychological effects". Deflection and girder depth limit checks are optional and should only be used if the design varies significantly from past successful engineering designs.

Plastic deformations are caused by stress in the material of the member in excess of the yield stress. In other words, when the yield stress is exceeded the material permanently deforms from its original geometric dimensions. The term plastic corresponds to the stress/strain relationship of the material. The ratio of stress/strain until the material reaches the yield stress is 1 to 1. However, once the yield stress is reached the ratio becomes a fraction and the material shows greater strain at lower magnitudes of stress. The design for plastic deformations is intended to prevent objectionable permanent deformations due to expected severe

traffic loadings that would impair rideability (AASHTO 2005). The provisions for these design specifications limit the flange stress in flexure to a percentage of the yield stress under the Service II load combination, as previously presented in Table 2.1. The load factors for live load and dead load are specified as 1.3 and 1.0 respectively.

Two flexural checks for the flanges of composite sections and one flexural check for the flanges of non-composite sections must be satisfied by the permanent deformation provisions of the LRFD Specifications (AASHTO 2005). Equations 2-2 through 2-4 are the permanent deformation flexural checks under the Service II load combination.

- For the top steel flange of a composite section:

$$f_f \leq 0.95 R_h F_{yf} \tag{2-2}$$

- For the bottom steel flange of a composite section:

$$f_f + \frac{f_l}{2} \leq 0.95 R_h F_{yf} \tag{2-3}$$

- For both steel flanges of a non-composite section:

$$f_f + \frac{f_l}{2} \leq 0.80 R_h F_{yf} \tag{2-4}$$

Where,

f_f = flange stress at the section under consideration due to the Service II loads calculated without consideration of flange lateral bending, (ksi).

f_l = flange lateral bending stress at the section under consideration due to the Service II loads, (ksi).

R_h = hybrid girder factor.

A major concern regarding the Service II Limit State is the frequency in which it places restrictions on and governs the design of compact section in flexure. This restriction stems from the flange stress limit provisions that are based on

successful past practice, which are not calibrated using LRFD methodology. It is unclear what stress limits are intolerable with regards to permanent deformations in girders due to repeated loading into the plastic range.

The flexural stresses calculated by Equations 2-2 through 2-4 under the Service II loads in the composite section may be computed using the short-term or long-term composite section, provided the member contains shear connectors along the entire length of the beam. If the factored modulus of rupture f_r of the concrete is exceeded by the Service II load combination in areas of adequate shear connection, the size or cracks in these regions is controlled by Equations 2-5 through 2-7.

- For normal weight concrete:

$$f_r = 0.24\sqrt{f'_c} \qquad (2\text{-}5)$$

- For sand-lightweight concrete:

$$f_r = 0.20\sqrt{f'_c} \qquad (2\text{-}6)$$

- For all light-weight concrete:

$$f_r = 0.17\sqrt{f'_c} \qquad (2\text{-}7)$$

Where,

f_r = modulus of rupture.

f'_c = specified strength of concrete (ksi)

The LRFD Specifications (AASHTO 2005) specifies the flange lateral bending stress f_l to be determined based on factored loads and as the largest value of the stress due to lateral bending throughout the unbraced length in the flange under consideration. Continuously braced flanges have a lateral bending stress equivalent to zero, while discretely braced flanges are evaluated through structural analysis and must satisfy Equation 2-8.

$$f_l < 0.6F_{yf} \qquad (2\text{-}8)$$

As previously mentioned, the purpose of Equations 2-2 through 2-4 is to prevent objectionable permanent deformations due to expected severe traffic loadings that would impair rideability (AASHTO 2005). Because these are serviceability specifications, the resistance factor, □, is equal to 1.00, and as a result is omitted from the equations. Hybrid steel sections often experience early web yielding as a result of increased flange stresses, therefore the hybrid girder factor R_h is included in the specifications and shown in Equation 2-9.

$$R_h = \frac{12 + \beta(3\rho - \rho^3)}{12 + 2\beta} \qquad (2\text{-}9)$$

The hybrid girder factor, R_h is taken as 1.0 for all rolled shapes, homogenous built-up sections, and built-up sections with higher-strength steel in the web than in both flanges; otherwise R_h is to be taken as specified in Equation 2-9.

The product of the hybrid girder factor, R_h, and the flange yield stress, F_{yf}, on the right-hand side of Equations 2-2 through 2-4 gives the stress that result in onset of yielding at the web-flange juncture in hybrid girders. This includes the effect of flange tip yielding, but does not consider flange residual stresses. Permanent deflections will remain small provided the flanges are nominally elastic at the web-flange juncture and the flange lateral bending stress; f_l is limited by Equation 2-8. It should also be noted that the values f_f and f_l from Equations 2-3 and 2-4 always be taken as positive. The flange lateral bending stress, f_l, is excluded from Equation 2-2 because the flange is continuously braced by the concrete deck. Equations 2-2 through 2-4 are not controlled by the following conditions as specified by the LRFD Specifications (AASHTO 2005):

- Composite sections in negative flexure for which the nominal flexural resistance under the strength load combinations is determined according to the provisions of Article 6.10.8. The computation of strength may be done according to Article

6.10.8 or Appendix A of Chapter 6, however when using Article 6.10.8 the increase in strength due to Saint Venant's Torsion is neglected.

- Non-composite sections with no flange lateral bending stress, f_l, and for which the nominal flexural resistance under the strength load combinations is determined according to the provisions of Article 6.10.8.

- Non-compact composite sections in positive flexure.

Equations 2-2 through 2-4 are not applicable under the following condition because it does not control:

- For the region extending from the pier section to the nearest flange transition or point of permanent-load contraflexure for continuous-span flexural members that satisfy the provisions of Article B6.2 and the procedures of either Article B6.3 or B6.6 of the LRFD Specifications (AASHTO 2005) with respect to moment redistribution procedures.

Except for composite sections in positive flexure where the web satisfies the aspect ratio of Equation 2-10, all sections must satisfy Equation 2-11.

$$\frac{D}{t_w} \leq 150 \qquad (2\text{-}10)$$

$$f_c \leq F_{crw} \qquad (2\text{-}11)$$

Where,

D = depth of the web.

t_w = thickness of the web.

f_c = compression-flange stress at the section under consideration due to the Service II loads calculated without consideration of flange lateral bending, (ksi).

F_{crw} = nominal bend-buckling resistance for webs with or without longitudinal stiffeners, as applicable, determined as specified by Equation 2-12, (ksi).

$$F_{crw} = \frac{0.9Ek}{\left(\frac{D}{t_w}\right)^2} \qquad (2\text{-}12)$$

Additionally, Equation 2-11 must be satisfied for those sections that satisfy the geometric provisions applicable sections for moment redistribution design under the standard Service II load combination or the refined method for moment redistribution design. These geometric provisions are presented in the subsequent section 2.1.3.2. The moment redistribution design procedures will be detailed in the subsequent sections of this chapter. In general, Equation 2-11 checks the web bend-buckling under the Service II load combination.

2.1.3 Moment Redistribution

2.1.3.1 Theory

The structural response for statically determinant structures (simply supported structures) in flexure is largely dependent on stability. Under stable conditions where local and global buckling does not govern, the bending resistance is governed by the plastic moment, M_p. As the cross-section reaches the plastic moment, additional rotation will occur at the section and a hinge resisting constant moment equal to the nominal moment capacity is developed. The disadvantage of simply supported bridge girders is that when the plastic hinge forms, so does a collapse mechanism.

However, statically indeterminate structures (continuous-span structures) offer additional load carrying capacity and do not form a collapse mechanism until multiple hinges form. This offers major advantages to design engineers and explains the continuing trend for the use of continuously supported structures in modern practice. These advantages include savings in cost, lower bending moments, and lower deflections. The additional load carrying capacity is taken advantage of through the moment redistribution design procedures, otherwise referred to as inelastic design. As increased loading causes the elastic behavior in a

continuously supported bridge girder to approach its limit, the moment at the interior pier support (negative moment region) reaches the yield moment, M_y. The interior pier support reaches the yield moment prior to the mid-span (positive moment region) because of the behavioral nature of a continuous-span structure. Increasing load beyond this point causes a plastic hinge to form with a constant moment equal to the nominal moment capacity at the interior pier support without resulting in a collapse mechanism. The positive moment regions have reserve capacity and continued loading results in the distribution of moment from the higher stressed interior pier support to these positive moment regions, assuming the structure provides sufficient rotation capacity.

Figure 2.1 illustrates the concept of moment redistribution for a two-span continuous girder. In a typical elastic design, the moment envelope is represented by the heavy black line labeled M_e. As previously mention, when the material at the interior pier yields, moment gets redistributed from the negative moment region to the positive moment regions. This redistributed moment envelope is represented with a light gray line labeled M_{rd}. The summation of the elastic moment envelope and the redistributed moment envelope results in the final design moment envelope for inelastic design procedures, represented by the dark gray line labeled $M_e + M_{rd}$. As illustrated in Figure 2.1, moment redistribution design results in a lower design moment at the negative moment region and higher design moment at the positive moment region. This is especially ideal for a composite continuous-span girder because the concrete is acting in compression at the positive moment region and in tension at the negative moment region. The concrete is ineffective at the interior pier, but is compensated for by the reduced design moments in this region. However, the concrete provides adequate moment resistance in the spans for the higher moments.

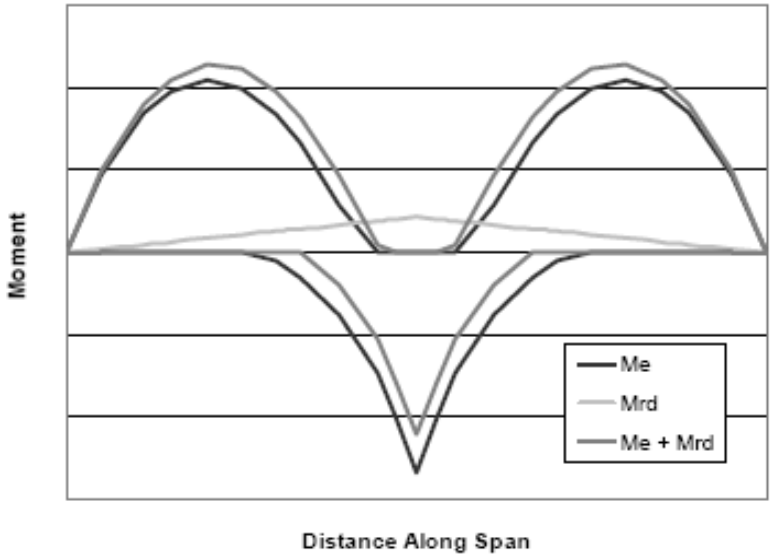

Figure 2.1 Illustration of Moment Redistribution Concept (Righman 2005)

It has been shown that the actual strength of continuously supported structures is best estimated through the use of moment redistribution procedures. Furthermore, moment redistribution design procedures offer significant advantages in economics and rating efficiency. The first major economic advantage as a result of moment redistribution design procedures is smaller cross-sections because of lower applied moments, therefore eliminating the need for cover plates in rolled beams to account for high stress. In addition to the economic advantage, the elimination of cover plates is more advantageous to a region in a girder in terms of greater fatigue resistance. The other major economic advantage is the large reduction in the number of flange transitions in welded plate girders. This results in savings of material and expensive fabrication costs. Additionally, the application of moment redistribution design procedures offers a major advantage with regard to already existing bridge structures. Moment redistribution rating procedures can more accurately predict the strength of existing bridges, resulting in higher load capacities. Although moment redistribution procedures for rating are not presently

incorporated in AASHTO specifications, such provisions would result in fewer bridges being rated as structurally deficient and reduce the need for rehabilitation and/or replacement.

2.1.3.2 Scope

The LRFD Specifications (AASHTO 2005) state that moment redistribution design procedures shall be only applied to sections within one unbraced length on each side of the interior pier if the following provisions are satisfied for these regions. These provisions are an attempt to ensure that there is sufficient ductility and robustness of the interior pier sections for moment redistribution behavior.

- Straight continuous span I-section members.
- Bearing lines are not skewed more than 10 degrees from radial.
- Nominal yield strength of the steel does not exceed 70 ksi.
- There are no staggered cross-frames in the bridge system.
- There are no holes in the tension flange within a distance equal to twice the web depth from each side of the pier where moments are redistributed from.
- The cross-section is prismatic within the unbraced length from which moment is redistributed.
- The shear force is less than the nominal shear capacity of the web neglecting tension field action and post-buckling shear resistance.
- $\frac{D}{t_w} \leq 150$, aspect ratio intended to eliminate the use of any benefits from longitudinal stiffening of the web at pier sections.
- $\frac{2D_c}{2t_{fc}} \leq 0.38\sqrt{\frac{E}{F_{yc}}}$, limit on the web slenderness.
- $D_{cp} \leq 0.75D$, limit on the depth of the web in compression.

- $\frac{b_{fc}}{2t_{fc}} \le 0.38\sqrt{\frac{E}{F_{yc}}}$, limit for compactness on the compression flange within the unbraced lengths adjacent to the interior pier

- $b_{fc} \ge \frac{D}{4.25}$, represents the largest allowable aspect ratio due to the negative influence of increasing aspect ratios on the strength and moment-rotation characteristics of I-sections.

- $L_b \le \left[0.1 - 0.06\left(\frac{M_1}{M_2}\right)\right]\frac{r_t E}{F_{yc}}$, represents the requirement for compact-section compression-flange lateral bracing.

Where,

D_c = depth of the web in compression in the elastic range (in.).

D_{cp} = depth of the web in compression at the plastic moment (in.).

L_b = unbraced length (in.).

M_1 = bending moment about the major-axis of the cross section at the brace point with the lower moment due to the factored loads, taken as either the maximum or minimum moment envelope value, whichever produces the smallest permissible unbraced length (kip-in.).

M_2 = bending moment about the major-axis of the cross-section at the brace point with the higher moment due to the factored loads, taken as the critical moment envelope value (kip-in).

R_t = effective radius of gyration for lateral torsional buckling (in.)

$\frac{M_1}{M_2}$ = ratio taken as negative when the moments cause reverse curvature.

2.1.3.3 General Discussion

The current LRFD Specifications (AASHTO 2005) allow the interior pier regions to be designed for lower levels of moment based on moment redistribution design procedures under the service limit state or strength limit state. A concern has been raised regarding the use of the design procedures for the service limit

state. The design procedures under the service limit state rarely, if at all, provide a more efficient design because Equation 2-11 governs. In addition, a question is raised regarding the inclusion of moment redistribution design under the service limit state. The additional concern is attributed to the conflicted intention of the service limit state to restrict undesirable deformations, while the moment redistribution design procedures will inevitably result in permanent deformations.

Calculation of the redistribution moments for the service limit state at interior pier supports is based on concepts of shakedown analysis of continuous-span girders under repeated application of moving loads (ASCE 1971; Schilling et al. 1997) utilizing an effective plastic moment that accounts for the interior pier section moment-rotation characteristics. An approximate upper-bound plastic rotation of 0.009 radians at the pier section serves as a base for the effective plastic moment M_{pe}, at the service limit state, as determined through direct inelastic analysis of several design trials (Schilling 1986). Equations 2-13 and 2-14 govern the redistribution moment for the Service II loads at each interior pier section.

$$M_{rd} = \left|M_e\right| - M_{pe} \qquad (2\text{-}13)$$

$$0 \le M_{rd} \le 0.2\left|M_e\right| \qquad (2\text{-}14)$$

Where,

M_{pe} = negative-flexure effective plastic moment for the service limit state (kip-in.), as subsequently detailed below in section 2.1.3.1.

M_e = critical elastic moment envelope value at the interior pier section due to the Service II loads (kip-in.).

Equation 2-13 provides the magnitude of moment redistribution and Equation 2-14 is included to prevent an exceptionally small section from potentially violating the upper-bound plastic rotation of 0.009 radians under the Service II loads.

The LRFD Specifications (AASHTO 2005) state that the redistribution moments, M_{rd}, at all other locations other than the interior pier support under the Service II loads shall be calculated by creating a redistribution-moment diagram. The redistribution-moment diagram is constructed with a straight line between adjacent interior pier supports and any adjacent supports that are locations of zero redistribution moment, including the abutments. The redistribution moments vary linearly between supports because the redistribution moments are held in equilibrium by reactions at the supports after the live loads are removed. Figure 2.2 illustrates an example of a three-span continuous girder redistribution-moment diagram.

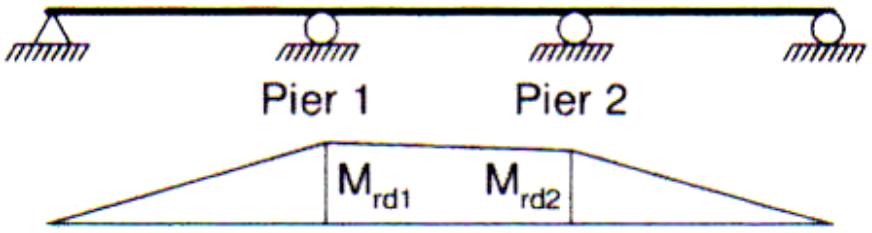

Figure 2.2 Redistribution-Moment Diagram (AASHTO 2005)

Chapter 6, Appendix B of the LRFD Specifications (AASHTO 2005) details moment redistribution design procedures from interior pier sections of continuous-span, I-section, flexural moments at the service and/or strength limit states. The provisions of the AASHTO LRFD Bridge Design Specifications, Third Edition (AASHTO 2005) for moment redistribution replace the 10 percent redistribution allowance in prior specifications and offer a design approach that includes compact and non-compact sections. The 10 percent redistribution allowance refers to the amount of design moment at the interior pier that may be redistributed to the positive

moment regions. The current specifications allow a 20 percent redistribution of moment. This current rational approach utilizes elastic moment envelopes and does not involve any inelastic analysis procedures.

2.1.3.4 Effective Plastic Moment

Tests conducted have shown that members with interior pier sections that satisfy either of the following conditions, exhibit an enhanced moment redistribution capacity (AASHTO 2005). This statement is in addition to the satisfaction of previously presented geometric provisions in the scope.

- Transverse stiffeners spaced at D/2 or less over a minimum distance of D/2 on each side of the interior pier section.
- $\frac{2D_{cp}}{t_w} \le 2.3\sqrt{\frac{E}{F_{yc}}}$

If either of these conditions is met, then the effective plastic moment M_{pe} is calculated for the service limit state and strength limit state using Equations 2-15 and 2-16.

$$M_{pe} = M_n \tag{2-15}$$

$$M_{pe} = \left(2.78 - 2.3\frac{b_{fc}}{t_{fc}}\sqrt{\frac{F_{yc}}{E}} - 0.35\frac{D}{b_{fc}} + 0.39\frac{b_{fc}}{t_{fc}}\sqrt{\frac{F_{yc}}{E}}\frac{D}{b_{fc}}\right)M_n \le M_n \tag{2-16}$$

Where,

M_n = nominal flexural resistance of the interior pier section taken as the smaller of the $F_{nc}S_{xc}$ and $F_{nt}S_{xt}$. For sections with compact or non-compact webs, M_n may be taken as the smaller of M_{nc} and M_{nt}.

Otherwise, the effective plastic moment for the service limit state and strength limit state is calculated using Equations 2-17 and 2-18 respectively.

$$M_{pe} = \left(2.90 - 2.3\frac{b_{fc}}{t_{fc}}\sqrt{\frac{F_{yc}}{E}} - 0.35\frac{D}{b_{fc}} + 0.39\frac{b_{fc}}{t_{fc}}\sqrt{\frac{F_{yc}}{E}}\frac{D}{b_{fc}} \right) M_n \le M_n \quad \text{(2-17)}$$

$$M_{pe} = \left(2.63 - 2.3\frac{b_{fc}}{t_{fc}}\sqrt{\frac{F_{yc}}{E}} - 0.35\frac{D}{b_{fc}} + 0.39\frac{b_{fc}}{t_{fc}}\sqrt{\frac{F_{yc}}{E}}\frac{D}{b_{fc}} \right) M_n \le M_n \quad \text{(2-18)}$$

As shown below in sections 2.1.3.5 and 2.1.3.6, the calculation of the effective plastic moment is essential to the moment redistribution design procedures and governs the upper bound limit of the redistribution moment under the service limit and strength limit load combinations.

2.1.3.5 Service Limit State Moment Redistribution

Moment redistribution design for the service limit state utilizing the Service II load combination is covered by Article B6.3 of the LRFD Specifications (AASHTO 2005). Flexure of the spans adjacent to the interior pier supports, extending to the nearest flange transition point or point of dead-load contraflexure must satisfy the web bend buckling check of Equation 2-11 before moment redistribution. However, the provisions included in the flange stress limit Equations 2-2 through 2-4 can be neglected because local yielding is accepted at the interior supports to allow for the redistribution of moments.

The permanent deformations are limited by the flange stress limits of $0.80F_y$ for non-composite and $0.95F_y$ for composite sections in the adjacent spans outside the nearest flange transition location or point of permanent-load contraflexure, whichever is closest to the interior pier support after redistribution. Flexure in these regions must satisfy the flange stress limit provisions of Equations 2-2 through 2-4 and the web bend buckling stress provision of Equation 2-11 as applicable. This is done by adding the redistribution moments to the elastic moments from Service II before performing the calculations for these provisions.

For composite members the long-term composite section shall be used to account for the repetition of stresses by continual passages of similar loadings.

2.1.3.6 Strength Limit State Moment Redistribution

Moment redistribution design for the strength limit state utilizing the various load combinations of the strength limit states is covered by Article B6.4 of the LRFD Specifications (AASHTO 2005). There is no check for the flexural resistance of unbraced sections adjacent to the interior pier supports because the strength and ductility influence is accounted for within the moment redistribution calculations. There is no change in the flexural resistance design for sections outside the unbraced lengths and adjacent to the interior pier sections from which moments are distributed. The provisions for I-section flexural members in Article 6.10 and the optional provisions for members with web slenderness well below the non-compact limit of A6.1 are applied when applicable with the exception that the redistribution moments shall be added to the elastic moments due to the factored loads at the strength limit state prior to calculations.

Redistribution moments, M_{rd}, at interior pier sections for the strength limit state are taken as the larger value of Equations 2-19 and 2-20, where flexural resistance is not checked for sections adjacent to the interior pier when they satisfy the geometric provisions listed in the scope. Equation 2-21 governs the range of M_{rd} values under the strength limit state. Based on various trial inelastic design analysis research (Schilling 1986), the effective plastic moment, M_{pe}, relies on an estimated upper bound plastic rotation of 0.03 radians at the interior pier supports.

$$M_{rd} = |M_e| + \frac{1}{3} f_l S_{xc} - \phi_f M_{pe} \qquad (2\text{-}19)$$

$$M_{rd} = |M_e| + \frac{1}{3} f_l S_{xt} - \phi_f M_{pe} \qquad (2\text{-}20)$$

$$0 \le M_{rd} \le 0.2\left|M_e\right| \qquad (2\text{-}21)$$

Where,

ϕ_f = resistance factor for flexure.

M_{yc} = yield moment with respect to the compression flange (kip-in.).

S_{xc} = elastic section modulus about the major axis of the section to the compression flange taken as M_{yc}/F_{yc} (in^3).

S_{xt} = elastic section modulus about the major axis of the section to the tension flange taken as M_{yt}/F_{yt} (in^3).

The reduction in the flexural resistance of the interior pier section is conservatively accounted for in Equations 2-19 and 2-20 with the inclusion of flange lateral bending effects. The flange lateral bending stress, f_l, is included to resist wind loads. Equation 2-21 is utilized to prevent an exceptionally small section from potentially violating the upper-bound plastic rotation of 0.03 radians under the strength limit state. The inclusion of the resistance factor, ϕ_f, accounts for the fact that the yielding within regions of positive flexure and the corresponding redistribution of positive bending moments to the interior pier sections is neglected in the equations. The redistribution moments under the strength limit state for all sections other than the interior pier support are calculated in the same manor as the service limit state by using the redistribution-moment diagram, see Figure 2.2.

2.2 AASHO Road Test

In the late 1950's, the American Association of State Highway Officials[1] (AASHO) conducted the historic and one-of-a-kind "Road Test" under the administration and direction of the Highway Research Board[2]. The test was

[1] American Association of State Highway Officials (AASHO) became known as the American Association of State Highway and Transportation Officials (AASHTO) on November 11th of 1973, (Schilling 1981).

[2] Now the Transportation Research Board (Fenves et al.).

conducted just northwest of Ottawa, Illinois, which is approximately 80 miles southwest of Chicago. The Bureau of Public Roads[3] (BPR) had the responsibility of assigning permanent staff and engineers to the project for 6 months. The original intention of the Road Test was to quantitatively evaluate the relationship between the service life of highway pavement to the magnitude of wheel loads, frequency of wheel loads, and characteristics of the pavement (Fenves et al.). Contributions and the funding of $27 million for the Road Test were provided by all 48 contiguous states, Hawaii, the District of Columbia, and Puerto Rico. In addition, 300 to 400 soldiers were used to drive the test vehicles.

In an effort to study the effect of repeated overstress on the service life of highway bridges, the scope of the Road Test was expanded to include bridges at the request of the AASHO Committee on Bridges (Fenves et al.). The committee decided to test eight bridges with steel beams, four with prestressed concrete beams, and four with reinforced concrete beams. Two steel bridges were replaced during the Road Test, as explained in the subsequent sections. All 18 bridges were designed to be a representative collection of bridges commonly found on the U.S. highway system. For the purpose of this thesis, only information regarding the steel bridges will be discussed, because the scope of this research and the Service II limit state is strictly applicable to steel structures.

The bridges included in the Road Test were all 50-foot simple-span slab-and-beam structures. The steel beams were all rolled wide flange sections with or without cover plates. The three types of steel beams used were non-composite with cover plates, non-composite without cover plates, and composite with cover plates. Maximum yield stress values of 27 ksi and 35 ksi were chosen for the

[3] Now the Federal Highway Administration (Fenves et al.).

design of the steel beams; however the actual test beams had a mean yield point varying from 34.7 ksi to 37.9 ksi, according to tension tests of flange coupons.

Table 2.4 Principle Design Features of AASHO Test Bridges* (AASHO 1962)

Steel Beam Type	Design Stress Level, Maximum Tension (psi)		No. of Bridges
	27,000	35,000	---
Non-composite, no cover plates	x	xx	3
Non-composite, cover plates	xy	y	5
Composite, cover plates	x	xx	2

Figures 2.3 and 2.4 show the AASHO Road Test configuration, which consisted of six test loops with double-lane tangents and turnarounds at each end of a tangent to allow for continuous test traffic (Fenves et al.). Four single-lane bridges were placed at the beginning of the tangent loop sections in these figures. Bridges 4A and 4B, as previously mentioned, were eventually replaced by bridges 9A and 9B in the identical locations of Figure 2.4.

* x represents one bridge; y represents one pair of duplicate bridges

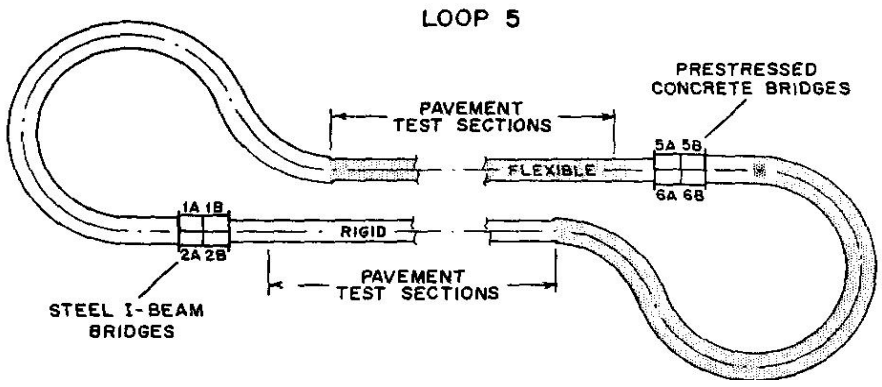

Figure 2.3 AASHO Road Test Bridge Locations, Loop 5 (AASHO 1962)

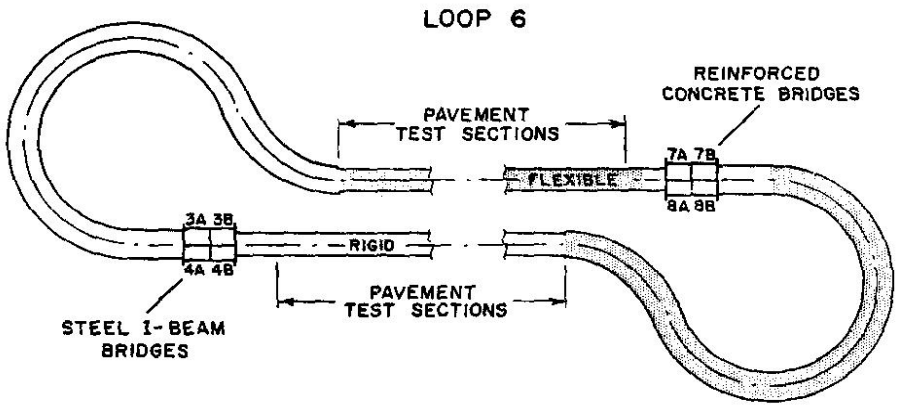

Figure 2.4 AASHO Road Test Bridge Locations, Loop 6 (AASHO 1962)

Each test bridge was actually one simple-span of a two-span bridge. For example, test bridges 2A and 2B were each simple-spans that formed one bridge. The simple-span bridges were supported by concrete substructures on spread footings at the pier and at the abutments. Figures 2.5 and 2.6 depict a longitudinal and transverse view of a typical AASHO Road Test steel bridge. As illustrated in the figures, each bridge consisted of 3 girders spaced 5-feet apart and either 3-feet

from the parapet or 2-feet from the center-line of the roadway, therefore making the width of each test bridge 15-feet. The height of the concrete supports was 6’-9” for all test bridges. The concrete slabs were 6-½ inches thick and provided 1-½ inches of cover between the top of slab and reinforcement steel. Reinforcement steel for the concrete deck of non-composite bridges and composite bridges was 3/8-inch in diameter and 5/8-inch diameter respectively.

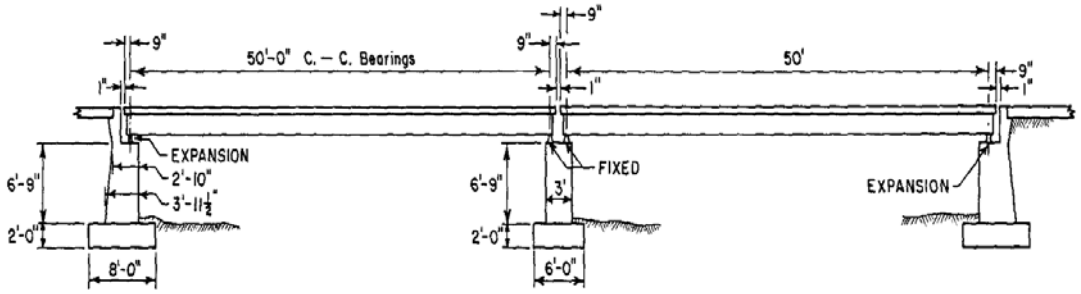

Figure 2.5 Longitudinal View of Typical Road Test Bridge (AASHO 1962)

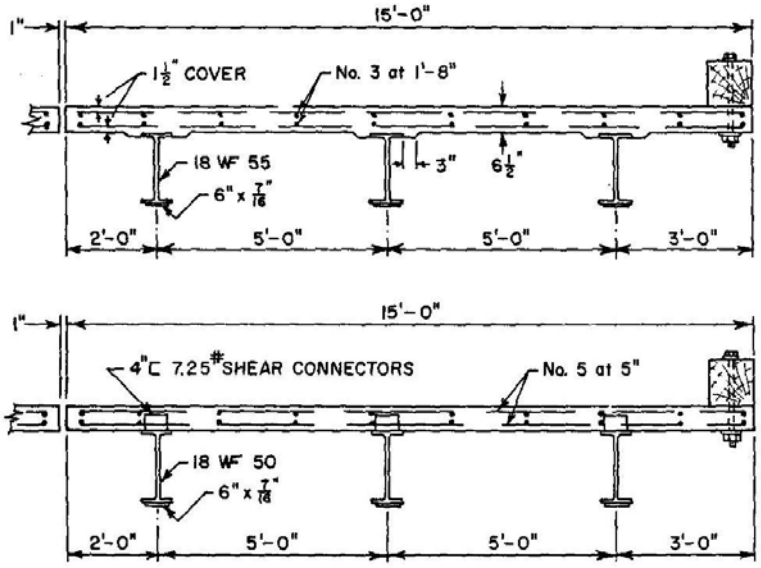

Figure 2.6 Transverse View of Typical Road Test Bridge (AASHO 1962)

Prior to the period of regular test traffic, initial reference tests were made to collect initial data on stresses and deformations. These initial reference tests were made at 6 month intervals and collected data for a standing vehicle, crawl speed vehicle (3 mph), and a regular speed vehicle (30mph). Table 2.5 displays the results of the initial reference test, which includes the stresses at critical sections, live load deflection, and permanent set. The live load deflection and permanent set are the average of the interior, center, and exterior beams of each bridge.

In general, the observed stresses of the initial reference test match well, within 10 percent of the design stresses, with the exception of bridges 2A, 4A, and 4B. The live load deflections are taken as the mean of 30-mph reference tests. Beams rarely experienced a live load deflection more than 10 percent from the mean. The initial reference tests resulted in a permanent set for all steel bridges and indicated yielding in various sections of the beams. As expected by the stress data, the largest permanent set was found in bridges 2A, 4A, and 4B. These three bridges yielded heavily during the initial reference test and the testing was terminated when the permanent set at mid-span was in excess of 3-in. in all three beams (AASHO 1962).

Testing of Bridge 1B was terminated shortly after regular test traffic began, when two vehicles from the adjacent lane crossed the bridge causing a 40 percent increase in the live load moment and thus a permanent set greater than 3-inches. Following the initial reference tests, regular test traffic began in October and ended in December. Table 2.6 shows the total number of trips made by test vehicles during the Road Test.

Table 2.5 Initial Reference Test Data (AASHO 1962)

Bridge		Bottom Flange Stress (ksi) Avg. of Beams	Design Stress	Live Load Deflection (in.)	Permanent Set (in.)
1A	18WF55	27.7	27.0	1.73	0.44
1B	18WF50	36.1	34.8	1.93	1.85
2A	18WF55	38.5	35.0	2.40	3.18
2B*	18WF50	33.3	35.0	1.06	0.29
3A	18WF50	31.6	37.3	1.67	0.85
3B*	18WF60	28.6	26.9	0.75	0.09
4A	18WF60	38.6	34.7	2.43	3.37
4B	18WF60	41.2	34.7	2.67	3.73
9A	18WF96	24.4	27.0	1.70	0.32
9B	18WF96	24.9	27.0	1.46	0.28

Table 2.6 AASHO Road Test Traffic Count Data (AASHO 1962)

Bridge	Number of Trips of Vehicles Regular Test Vehicles	Lighter than Reg. Test Veh.	Heavier than Reg. Test. Veh.
1A	557,400	275	8
1B	235	131	2
2A	26	174	0
2B	558,400	335	0
3A	392,400	722	1
3B	557,800	722	2
4A	106	188	0
4B	106	188	0
9A	447,900	100	0
9B	447,900	100	0

As previously mentioned, the Service Limit State originates from the overload check of the 1992 AASHTO Standard Specifications and is based on past practice. It is the AASHO Road test which forms the bedrock for which the flange

* Composite Beam

stress limits of the Service II Limit state are founded. According to Hansell & Viest (1971) the bridge experiments of the AASHO Road Test demonstrated that, under some circumstances, permanent deformations can take place in steel beams at stresses lower than the nominal yield point of the steel. Hansell & Viest (1971) state that the regular test traffic intentionally caused yielding in all steel beams at test stresses approaching $0.8F_y$ and $0.9F_y$. As shown in Figure 2.7, a test stress to yield stress ratio versus the cumulative permanent set at the end of regular test traffic for all six steel bridges that survived 390, 000 passes is the founding justification for the stress limits.

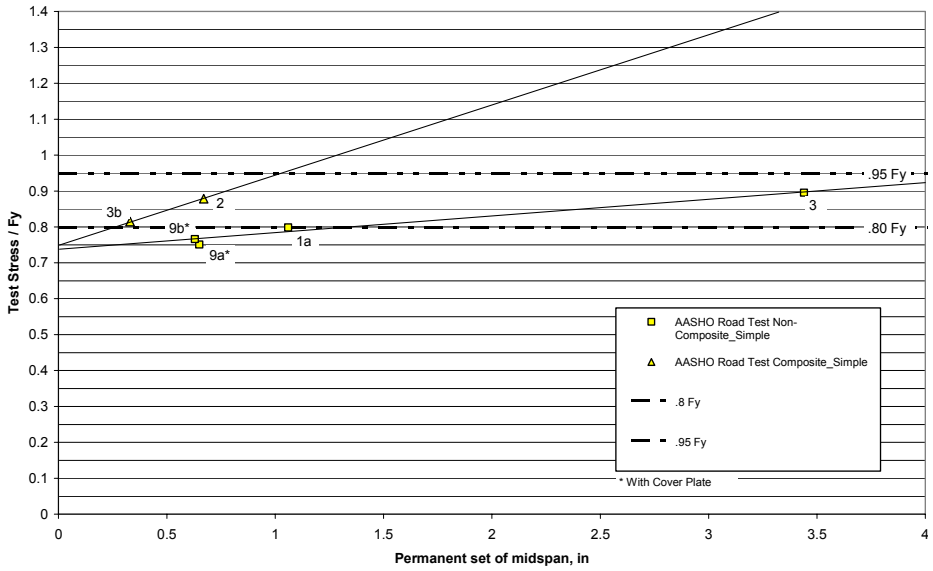

Figure 2.7 AASHO Road Test Data for Service II Stress Limits (Hansell & Viest 1971)

Because the flange stress limits of the Service II are founded on Figure 2.7 and the AASHO Road Test, several concerns are raised. The first concern is the fact that the limit state is based on limited experimental data obtained from a single study that included variation of relatively few parameters. This collection of data is

not significant enough in forming the basis for these flange stress limitations. In fact, there are only two experimental data points which form the basis of the composite beam and the 95 percent flange stress limit. Obviously, a Service Limit State that has such a governing effect on the design of modern bridges should be justified by a greater pool of experimental data. The bridges excluded from Figure 2.7 and thus the evaluation of the flange stress limits for the Service II Limit State because of their failure prior to the regular test traffic have been added to Figure 2.8. Additionally, one experimental data point of a 200-ft, 3-span, continuously-supported, composite structure has been added in an attempt to include more data points. This experimental test data came from experimental testing of a bridge in Ontario for deflection (King et al.)

The second concern is the alternative flange stress limits for composite girders and non-composite girders are intended to result in the same permanent set. However, there is an apparent discrepancy between values of permanent set at the respective composite and non-composite flange stress limits. As shown in Figure 2.8, the discrepancy is 0.35-inches, which indicates that the flange stress limit for a composite beam could potentially be $1.01F_y$. This assumes that the non-composite flange stress limit and its corresponding permanent set are accurate design criteria. The potential flange stress limit for composite sections comes from following the permanent set vertical line of the non-composite section until it intersects the line for experimental composite data in Figure 2.8 at a stress ratio of $1.01F_y$. If the flange stress limit for composite compact sections was greater than the yield stress, then the Service II Limit State would not govern the design of these sections and no longer be an issue. The Service II Limit State is intended to prevent objectionable deformations, however a flange stress limit greater than yield would in fact promote deformations in the flange.

The third concern of the basis for the Service II design criteria on the data in Figure 2.7 is that the deflection data recorded for the experiment was the result of all test bridges having the equivalent span length of 50-feet. The deflection and permanent set of a girder is directly related to span length, therefore experimental data should have included varying span lengths. Inclusion of the effects of span length in the design criteria for the Service II Limit State would make it a more efficient design criterion for basing the flange stress limits.

The fourth concern is that the majority of modern bridges are continuous-span structures, however all test bridges used for the Road Test were simple-span structures. Continuous-span structures will result in lower levels of deflection and permanent set compared to a simple-span structure. Using this logic, the flange stress limits of the Service II Limit State would be reduced because of the lower resulting permanent set of continuous-span structures. Therefore, Figure 2.7 must be updated to include experimental data on continuous-span structures in order to evaluate the current flange stress limits for a more efficient design criterion.

The final concern is the conservatism of the AASHO Road Test. Figure 2.7 is based on bridges that survived more than 390, 000 vehicle passes, which according to Hansell & Viest (1971) is equivalent to 20 overload crossings everyday for more than 50 years. This is clearly significantly greater than any bridge would ever experience during its lifetime. Therefore, the permanent sets displayed in Figure 2.7are greater than would ever be realized by a bridge.

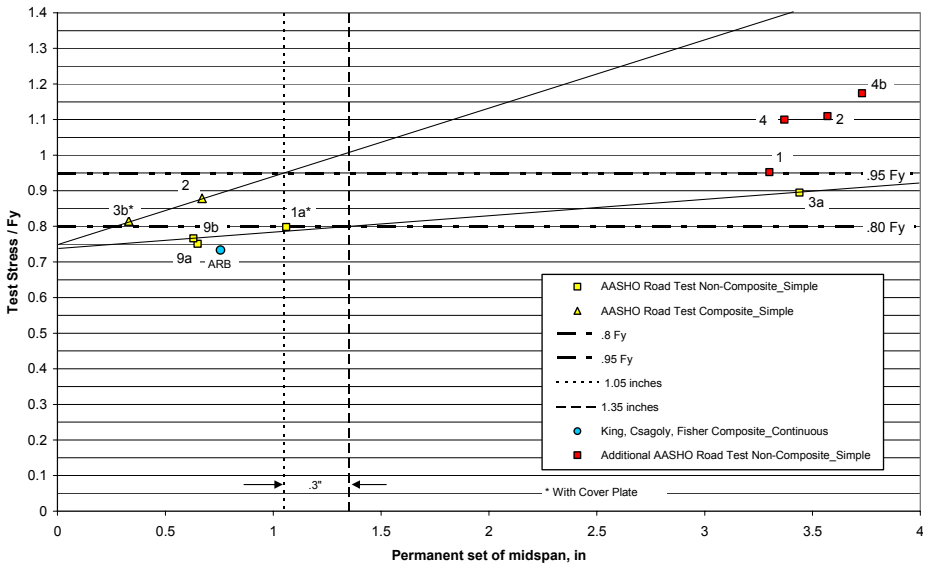

Figure 2.8 Updated AASHO Test Data for Service II Stress Limits

Table 2.7 Data for Figures 2.6 and 2.7

Bridge	Final Mean Permanent Set (in)	Test Stress / Flange F_y
1A	1.06	0.80
1B	3.30	0.95
2A	3.57	1.11
2B	0.67	0.88
3A	3.44	0.90
3B	0.33	0.81
4A	3.37	1.10
4B	3.73	1.17
9A	0.65	0.75
9B	0.63	0.77

2.3 Criteria for the Service II Limit State

With regard to the intentions of the Service II Limit State, the ambiguity of the phrase "to prevent objectionable deformations due to expected severe traffic

loadings which would impair rideability" raises questions. What magnitude of deformation is "objectionable" and when does the public characterize the bridge as having impaired rideability? The term "rideability" can be thought of in other words as the functionality or serviceability of the bridge.

The public will characterize unacceptable deformation based on their personal perception and experience on the bridge. The amount of deflection or permanent set of a bridge girder is relative to the span length of the bridge. For example, a permanent set of 3-inches may be unacceptable for a 50-foot span length, but acceptable and go unnoticed for a 200-foot span. If the intention of the Service II Limit State is to limit deformation, then the justification and calibration of the criteria must account for variations in span length. As previously discussed, the current Service II limit state is implemented to maintain rideability by controlling girder deformation, however Walker and Wright (1971) have shown that deflection and deformation limits are not a good method for controlling bridge vibrations.

Additionally, research has shown that the public defines an unacceptable bridge in terms of sensation. Within reason, the permanent set of a bridge span can not be felt or viewed by those driving across; instead, human perception is more sensitive to vibrations. As previously discussed, the current Service II limit state is implemented to maintain rideability by controlling deformation, however Walker and Wright (1971) have shown that deformation limits alone are not a good method of controlling bridge vibrations or assuring human comfort. Accelerations in the bridge are the root of these unacceptable vibrations; whether the result of an overload vehicle, wind, or earthquake. If the service limit states are to ensure the rideability of a bridge is maintained, then accelerations must be quantified and accounted for in the design criteria. There is limited research available for controlling human comfort due to bridge vibration, most of which limits either vertical acceleration or the natural frequency of the bridge. However, Walker and

Wright (1971) have developed an alternative method that utilized deflection and vertical acceleration limits in an effort to control bridge vibration. In short, the static deflection due to live load and the natural period of each bridge girder is computed. Truck speed, impact factors, and natural period are all correlated to result in a maximum deflection. They have determined that a bridge exceeding a vertical acceleration greater than 100 in/s^2 must be redesigned (Roeder et al. 2004).

Currently, the Ontario Bridge Code (Ministry of Transportation 1991) has provisions similar to the method developed by Walker and Wright (1971). To evaluate and control the bridge vibration, the Ontario Bridge Code utilizes a relationship between natural frequency and maximum superstructure static deflection. Human perception to vibration is used to calibrate the deformation limits (Roeder et al. 2004). The following questions are raised regarding the acceleration of a bridge in terms of the service limit state and the public perception:

1 What magnitude and direction of acceleration does the public find unacceptable?

    a. This question has only been addressed by the Ontario Bridge Code (Ministry of Transportation 1991). Background and literature reviews of this provision should be researched for design criteria in incorporation of the AASHTO LRFD Specifications.

2 What magnitude of acceleration should be accounted for in a bridge design in an effort to eliminate unacceptable rideability?

    a. This question has only been addressed by Walker and Wright (1971), therefore needing greater data for validation and incorporation in the LRFD Specifications.

3 What methods of bridge design and construction should be implemented to satisfy the service limit state acceleration criteria?

Chapter 3

3. Experimental Design

3.1 Scope

The original scope for the test specimens of the experimental testing portion of this research included five steel I-girders - one simply supported and four two-span continuously supported. The testing of a simply supported beam was desired in order to provide direct correlation with the AASHO Road Test data shown in Figure 2.7, on simply supported beams. Experimental results collected from a simply supported beam will also help validate the scaling of the experimental test specimens and the testing procedures used. The other beams are to be tested as continuously supported structures because of the current and future bridge design trend of engineers and owners towards these structures. Additionally, continuous-span structures will be tested to meet the interests of this research with regard to the objectives and problem description surrounding the Service II Limit State and moment redistribution design. There is a lack of founding data for the Service II design criteria on continuous-span structures and moment redistribution design procedures are only applicable to continuous-span structures.

Stress limits are a function of the steel yield stress, but research has not been performed to look at these limits for High Performance Steel (HPS) and Grade 50 steel. Therefore, the initial scope for the testing of the continuous-span structures include details for two High Performance Steel (HPS) and two Grade 50 beams, yield strength 70 ksi and 50 ksi respectively. The Service II flange stress limits are 0.95Fy and 0.80Fy for composite and non-composite specimens, therefore

the initial scope of test specimens includes the testing both specimen types. The goal behind this collection of test specimens is to provide a direct correlation back to the AASHO Road Test data, while concentrating on the service stress and moment redistribution behavior of modern structures. This modernized scope of testing for these parameters will help evaluate the flange stress limits of the service limit state by providing data that may strengthen or weaken the basis for these limits, with the long term goal of making them more efficient for design criteria.

With the basic target parameters of the test specimens determined, it was decided that the design of the test specimens needed to satisfy two key geometric criteria: (1) the specimens must have geometric properties and strength capacities such that they may be efficiently tested in the structures laboratory at the University of Delaware, and (2) the specimens must adequately represent a scaled-down model of typical bridge girder. After evaluation of the geometric constraints in the laboratory, the primary limitation was determined to be a maximum test specimen length of 30-feet. Thus, the maximum permissible span length for the two-span continuous beams was set at 15-feet. Figure 3.1 shows the basic test layout for a continuous-span beam based on these geometric constraints. The point load will be applied in both spans by hydraulic actuators 4-feet from the interior pier. Simple-span testing was to be done using three-point bending and continuous-span testing was to be done by applying a concentrated load in each span. The 4-foot spacing was selected to satisfy lateral bracing specifications as specified in subsequent sections.

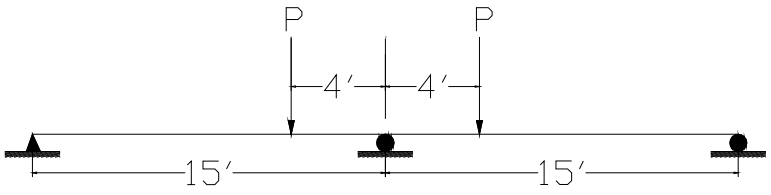

Figure 3.1 Basic Experimental Set-up, Continuous-Span Structure

3.2 Specimen

The Service II flange stress limits of 95 percent and 80 percent of the yield stress for composite and non-composite girders respectively, regularly govern the design of compact girders. However, these girders retain much more reserve capacity, and thus limit the efficiency of the final design. Additionally, the LRFD Specifications currently limit the amount of allowable moment redistribution to 20 percent of the negative moment at the pier. This is known to be a conservative limit and, in fact, previous inelastic design provisions (ALFD 1986) did not contain this restriction. It is the position by Dr. Righman of the University of Delaware, that this allowable moment redistribution limitation is conservative and a 30 percent allowable moment redistribution may be more efficient and advantageous.

Accordingly, the focus for the design of the continuous-span, composite girder test specimen for this research included the service flange stresses and percentage of moment redistribution. The goal was to design a test specimen that would violate the flange service stress limit of 95 percent for composite girders and the 20 percent allowable redistribution moment under moment redistribution design, as required by the LRFD Specifications. All other LRFD Specification design criteria is to be satisfied except for these two provisions. The violation of these two criteria is done in an effort to study the extent of their conservatism and inefficiency.

In an effort to adequately represent a scaled-down model of a typical bridge girder, a large suite of bridge designs were evaluated. As shown in Figures 3.2, 3.3, and 3.4 key geometric properties such as web depth, flange area, moment of inertia, et cetera were plotted as a function of span length. This evaluation provides the geometric properties necessary to choose an initial test specimen for evaluation of the design criteria.

The selection for a test specimen considers design criteria related to reaching the goal objectives of the research with regards to the flange stress limits of the Service II limit state and moment redistribution procedures of the AASHTO LRFD Specifications. The goal is to exceed the flange stress limits at a specific magnitude of moment redistribution. Trends in this data were established resulting in varying levels of correlation and used to determine target geometric values for a 15-foot span length. Table 3.1 displays these trends for the geometric properties of a 15-foot span length for Grade 50 composite girder designs based on 20 percent and 30 percent moment redistribution.

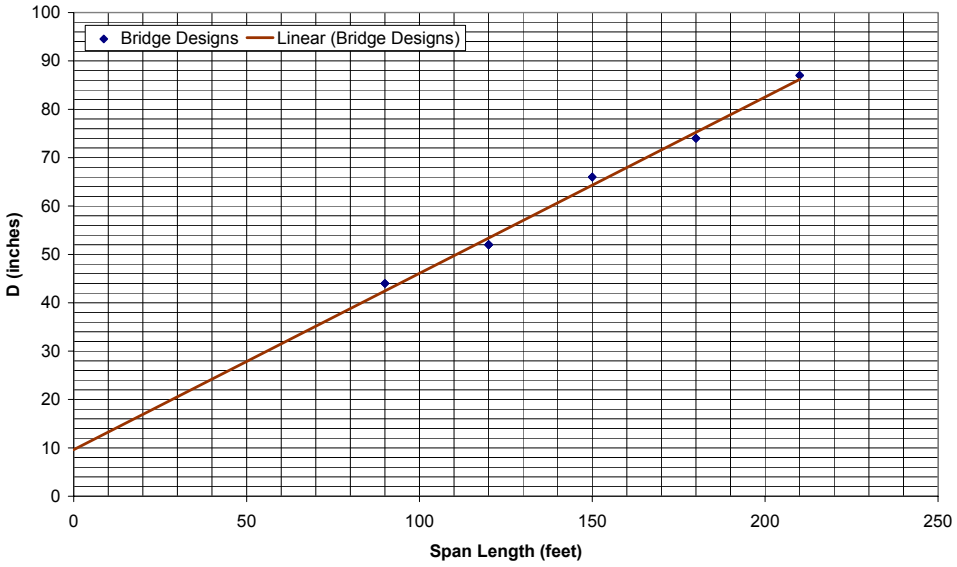

Figure 3.2 Trend of Girder Depth Based on Bridge Designs for Grade 50 Steel and 20 Percent Moment Redistribution

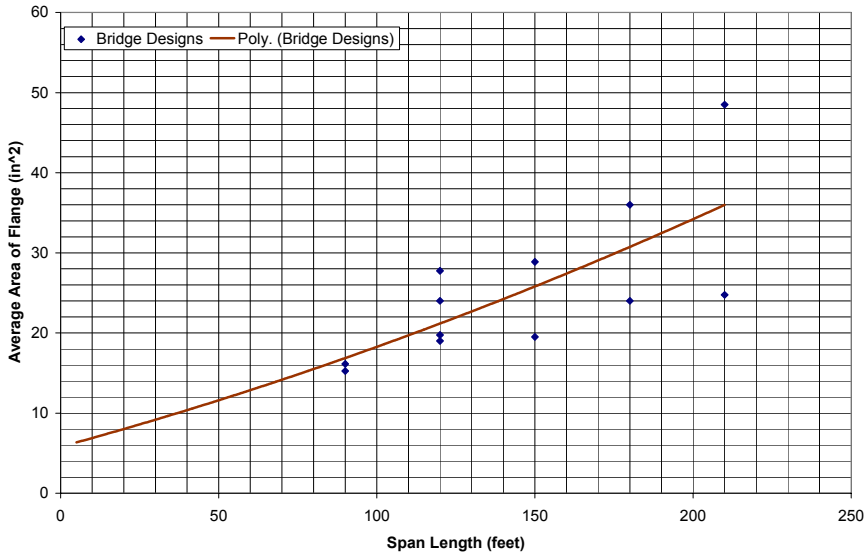

Figure 3.3 Trend of Average Flange Area Based on Bridge Designs for Grade 50 Steel and 20 Percent Moment Redistribution

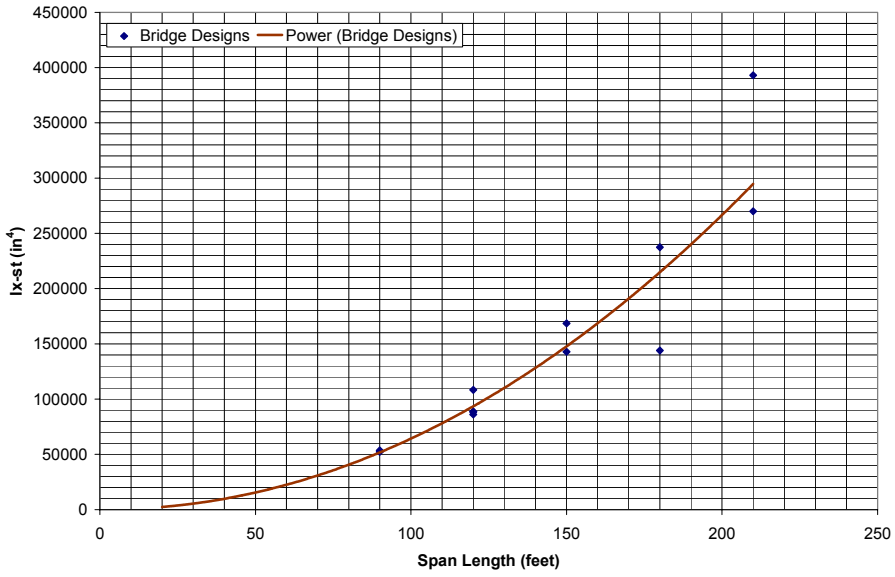

Figure 3.4 Trend of Short Term Moment of Inertia based on Bridge Designs for Grade 50 Steel and 20 Percent Moment Redistribution

Table 3.1 Geometric Design Trends Extrapolated for 15-Foot Span Length

Geometric Parameter	Grade 50 20% Moment Redistribution	Grade 50 30% Moment Redistribution
Span Length, L (ft)	15.	15
Depth, D (in.)	15.10	12.04
Compression Depth, D_{cp} (in.)	5.59	3.77
D_{cp}/D	0.37	0.31
Flange Area-avg, A_f (in.$^{2)}$	3.52	2.69
$I_{x\text{-}steel}$ (in.^{4})	150	64
$I_{x\text{-}st}$ (in.4)	1309	674
$I_{x\text{-}steel}/I_{x\text{-}st}$	0.11	0.10

Based on preliminary designs and cost estimates, it was quickly realized that the research budget would not allow for the experimental testing of the 5 beams comprising the initial scope. After careful review, it was decided that two composite continuous-span beams would be tested – one of these consisting of

Grade 50 steel and the other being constructed from HPS70 steel. These were determined to be the most important specimens based on placing a higher priority on the continuous-span testing, compared to the simple-span testing and the modern practice of composite construction versus non-composite construction.

It became a difficult task to obtain HPS70 steel within the economic and time budget for this research project. Because HPS70 steel is primarily used for bridge construction, the availability is primarily limited to a select few steel fabricators that specialize in this field. The steel fabricator must be familiar with HPS70 steel because of differences in the fabrication process for the plate girders compared to Grade 50 steel. The only fabricator able to meet the demands for HPS70 steel availability and fabrication ability in the region gave a cost estimate triple the entire research budget. After further discussion, they agreed to donate the steel; however they would not fabricate the girder within the economic budget of the research. Therefore, it was decided for the purposes of this research thesis; one continuous-span, composite, Grade 50 girder would be experimentally tested. This test specimen was determined to be the best available representation of a modern bridge girder. Additionally, this test specimen will be most beneficial for future research in this area by contributing to the lack of available experimental data for evaluation on the Service II limit state and moment redistribution design procedures.

The final design of the compact, continuous-span, composite test specimen meets the desired design objectives for Service II and moment redistribution criteria. The yield moment capacity and plastic moment capacity of the specimen are 195 ft-kips and 216 ft-kips respectively. At a redistribution moment of 20 percent of the elastic moment the specimen will theoretically violate the service flange stress specifications by reaching 101.5 percent of the yield strength. At a live load moment redistribution of 30 percent the specimen will

theoretically violate the service flange stress specifications by reaching 109.7 percent of the yield strength. Table 3.2 summarizes these design results and their corresponding flange stresses. Table 3.3 provides a comparison between the selected experimental test specimen geometric properties and the geometric trends of the multiple beam design study.

Within reason, the geometric design properties between the selected test specimen and the trend study match well. Because there are numerous factors that affect the final selection and design of a bridge girder, it is unreasonable to believe the test specimen and design studies would prove an exact match. However, considerable effort was made to select a test specimen within the range of the design trend study, meeting the laboratory constraints and research objectives. The design of the test specimen was done without considering the load factors of 1.75 and 1.30 for strength and service respectively. This was done because the capacity of the actuators was not capable of applying enough force to reach high levels of stress in the specimen; therefore a slightly smaller test specimen resulted. The load factors are included in the design criteria for purposes of safety; therefore this consideration has no effect on the objectives and behavior of the test specimen for the purpose of this research and may explain some of the difference in values of Table 3.3.

Table 3.2 Test Specimen Final Design for Service II and Moment Redistribution Criteria

Parameter	20% Moment Redistribution	25% Moment Redistribution	30% Moment Redistribution	35% Moment Redistribution
Live Load Moment (ft-kips)	143	150	156	162
Flange Stress (ksi)	50	52	54	56
$\%F_y$	101.5	105.6	109.7	117.9

Table 3.3 Geometric Design Trend Comparison for Bridge Designs and Final Test Specimen

Geometric Parameter	Grade 50 20% Moment Redistribution	Grade 50 30% Moment Redistribution	Test Specimen
Span Length, L (ft)	15	15	15
Depth, D (in.)	15.10	12.04	8.02
Compression Depth, D_{cp} (in.)	5.59	3.77	2.39
D_{cp}/D	0.37	0.31	0.30
Flange Area-avg, A_f (in.$^{2)}$	3.52	2.69	3.97
$I_{x\text{-}steel}$ (in.^{4})	150	64	127
$I_{x\text{-}st}$ (in.4)	1309	674	801
$I_{x\text{-}steel}/I_{x\text{-}st}$	0.11	0.10	0.16

After a thorough evaluation of various rolled W-sections and concrete slab dimensions, while accounting for these design considerations, a 30-foot long W8X35 beam with a 36-inch wide by 7-inch deep concrete slab was selected. The design was based on Grade 50 yield strength steel and 4,000 psi compressive strength concrete. Figure 3.5 shows the cross-sectional geometric properties for a W8X35 steel beam.

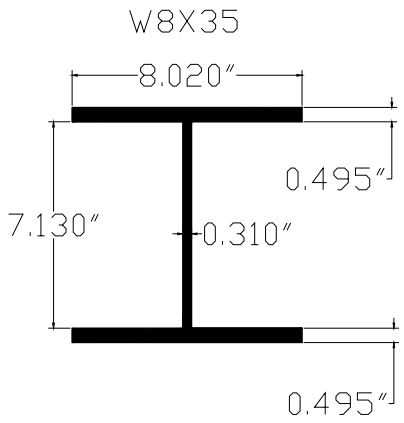

Figure 3.5 Cross-Sectional Geometric Properties, W8X35

Figure 3.6 shows a transverse view of the continuous-span composite test specimen, which includes the reinforcement steel layout. The reinforcement steel consists of a total of nine longitudinal bars in the concrete slab. Six bars transversely spaced at 6-inches are located 1-¾ inches from the top of the concrete slab, while three bars transversely spaced at 12-inches are located 6-inches from the top of the concrete slab. The number of reinforcement bars is directly related to the required area of reinforcement steel specified in LRFD Specifications. The specifications state that the total area of the reinforcement steel should be 1 percent of the area of the concrete slab, with two-thirds of the required area in the top of the slab and one-third of the required area in the bottom of the concrete slab. All reinforcing steel consists of #5 bars (0.625-inch diameter) for simplicity and runs the entire longitudinal length of the beam, with 18-inch splices located 5 feet from both ends of the beam. The transverse spacing of the reinforcement steel meets the required minimum spacing of 1.5 times the diameter and the maximum spacing of 1.5 times the concrete slab thickness or 18-inches.

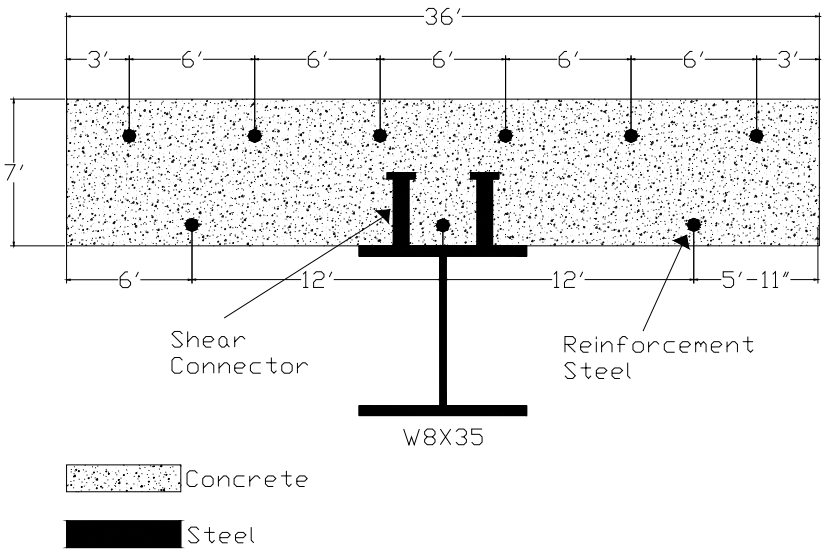

Figure 3.6 Transverse View of Test Specimen, with Reinforcing Steel Layout

Figure 3.7 also displays the longitudinal location of the stiffeners, which are all Grade 50 steel. All stiffeners are full-height stiffeners, extend to the flange edge at a width of approximately 3-¾ inches, and are 1-inch thick. They provide the necessary bearing resistance at the applied load points. The stiffeners at 4-foot from mid-span are provided because of the application of the load for the experiment at these points. The stiffener design is conservative and maintains a safety factor greater than two, which is ideal because yielding of the steel in a buckling fashion will disrupt the objectives of the experimental testing. The stiffeners serve two main purposes; the first is to provide adequate bearing resistance, and the second is to provide a point of connection for lateral bracing members.

Figure 3.7 and 3.8 show the layout of the shear connectors, which are ¾-inch in diameter and 3½-inches tall. The original design detailed 7/8-inch diameter shear connecters, however based on availability 3/4-inch diameter shear connectors

were chosen. The number and size of the shear connectors is based on full composite action between the steel beam and the concrete slab. For full composite action, the number of shear connectors is a function of the total area of the steel and the yield strength of the steel. The strength of ¾-inch diameter shear connectors is 26.1 kips. Therefore, full composite action for a W8X35 beam requires a minimum of 20 shear connectors between locations of zero and maximum moment. Due to spacing requirements, there are 20 shear connectors between stiffeners, as shown in Figure 3.7, for a total of 80 shear connectors used in the fabrication of the test specimen. The height of the shear connector is determined by providing a minimum of 2-inch concrete cover over the top of the shear connector and penetration of at least 2-inches into the concrete slab. The pitch (longitudinal spacing) is determined by providing a center-to-center spacing greater than six times the shear connector diameter. The transverse spacing is determined by providing a center-to-center spacing greater than four times the shear connector diameter, while providing a distance greater than 1-inch from the flange edge to the edge of the connector.

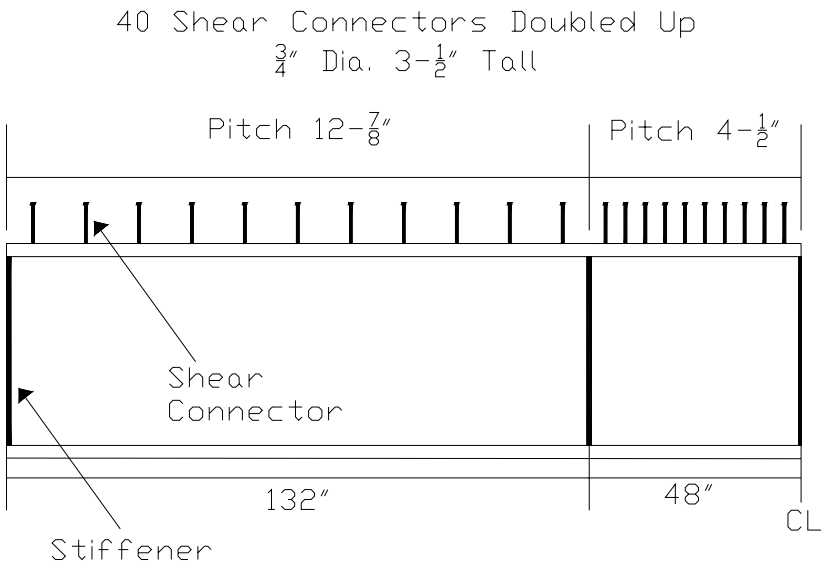

Figure 3.7* Longitudinal View of Test Specimen, with Shear Connector Spacing

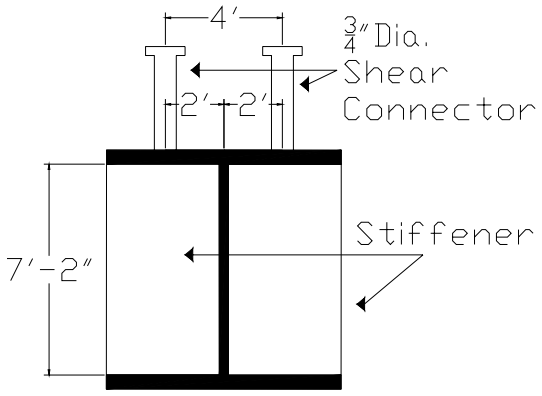

Figure 3.8* Transverse View of Test Specimen, with Shear Connector and Stiffener Dimensions

* The concrete slab is not shown in Figure 3.7 for clarity, although the test specimen is composite and the concrete slab runs the entire 30-foot length of the beam. The test specimen in Figure 3.7 is symmetric about the center line (CL).

3.3 Bracing

All of the lateral bracing included in the scope of the experimental design and testing for this research achieves two main purposes: (1) for strength bracing and (2) for safety. The strength bracing members act as lateral brace points to limit the length of the unbraced sections on the test specimen. This lateral bracing increases the lateral torsional buckling (LTB) capacity of the beam. LTB may cause two types of torsion in the section. The purpose of the lateral bracing for safety is because of the extreme magnitude in vertical loading to be applied by the actuators on the test specimen, large lateral forces will develop. Eccentric loading, failure of the test specimen, or some unexpected event causing the beam to "kick" off of the supports is a real and potentially life threatening situation for the researchers and lab technicians. Therefore, it was necessary to secure the test specimen to each support by means of lateral bracing. Two different types of lateral bracing were used for this experimental research; the first type is used in areas were the vertical displacement of the test specimen is to be restricted and the second type is used in areas were the vertical displacement is unrestricted.

As mentioned, the first type of lateral bracing is in locations were the vertical displacement is restricted. The support locations for this type of lateral bracing is shown in Figure 3.1, where the lateral bracing was constructed on each side of the test specimen. Figure 3.8 shows the first step of construction, a bolted steel plate to the top of the concrete support, while the steel beam is suspended over the supports with a 5-ton overhead crane. Additionally, Figure 3.8 shows the "roller" support welded to the plate. The "roller" support is constructed of a 1-inch round bar welded to a 1-inch thick steel plate. The term "roller" in this case does not imply any rotation or movement of the 1-inch round bar.

---

* The concrete slab is not shown in Figure 3.6 for clarity, although the test specimen is composite and the concrete slab runs the entire 30-foot length of the beam.

Figure 3.8 Steel Plate Bolted to the Concrete Pier

The next step was to construct steel members to connect the lateral bracing to the steel plate. Figure 3.9 shows a tee shaped 7-½ inch tall member, WT5X15 welded to two 1-inch steel plates with two ¾ inch holes drilled for the attachment of the lateral bracing. The WT5X15 tee shaped member was then welded to the steel plate on tope of the concrete slab. The welded angle on the WT5X15 steel member was added to strengthen the piece and eliminate the effects of any eccentric loading.

Figure 3.9 WT5X15 Steel Member Used for Lateral Bracing

Figures 3.10, 3.11, and 3.12 show the WT5X15 steel member welded to the steel plate and connected to the stiffener on both sides of the test specimen with two L3X3X5/16 inch steel angles. The L3X3X5/16 inch steel angles were connected to the WT5X15 tee member and the test specimen stiffeners with A325 ¾ inch bolts. Again, this lateral bracing is on both sides of the test specimen at each vertical support for a total of three points along the length of the beam with this type of lateral bracing.

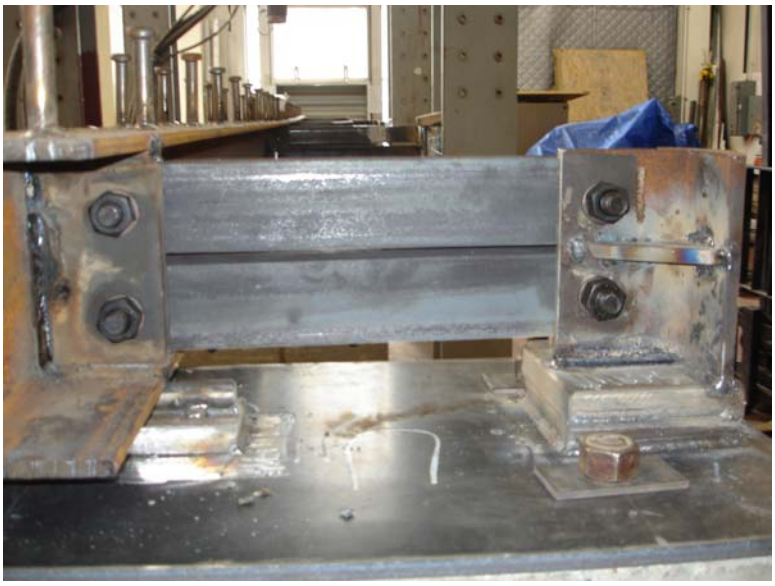

Figure 3.10 Lateral Bracing, East View

Figure 3.11 Lateral Bracing, West View

Figure 3.12 Lateral Bracing at the Interior Pier, North View

As previously mention, the second type of lateral bracing for the experiment is at locations were the vertical displacement is unrestricted. The vertical displacement of the test specimen must be unrestricted at the actuator applied load locations. Figure 3.1 shows these locations at 4-feet from the center support in both spans. An unbraced length of 4-feet allows the nominal moment capacity in negative bending to equal the plastic moment capacity of the test specimen.

The lateral bracing along the span of the test specimen was needed to resist lateral movement, but allow for vertical deflection. As a result, L3X3X5/16 inch angles were bolted to the stiffeners at 4-foot from mid-span and welded to an industrial strength steel wheel at the end as shown in Figure 3.13. The steel wheel was designed to allow for vertical travel along the actuator testing frame as shown in Figure 3.14. The actuator testing frame provided the necessary lateral resistance to create a lateral brace point.

Figure 3.13 Lateral Bracing for LTB Resistance, Close View

Figure 3.14 Lateral Bracing for LTB Resistance at West Actuator

3.4 Instrumentation

The scope of the instrumentation for the experimental testing of this research included 16 strain gages for steel, 9 strain gages for concrete, and 4 Linear Variable Differential Transducers (LVDT's). The strain gages for steel were placed at both points of load application and at the interior pier. The gages were placed on both sides of the test specimen where possible to allow for an average strain calculation. This is important because it accounts for minor unavoidable unsymmetrical aspects of the test set-up, which may otherwise provide atypical data results. Strain gages were placed on the top flange, middle of the web, and bottom flange of the test specimen. As shown in Figure 3.15,they were offset 6-inches towards mid-span at each actuator location and offset 6-inches at the interior pier due to the conflicting location of the stiffeners. Figure 3.16 shows the location of the strain gages on the test specimen and Figure 3.17 displays a typical strain gage for steel at a web location.

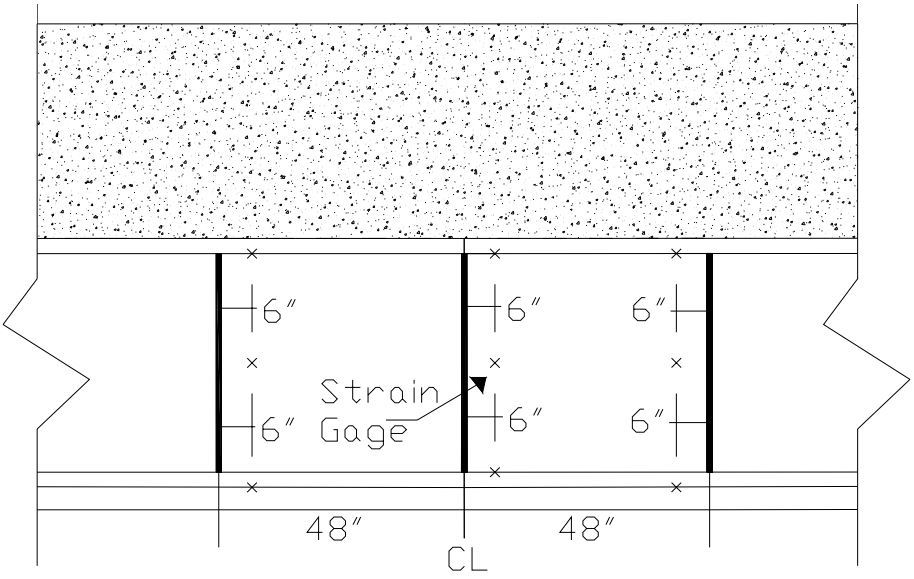

Figure 3.15 Longitudinal Location of Steel Strain Gages

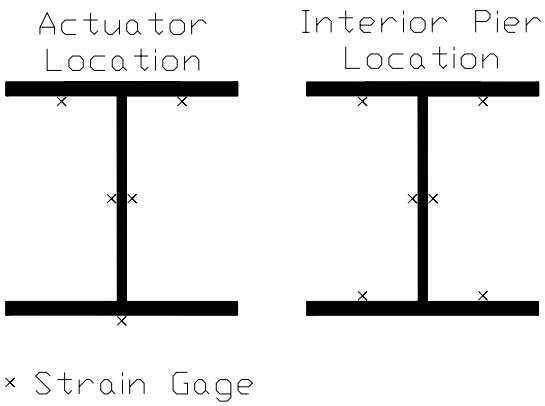

Figure 3.16 Cross-Sectional Locations of Steel Strain Gages

Figure 3.17 Typical Stain Gage for Steel

The primary purpose of the steel strain gages is to collect experimental data on service strains, from which stress and moment can subsequently be calculated. This relates to the second objective of this research, collection and evaluation of experimental service stresses at various levels of moment distribution. The long

term goal of this experimental data is to evaluate service requirements for various moment redistribution designs.

The concrete strain gages were added to the scope of testing to monitor the cracking of the concrete slab at the interior pier support. The concrete is in tension at this location and experiences large amounts of strain at small amounts of moment, relative to the concrete at other locations along the span. Figures 3.18 and 3.19 shows the layout of strain gages at the interior pier support and Figure 3.20 shows a close view of a typical concrete strain gage.

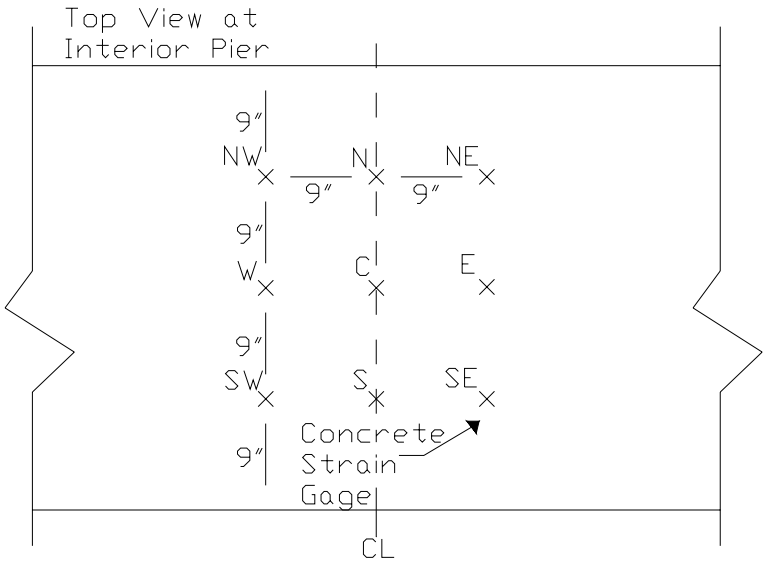

Figure 3.18 Concrete Strain Gage Layout, Top View

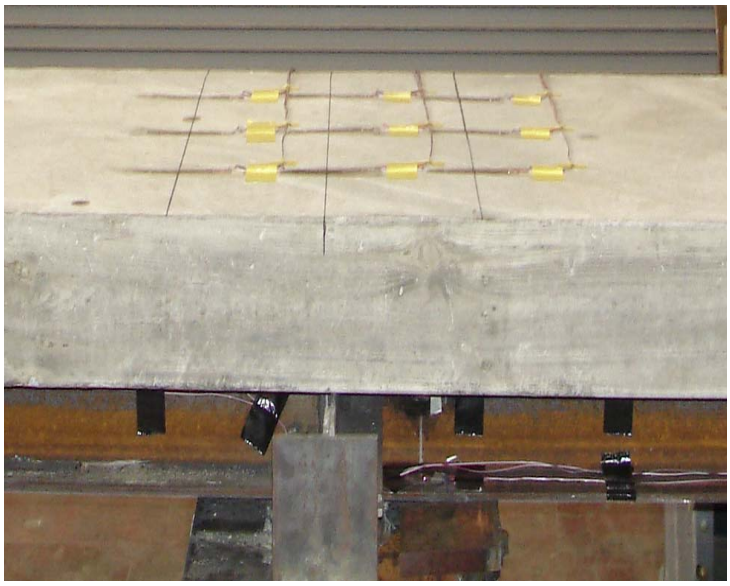

Figure 3.19 Concrete Strain Gages at the Interior Pier

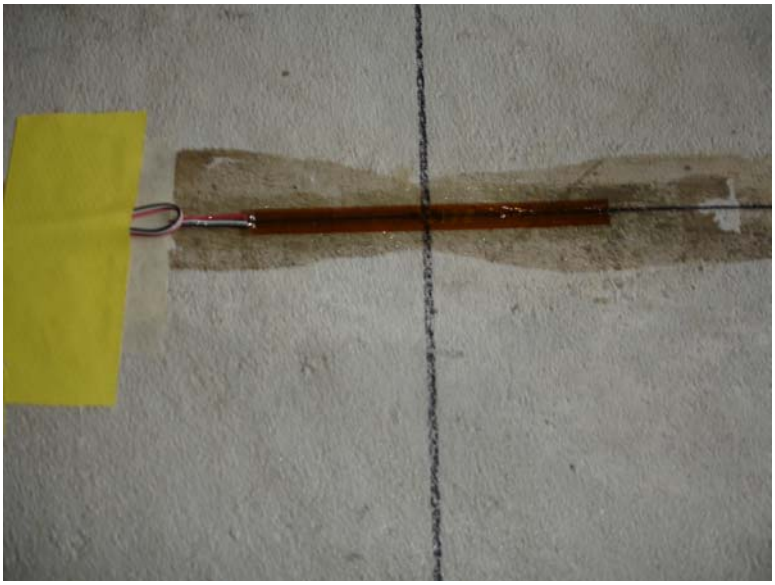

Figure 3.19 Typical Concrete Strain Gage

The LVDT's were added to the instrumentation scope for this research to collect specific experimental deflection data related to the first research objective.

This objective is to provide experimental data on service stresses versus deflection. Much of the criticism of the Service II limit state and moment redistribution is related to deflection. One LVDT was positioned at each actuator to collect deflection data of the test specimen at the point of load application. LVDT's were also placed at 84-¾ inches from the ends of the test specimen because this is the theoretical location of maximum deflection under the applied loads. Figure 3.20 shows a typical LVDT set-up for collecting experimental deflection data.

Figure 3.20 Typical LVDT Test Set-Up

Chapter 4

4. Experimental Testing

This chapter discusses construction of the test specimen, testing procedures, and the material testing. The construction of the specimen primarily consisted of three phases: general test setup, deck casting, and instrumentation installation. Each of these three phases is discussed and pictured in Section 4.1, in chronological order. Completion of all three phases was completed over the course of six weeks in the Structures Laboratory at the University of Delaware. The deflection controlled testing procedures for the application of the incremental applied loads by the actuators is discussed in detail. This includes a description of the beam behavior during the individual load increments and reasons for deflection control of the actuators. This section also provides figures of the cracking in the concrete slab and the bending of the test specimen under loading. Finally, the material testing for the W8X35 steel beam and the concrete slab is detailed. The testing of the steel tensile coupon resulted in the yield stress and modulus of elasticity, while the concrete cylinder test provided the compressive strength of the concrete.

4.1 Construction

4.1.1 Phase One – General Test Layout

The first phase for the construction of the experimental test set-up and test specimen consisted of a several steps. These steps included aspects regarding positioning the actuators, supports, bearings, lateral bracing members at the supports, and lateral bracing members at the locations of load application.

4.1.1.1 Actuator Positioning

The first step in constructing the experimental set-up was positioning the load frames. The "strong-floor" in the structures laboratory at the University of Delaware is 2-½ feet thick and has bolted connection points in a linear direction at 2-foot intervals. The load frames consist of two steel beam columns connected by one steel cross-beam in an "H" fashion, as shown in Figure 4.1.

Figure 4.1 East Load Frame Prior to Positioning

The beams are connected to each other with bolts, allowing the position of the cross-beam to vary in vertical position. The bottom of the steel beam columns are connected to plates, which are then secured to the "strong-floor" with a bolted connection. Because the point load in each span was designed to be applied 4-feet from mid-span, the load actuators were placed 8-feet apart.

As shown in Figure 4.2, the loading actuators are bolted to the bottom of the cross-beam with a slotted connect to allow the position of the actuator to vary

transversely. The actuators are have a +/- 6-inch vertical travel and is shown in Figure 4.2 at a fully extended position. The vertical position of the cross-beam was fastened to the steel beam columns at a height were the actuator in a fully extended position would come just short of the test specimen concrete slab. This was done to avoid any potential for an accidental or unexpected loading of the test specimen, and thus destruction of the experiment. The loading actuators were transversely positioned over the web of the test specimen.

Figure 4.2 West Load Actuator in a Fully Extended Position

4.1.1.2 Supports

The substructure for the test set-up consisted of three concrete supports, located at both ends and at the mid-span of the test specimen. These supports were 48 in. high, 48 in. wide, and 18 in. deep. The concrete supports were roughly centered with respect to the load actuators (in the transverse direction of the beam) and the beam's stiffeners (in the longitudinal direction of the beam).

4.1.1.3 Bearings

An 18X48X½ inch steel plate was bolted to the top of the concrete supports. This was done to provide a smooth, level surface for the experimental test set-up and, more importantly, to secure the bearings and bracing to the supports by means of welding. After the 18X48X½ inch steel plate was bolted to the top of the concrete support, the rolled W8X35 steel beam, fabricated with shear connectors and stiffeners, was lifted over the supports with a 5-ton overhead crane. With the steel beam suspended over the supports, the two end bearings were welded to the 18X48X½ inch steel plate to be transversely and longitudinally centered with respect to the stiffeners. The two end bearings are identical and are constructed of a 3X12X1 inch steel plate welded to a 1-inch diameter steel bar. At the end supports, the beam rests on the steel bar and is used to represent a roller support, although the end bearings are fixed to the 18X48X½ inch steel plate and do not actually "roll". At the mid-span support, the beam rests on a neoprene rubber bearing pad. Figures 4.3 and 4.4 display the results of these first few construction steps included in Phase One.

Figure 4.3 Steel Plate Bolted to the West End Concrete Support with the W8X35 Beam Suspended Over the End Bearing

Figure 4.4 Close View of the West End Bearing Support

4.1.1.4 Lateral Bracing at Supports

The next few steps of the construction for Phase One included the construction of bracing components and connecting these to the test specimen and supports. The component of the support bracing member to be welded to the 18X48X½ inch steel plate at each support was constructed with a WT5X15 steel member as the primary member and two 1-inch steel plates attached to the member as shown in Figure. 4.53. The WT5X15 steel members were cut at a height of 7-½ inches and drilled for the ¾-inch bolt holes prior to the construction of the bearings. This minor oversight resulted in a 2-inch offset in height for the lateral bracing connection points. The two 1-inch plates were welded to the bottom of the WT5X15 steel member to make up for the height difference. Six of these bracing components were constructed, one of which was installed on each side of the beam at each vertical support.

Figure 4.5 Support Bracing Welded Component

These support bracing components were then welded to the 18X48X½ inch steel plate at all three supports and was connected to the test specimen. The connection was made to the stiffeners with two L3X3X5/16 steel angles and four A325 ¾ inch diameter bolts. Figure 4.6 and 4.7 show the final construction and application of the support bracing to the test specimen. Figure 4.6 also shows the neoprene rubber bearing pad under the stiffener at the mid-span support mentioned previously.

Figure 4.6 Support Bracing at the Mid-Span Support

Figure 4.7 Support Bracing at the East End Support

4.1.1.5 Lateral Bracing at Actuators

As mentioned in Chapter 3, the bracing at the actuators included a steel wheel that would allow vertical translation, but restrict any lateral movement. A steel bar was used to form an axle for each steel wheel. The axles were then welded to steel plates that were parallel to the wheel as pictured in Figure 4.8. These plates were in turn connected via a third plate, which was welded to the end of two L3X3X5/16 inch steel angles and were connected to the test specimen. The connection to the test specimen was made using two A325 ¾ inch diameter bolts. Figures 4.9 and 4.10 show the connection detail of the actuator bracing to the test specimen.

Figure 4.8 Steel Wheel Actuator Bracing Component

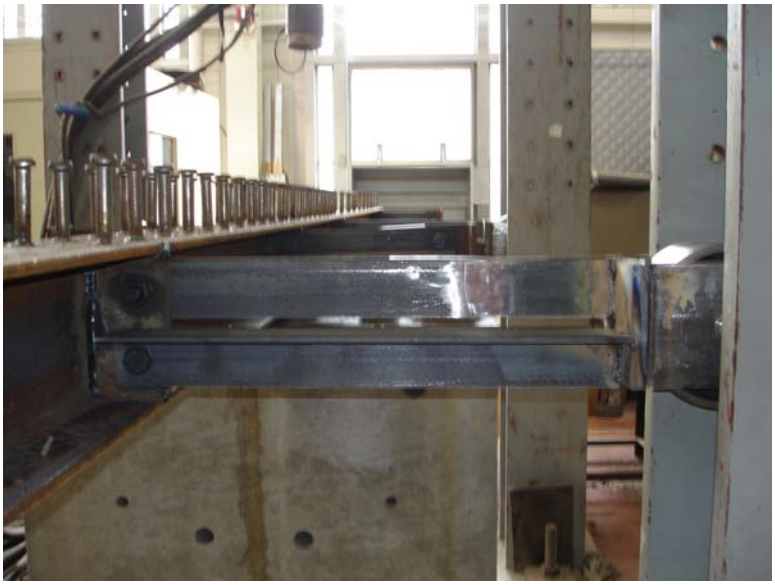

Figure 4.9 Actuator Bracing at the West Actuator

Figure 4.10 Alternate View of Actuator Bracing at the West Actuator

4.1.2 Phase Two – Composite Construction

The second phase of construction of the experimental test set-up and test specimen consisted of tasks regarding the construction of the concrete slab, and thus final construction of the composite test specimen. The first of these tasks in Phase Two was to build formwork around the W8X35 steel beam for the casting of the composite concrete slab. The formwork was constructed entirely of wood and fastened with standard wood screws. Additionally, the formwork was constructed to be level with the top edge of the top flange and provide for a 7 inch deep by 36 inch wide concrete slab. Vertical supports were sufficiently attached to the form work every two feet along the longitudinal length of the test specimen to carry the weight of the concrete slab during the initial pour and curing stage. The inside of the formwork was coated with a thin layer of used motor oil to prevent any bonding between the concrete slab and the wood formwork. Figure 4.11 through 4.13 show the final construction of these initial construction steps included in Phase Two.

Figure 4.11 Construction of the Wood Formwork, Top View

Figure 4.12 Construction of the Wood Formwork, Side View

Figure 4.13 Application of Thin Oil Layer to the Wood Formwork

The reinforcement steel was then attached to plastic rebar chairs. The chairs were spaced at 18 in. in the longitudinal direction. Two heights of plastic chairs were used for the construction of the composite concrete slab. The plastic chairs were connected to the reinforcement steel with plastic zip ties. Reinforcement steel was then lifted into place within the concrete slab wooden formwork. Figures 4.14 through 4.16 show the reinforcement steel construction and layout. Specific details regarding the layout of the reinforcement can be found in Chapter 3.

Figure 4.14 Zip Tie Connection of the Plastic Chair to Reinforcement Steel

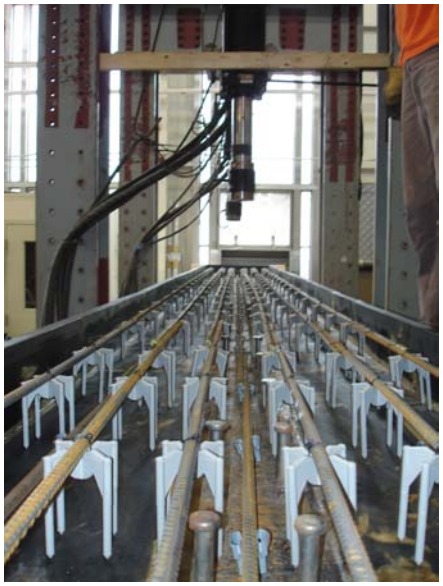

Figure 4.15 Longitudinal Layout of Reinforcement Steel

Figure 4.16 Vertical Layout of Reinforcement Steel

The next step in the Phase Two construction was the pouring of the concrete for the composite concrete slab. The specified 4000 psi concrete was supplied by Newark Concrete LTD by a front end unloading concrete truck. The concrete was placed in the wooden formwork and vibrated to prevent air pockets from forming within the concrete slab. Figure 4.17 and 4.18 show the placement, vibrating, and finishing of the concrete for the construction of the composite concrete slab.

Figure 4.17 Placement and Vibrating of the Concrete

Figure 4.18 Leveling of the Poured Concrete

After allowing the concrete to cure for 8 days, a concrete cylinder test was performed to determine the compressive strength of the concrete. Because the

strength was sufficient enough to carry the dead load of the concrete, the wooden formwork was removed. Figures 4.19 and 4.20 show the final construction of the test specimen with the wooden formwork removed.

Figure 4.19 Total Overall View of Constructed Composite Test Specimen

Figure 4.20 East End Bearing View of Constructed Test Specimen

4.1.3 Phase Three - Instrumentation

The third and final phase for the construction of the experimental test set-up and test specimen was the application of the instrumentation to the test specimen. A total of 15 CEA-06-W250A-350 ¼-inch long weldable strain gages were applied to selected locations of the steel beam, 9 EP-08-40CBY-350 4-inch long concrete strain gages were applied to the concrete slab near mid-span, and 4 RDP model DCT 3000A LVDT's were set-up at select locations under the test specimen to capture vertical deflection. All of the instrumentation was connected to a VISHAY model 5000 data acquisition system. The data acquisition system collected and reduced the data using StrainSmart software version 4.01. Figures 4.21 through 4.24 show the construction steps and application of each type of instrumentation to the test specimen. Figures 3.15, 3.16, and 3.18 of Chapter 3 show a schematic of the strain gage layouts for steel and concrete. As previously mentioned in Chapter 3, the LVDT's were placed underneath the beam at the

actuators and 84-¾ inches from both ends of the beam because these are the locations of theoretical maximum deflection.

Figure 4.21 Typical Steel Strain Gage

Figure 4.22 Concrete Strain Gages at Mid-Span

Figure 4.23 LVDT Set-Up at the West Actuator

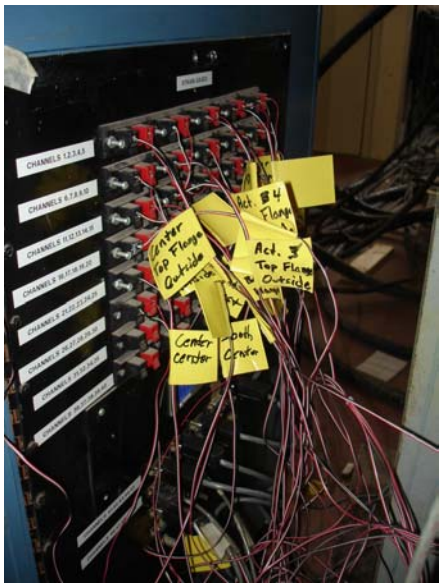

Figure 4.24 Connection of All Testing Instrumentation to Data Collection Box

The installation of the testing instrumentation signified the end of the construction for the test set-up and composite test specimen except for one last step. Finally, two 3-inch thick steel members constructed of welded 1-inch plates were placed under the load actuators in order to provide an interaction between the actuators and the test specimen. With the construction complete, preparations were finalized for the experimental load testing of the specimen.

4.2 Experimental Testing Procedure

The continuous-span composite test specimen was loaded with one point load in each span at the transverse centerline of the beam and located 4-feet from mid-span. The load actuators were originally designed to apply a maximum of 110,000 pounds of compressive force, but were subsequently upgraded to reach a maximum of 150,000 pounds of compressive force. Based on this upgraded strength, 150,000 pounds of compressive force was determined to be significant enough to reach the ultimate capacity of the test specimen. Theoretically, an

applied load of 150,000 pounds of compressive force by the actuators would result in a moment 76 percent larger than the plastic moment, M_p, of the test specimen, assuming the ultimate capacity is not reached.

For reasons of laboratory safety and protection of the test specimen, the experimental load testing was controlled by inputs of deflection rather than applied loads. The reason for the greater control with deflection input is especially due to the inelastic nature of the test specimen at and beyond the plastic moment. Once the test specimen begins to yield, the same force that resulted with a small deflection during the elastic range may now cause large unexpected and uncontrolled deflections. This is avoided with deflection controlled inputs because the technician has the discretion to decrease the amount of desired deflection as the test specimen starts to show inelastic behavior, and thus indirectly decrease the applied load to an appropriate magnitude.

The expected deflection at the east and west actuator was calculated for various applied moments up to the plastic moment capacity of the beam. Based on these calculations, the initial load deflection increment was set at 0.1 inches. This applied deflection increment was used for deflection steps 1 through 4. It was important to choose small enough increments for the deflection steps to ensure sufficient data to analyze the behavior of the test specimen. During deflection step 2 the concrete initially cracked down the transverse centerline. During deflection step 3 the cracking spread throughout the interior pier region of the concrete slab. Figure 4.25 and 4.26 show the cracking in the concrete slab with the cracks outlined in black. There was period of time between each load deflection step where the actuators were held stationary. This was done to allow the load being applied by the actuators to stabilize as all of the forces in the test specimen were redistributed until they reach a relatively static state. This is important for capturing the true behavior of the test specimen in terms of load versus deflection data. Each data

reading of strain, deflection, and load was recorded just before the next deflection step, after the forces in the test specimen from the previous deflection step were stabilized.

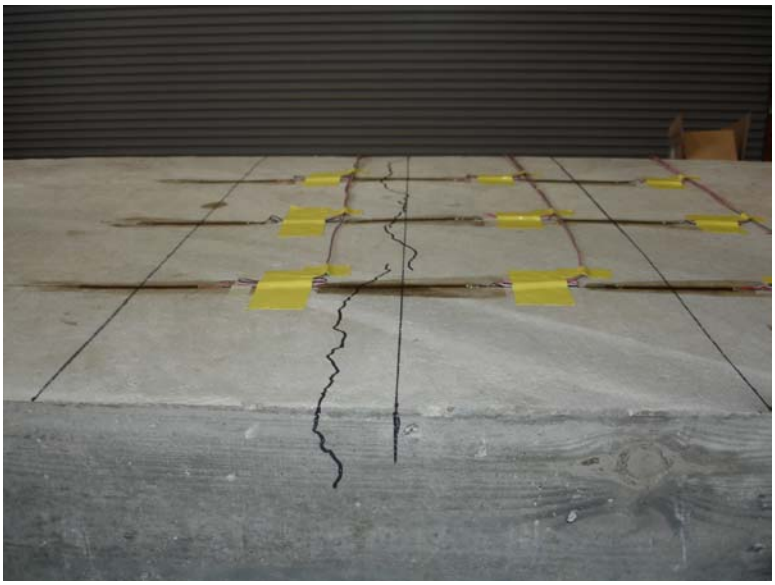

Figure 4.25 Initial Cracking through the Transverse Centerline of the Concrete Slab during Deflection Step 2

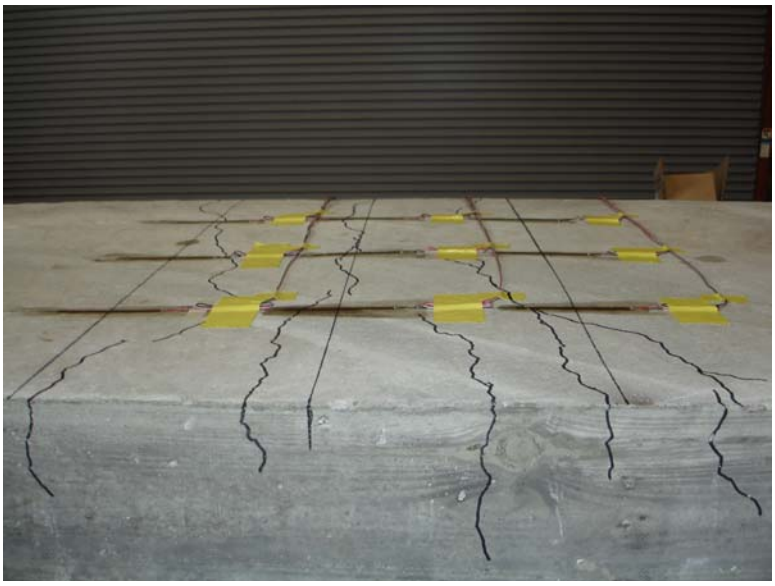

Figure 4.26 Continued Cracking throughout the Interior Pier Concrete Slab Region during Deflection Step 3

The theoretical loads necessary to reach various levels of moment at the critical interior pier section were calculated at increments leading up to the plastic moment capacity. Because the actuators provide feedback through the computer software on the amount of load being applied, these theoretical calculations were used to lessen the load deflection input as necessary. Deflection steps 5 through 8 used a load deflection increment of 0.05 inches because the test specimen was approaching the theoretical plastic moment of the beam. Figure 4.27 shows additional cracking of the concrete throughout the interior pier concrete slab region during these deflection steps.

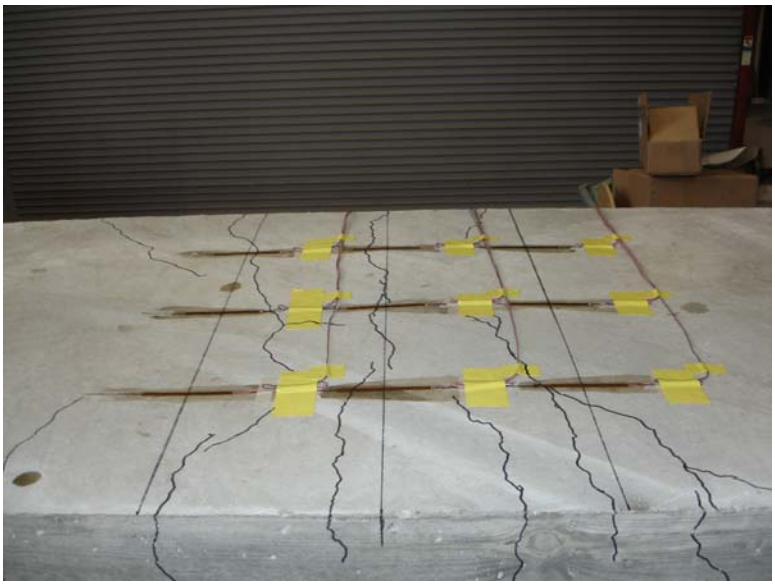

Figure 4.27 Continued Cracking throughout the Interior Pier Concrete Slab Region during Deflection Steps 5 through 8

Deflection steps 9 through 14 all used a load deflection increment of 0.025 inches because the load was nearing the predicted maximum capacity where additional data was desired. At these relatively high levels of applied load the deflection of the test specimen was clearly visible. Figure 4.28 and 4.29 show the positive bending of the test specimen over the spans and the negative bending of the test specimen over the interior pier support.

Figure 4.28 Positive Bending Behavior of the Test Specimen over the Span during Experimental Testing

Figure 4.29 Negative Bending Behavior of the Test Specimen over the Interior Pier during Experimental Testing

During deflection step 14 the actuators failed to respond to the manual input at an applied load of approximately 119,000 pounds. The testing was terminated after load deflection step 14 because the actuators were incapable of applying additional load. As shown in Figure 4.30, inspection of the test specimen after the applied loads were removed revealed a large crack on the bottom of the concrete slab. The crack developed sometime during deflection steps 9 through 14 and ran from the stiffener at the north side of the east actuator to the slab edge.

Figure 4.30 Large Crack on the Bottom of the Concrete Slab at the East Actuator as Revealed after Experimental Testing

4.3 Material Testing

The steel and concrete used for the construction of the test specimen were tested according to the standards of the American Society of Testing Materials (ASTM) to determine the strength properties. These properties are essential for the

evaluation of the experimental data and analysis of that data for stress and moment calculations as discussed in Chapter 5.

4.3.1 Concrete Testing

During the concrete pour, nine concrete cylinders were made for future testing and evaluation of the compressive stgrength. The concrete composite slab was then left to cure for 8 days before a compressive test was performed on two of the concrete test cylinders on February 9, 2007. The compressive strength was approximately 3,700 psi after the 8 day curing and was determined sufficiently strong to allow for the removal of the wooden formwork.

Three concrete cylinders were tested on the same day as the experimental loading of the test specimen to determine the actual concrete compressive strength during testing. This was done on March 7, 34 days after the initial pour of the composite concrete slab, therefore exceeding the generalized minimum 28 day curing period for full compressive strength. The results of the concrete cylinder testing yielded an average concrete compressive strength of 4,821 psi, which as expected is greater than the design specified compressive strength of 4,000 psi. Figure 4.31 is an example of one of the concrete cylinder tests.

Figure 4.31 Example of Concrete Cylinder Test

4.3.2 Steel Testing

After experimental testing was completed, standard steel tension coupons were taken from areas of the web that theoretically experienced small strains. These areas were located near the center-line of the web and near the ends of the test specimen. Figure 4.32 show the location of the steel tensile coupon sample taken from near the east end support. These coupons were used to determine the actual yield strength and modulus of elasticity of the steel. The steel tensile yield strength and modulus of elasticity was found to be 51.8 ksi and 26,450 ksi respectively. This values match well with the expected design values for tensile strength and modulus of elasticity of 50 ksi and 29,000 ksi respectively.

Figure 4.32 Steel Tensile Testing Coupon Sample at East End Support Location

The subsequent chapters will summarize, display, and detail the resulting data recorded during the experimental testing and the analysis of this data. Conclusions and discussions regarding the resulting experimental test data in connection with the objectives of this research will also be provided.

Chapter 5

5. Experimental Results

This chapter provides the results of the experimental testing for this research thesis. The first half of the chapter presents graphical displays of the experimental data collected during testing. This includes the load versus deflection data and the load versus strain data for steel and concrete. In addition to the graphical display of collected data, an evaluation and discussion of this data is provided to establish the behavior of the test specimen during the experimental testing. The second half of the chapter is an analysis of the data collected from the experiment. Using the collected strain data, stress and moment values are calculated for the test specimen. Figures and discussion regarding the analysis data from the experiment is also presented. Conclusions are based on the behavior of the experimental test specimen and how the collected experimental data relates to the research objectives.

5.1 Experimental Data

This section presents a graphical display of the data collected by the test specimen instrumentation. This instrumentation consisted of steel strain gages, concrete strain gages, and LVDT's. Figures 3.15, 3.16, and 3.18 of Chapter 3 show a schematic of the strain gage layouts for steel and concrete. Steel strain data was collected in the top flange, center-line of the web, and the bottom flange at three locations along the beam. These longitudinal locations included the interior pier and both actuator locations, which were 4-feet on both sides of the interior pier. Concrete strain data was collected over a 27 by 27 inch grid on the top of the

concrete slab over the interior pier. Deflection data was collected by LVDT's located at the theoretical maximum deflection points in both spans and at the east and west actuators. The theoretical maximum deflection in the spans is 84-¾ inches from both ends of the beam. As previously mentioned, data was collected after the internal forces in the test specimen were redistributed and stabilized for each deflection increment. Therefore, the collection of strain and deflection data at each increment corresponds to a single magnitude of applied load.

5.1.1 Applied Load versus Deflection

Figure 5.1 is a graphical display of the applied load versus the deflection data at all four locations of LVDT instrumentation. The figure includes the data for all 13 deflection increments beginning with an applied load of 8 kips and ending with an applied load of 119 kips. The corresponding deflections range from 0.035 to 0.042 inches at the first deflection step and 0.548 to 0.591 inches at the final deflection step. The expected deflections for the test specimen were small; therefore there is little difference in the applied load versus deflection data at all four locations. Theoretically the East and West LVDT's should have resulted in the exact same deflection, and the East Actuator and West Actuator LVDT's should have resulted in the exact same deflection. This discrepancy shown in Figure 5.1 is due to minor variances in the symmetry of the test set-up and test specimen. However, as expected, the LVDT's located at the theoretical points of maximum deflection in the spans show slightly larger deflections than the LVDT's at the east and west actuators.

The linear slope throughout the majority of the load range indicates that the test specimen behaved elastically at loads up to approximately 107 kips. After this load was exceeded, deflection begins to increase more rapidly with increasing load. The two possible reasons for this to occur are: (1) decreased stiffness caused

by yielding of the specimen or (2) decreased moment of inertia caused by loss of composite action. As will be shown by the analysis of the strain data, it is more likely that, in this case, there was a loss of composite action.

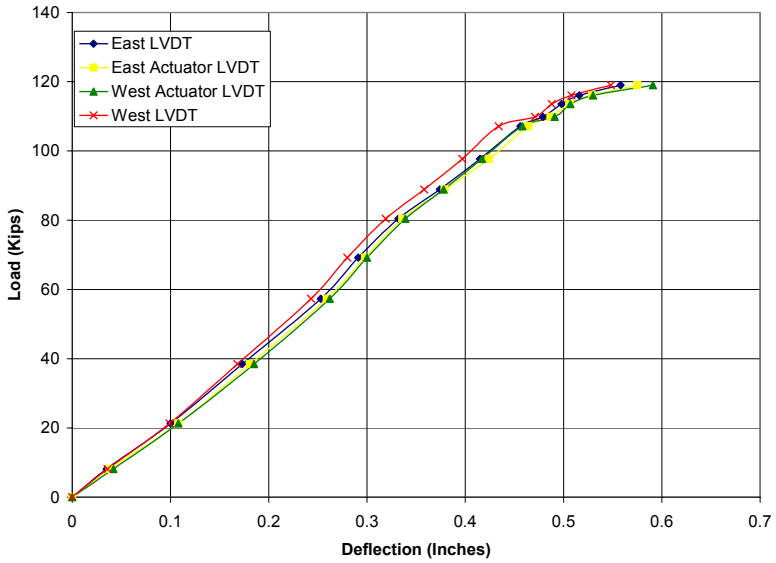

Figure 5.1 Applied Load versus Deflection Data at all LVDT Locations

From Figure 5.1 it is evident that the slope in the linear range is not constant. In fact, three distinct linear elastic regions can be identified, as shown in Fig. 5.2. Here three linear slopes, which are typical of all four instrumented locations, are identified. During the experimental loading there was a large popping noise at the deflection increment where the first and the second linear elastic region meet. At this point the test specimen becomes stiffer for the next two deflection increments. Following this, a third linear elastic region exists, where the test specimen stiffness decreased. Figure 5.2 shows the slope of each linear elastic portion of the applied load versus deflection data. The first and third linear elastic regions have the same slope with the second linear elastic slope approximately 30

percent larger. It is believed that torsional effects in combination with resistance from the lateral bracing caused the momentary increase in stiffness of the test specimen.

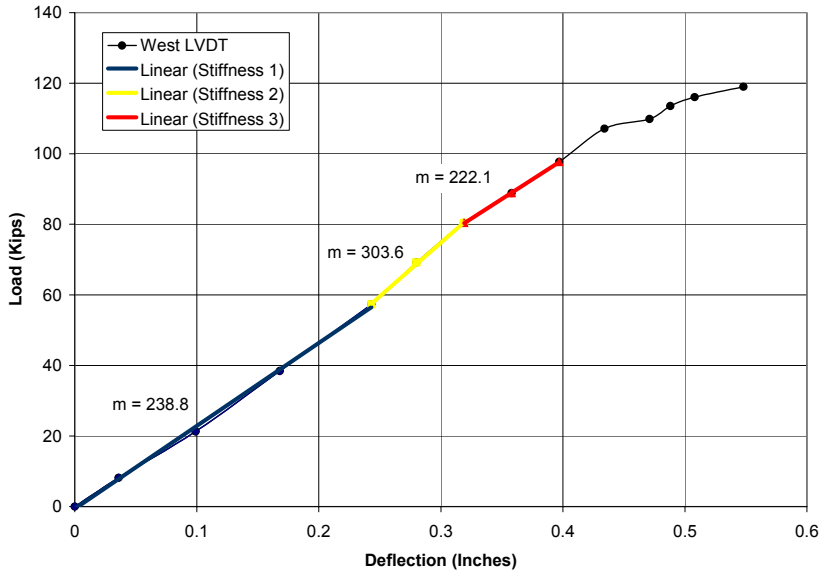

Figure 5.2 Typical Linear Elastic Regions of the Test Specimen during Loading

5.1.2 Applied Load versus Strain

As previously described, strain data was collected for the steel beam and the concrete slab at select locations using strain gages. Strain data was recorded from the 0 kips to the final applied load of 119 kips. The data is reported and graphically displayed as either positive or negative values, which mean tensile or compressive strains respectively. In other words, the positive strains reflect an expansion of the material and the negative strains reflect a contraction of the material.

5.1.2.1 Strain in the Steel Beam

Figure 5.3, 5.4, and 5.5 graphically display the applied load versus strain data for the interior pier, east actuator, and west actuator locations respectively. Tables 5.1, 5.2, and 5.3 provide the strain values for all gages at the interior pier, east actuator, and west actuator locations respectively. Strains located on the north side of the beam are labeled in the tables as "N" and those located on the south side of the beam are labeled in the tables as "S". The tables are given to provide all collected experimental strain data because the strain values in the figures are taken as an average where two gages were used at the top flange, web, or bottom flange. The top flange at the interior pier experienced the largest strains, while at the east and west actuators the bottom flange experienced the largest strains. These maximum strains were all tensile strains. This strain data accurately reflected the expected strain behavior of a continuous-span structure with positive bending in the spans and negative bending over the interior pier.

The bottom flange and web at the interior pier along, top flange and web at the east actuator and all three locations at the west actuator proved linear data trends as expected by the assumed linear elastic behavior. Figure 5.3 shows that the web strain gage was located near the neutral-axis of the test specimen at the interior pier. All of the locations on the figures should theoretically show linear data trends assuming linear elastic behavior; however the top flange at the interior pier and the bottom flange at the east actuator do not portray this data trend. The momentary variation from linear elastic behavior for three deflection increments is believed to be related to the unexpected torsional behavior of the test specimen that was mentioned above when discussing the deflection results. It is noted that the load levels corresponding to these large strains are the same as those where the higher stiffness is observed in the above deflection plots.

When reviewing the following figures related to the strain in the steel, it is important to note that the 51.8 yield stress of the steel translates to a steel yield strain value of 1724 microstrain. Therefore, with the exception of these few outlying data points, it can be concluded that the steel did not yield and thus indicates linear elastic behavior.

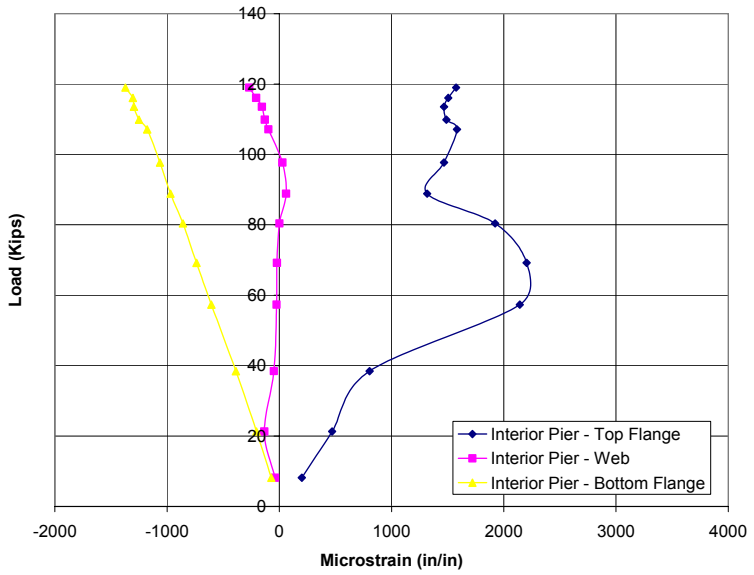

Figure 5.3 Applied Load versus Steel Strain Data at the Interior Pier

Table 5.1 Strain Data for All Gages at the Interior Pier

Load (kips)	Strain @ Interior Pier (Microstrain)					
	Top Flange +3.565		Web 0		Bottom Flange -3.565	
	N	S	N	S	N	S
8	-4	404	-40	-36	-73	-69
21	14	926	-203	-64	-203	-203
38	187	1421	-60	-36	-386	-388
57	400	3884	-48	0	-604	-606
69	521	3886	-53	10	-734	-740
80	695	3149	-34	37	-848	-869
89	859	1776	24	98	-944	-995
98	1058	1876	66	-11	-1021	-1107
107	1206	1958	-35	-160	-1112	-1243
110	1248	1728	-30	-227	-1165	-1335
114	1285	1650	27	-337	-1189	-1402
116	1345	1666	-80	-332	-1190	-1421
119	1451	1699	-426	-107	-1232	-1512

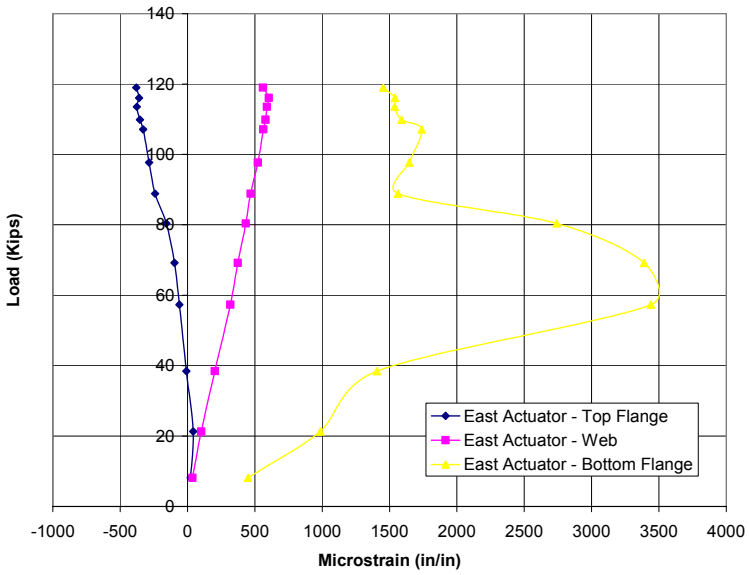

Figure 5.4 Applied Load versus Steel Strain Data at the East Actuator

Table 5.2 Strain Data for All Gages at the East Actuator

	Strain @ East Actuator (Microstrain)				
Load (kips)	Top Flange +3.565		Web 0		Bottom Flange -4.06
	N	S	N	S	---
8	21	24	37	37	449
21	36	49	102	100	987
38	-36	20	199	206	1406
57	-88	-32	311	324	3441
69	-121	-73	366	380	3390
80	-190	-125	424	441	2741
89	-280	-203	459	478	1563
98	-330	-240	511	533	1647
107	-375	-285	551	574	1739
110	-402	-305	569	591	1589
114	-425	-328	578	602	1538
116	-412	-308	590	617	1540
119	-432	-330	545	575	1453

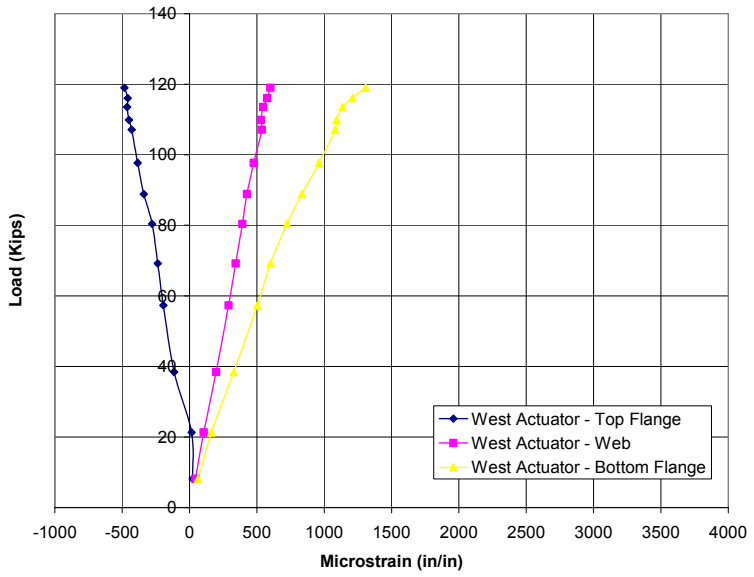

Figure 5.5 Applied Load versus Steel Strain Data at the West Actuator

Table 5.3 Strain Data for All Gages at the West Actuator

	Strain @ West Actuator (Microstrain)		
Load (kips)	Top Flange +3.565	Web 0	Bottom Flange -4.06

	N	S	N	S	---
8	24	21	42	45	63
21	45	-13	103	108	162
38	-93	-136	190	204	328
57	-159	-229	277	302	503
69	-193	-279	329	358	601
80	-232	-324	377	408	724
89	-290	-391	411	442	833
98	-332	-439	463	491	961
107	-384	-475	524	548	1081
110	-414	-487	519	540	1091
114	-432	-495	537	555	1136
116	-435	-483	568	586	1211
119	-472	-496	594	608	1308

Figures 5.6, 5.7, and 5.8 show the resultant strain through the cross-section at the interior pier, east actuator, and west actuator locations, respectively. The strain data is recorded at the locations of instrumentation and interpolated between gages. The abscissa represents the recorded strain values and the ordinate marks distance from mid-depth of the web. The bottom flange strain gages at the east and west actuators were located further from the center-line of the steel beam than the interior pier because they were applied to the outside of the flange, while those at the interior pier were fixed to the top surface of the bottom flange. The data demonstrates that the strain through the cross-section becomes less linear as the applied load increases. This is due to the increased bending of the beam and the resulting increase in the strains at the top or bottom flanges to reflect this bending behavior. The point where the interpolated trend lines cross the ordinate approximates the location of the neutral-axis at that respective cross-section. These experimental neutral-axis values are later used to accurately calculate the experimental moments. The applied load increments selected for Figure 5.6, 5.7, and 5.8 were subjectively chosen for clarity.

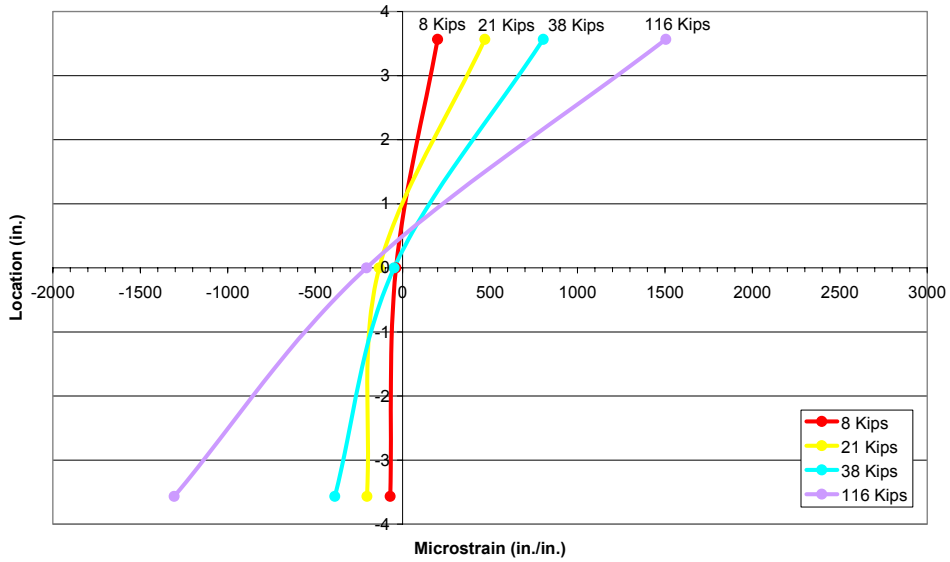

Figure 5.6 Resultant Strain through the Interior Pier Cross-Section at various Applied Loads

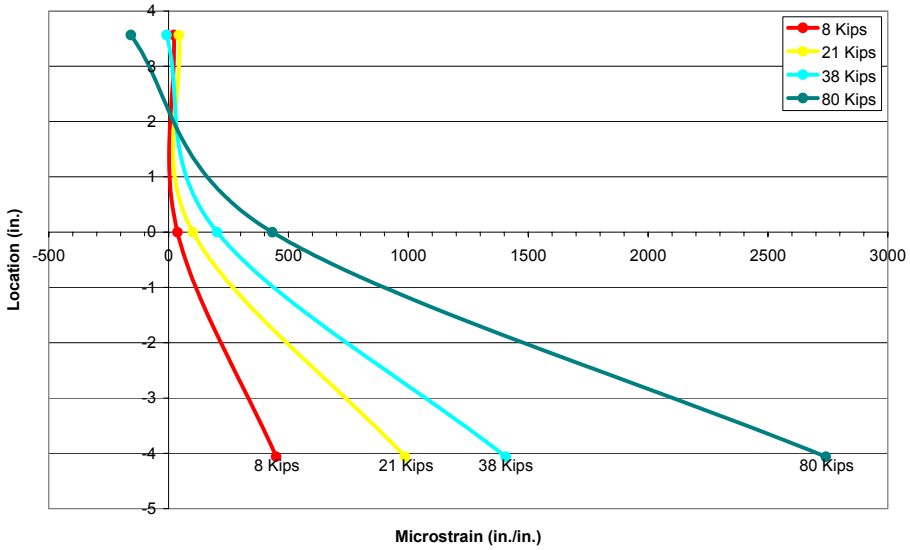

Figure 5.7 Resultant Strain through the East Actuator Steel Cross-Section at various Applied Loads

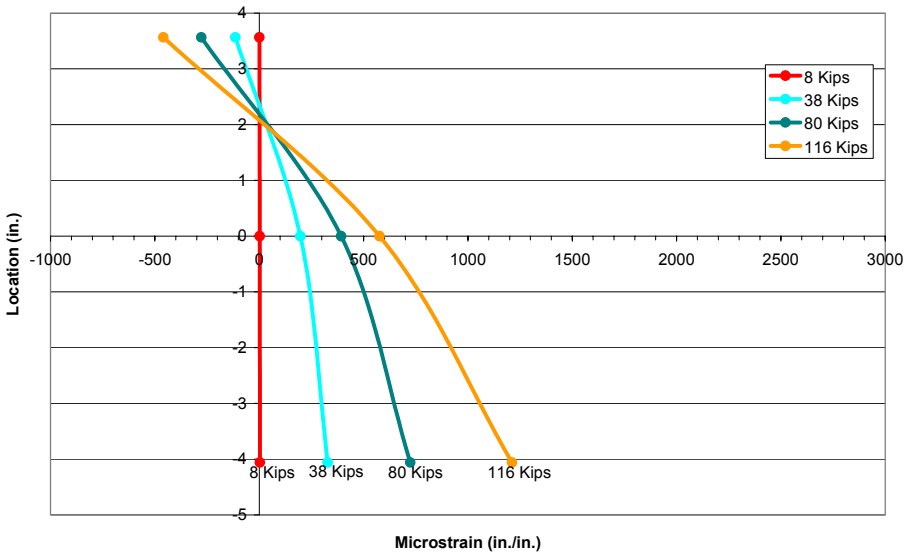

Figure 5.8 Resultant Strain through the West Actuator Steel Cross-Section at various Applied Loads

5.1.2.2 Strain in the Concrete Slab

Strain data was collected with nine concrete strain gages instrumented on the top of the concrete slab over the interior pier. Figure 3.18 in Chapter 3 provides a schematic for the concrete strain gage locations. Theoretically all concrete strain gages should have recorded tensile strain at this extreme location from the neutral-axis due to the negative bending of the test specimen over the interior pier. The W Gage and E Gage both recorded compressive strain data, which is believe to be related to torsional behavior of the test specimen. The N Gage, C Gage, and S Gage show limited data because they were located along the transverse center-line of the beam where cracks immediately occurred during the second deflection increment, as shown in Figure 4.24 of Chapter 4. Additionally, the NW Gage shows limited data because a crack occurred through this region during the third deflection step, as shown in Figure 4.25 of Chapter 4.

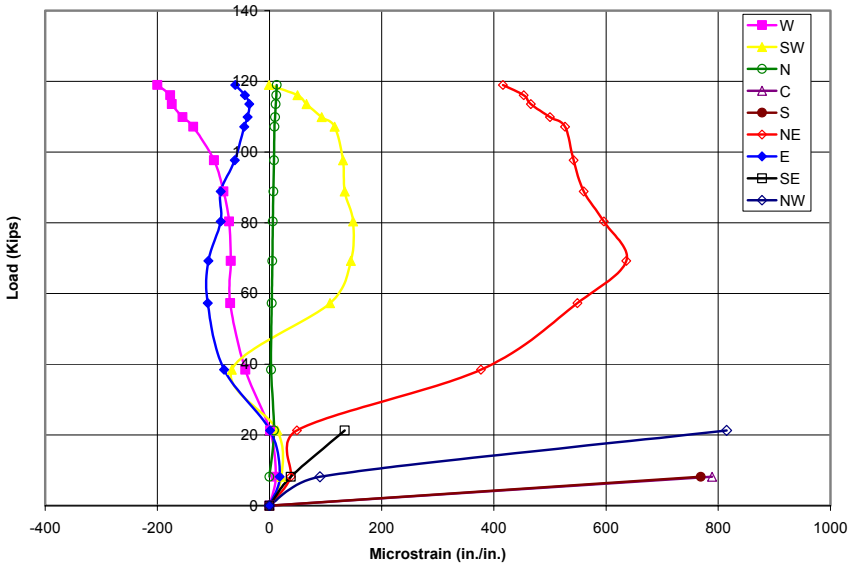

Figure 5.9 Applied Load versus Concrete Strain Data at the Interior Pier

5.2 Analysis of Experimental Results

The data recorded through the instrumentation of the test specimen was further analyzed by calculating the service stresses and moments that resulted from the experimental test. Calculation of service stresses and moments from the experimental test data was vital to achieve and evaluate the objectives of the research. Service stresses were calculated to meet the first objective of providing experimental data on service stresses versus deflection and permanent set. Moments were calculated in an effort to meet the second objective of providing experimental data on service stresses at various levels of moment redistribution.

As previously mentioned in the material testing section of Chapter 4, the steel yield stress and modulus of elasticity were determined to be 51.8 ksi and 26,450 ksi respectively. This actual modulus was used to convert the experimental strains into stresses using Hooke's Law. These stresses were then compared to the yield stress of 51.8 ksi to determine if yielding occurred at any of the locations

where data was recorded. From the analysis of the stresses and moments, key aspects and final conclusions regarding the experimental behavior of the test specimen were determined and/or verified.

5.2.1 Applied Load versus Stress

Table 5.1 shows the stresses computed by multiplying the strain data in Figure 5.3, 5.4, and 5.5 by the modulus of elasticity. The table shows the stress at each steel strain gage location for each deflection increment, and thus each level of applied load. Again, it is important to note that the negative stress values mean compressive stress and the positive stress values represent a tensile stress. The much larger magnitudes of stress at the top flange over the interior pier and bottom flange at the east and west actuator compared to the other locations of instrumentation are apparent in the table. As previously discussed, this behavior is expected due to the continuous-span nature and bending behavior of the test specimen.

The most important finding from this calculation and display of experimental service stresses is that the steel did not reach the yield stress of 51.8 ksi at any strain gage location. Therefore, this verifies the conclusion that all data trends from the experiment should be linear elastic, assuming behavior of the specimen was consistent with the theoretically assumed behavior, i.e., no torsion or loss of composite action in the specimen.

The first objective, to provide experimental service stress versus deflection and permanent set data, is only met on the surface. The underlying reason for providing this information was to evaluate what live load deflections and permanent set deformations can be expected for high levels of service stress. High levels of service stress were not attained; therefore the resulting information from

the experimental test reveals nothing with regard to the first objective of the research.

Table 5.1 Applied Load versus Service Stress

Applied Load (kips)	Stress @ Interior Pier (ksi)			Stress @ East Actuator (ksi)			Stress @ West Actuator (ksi)		
	Top Flange	Web	Bottom Flange	Top Flange	Web	Bottom Flange	Top Flange	Web	Bottom Flange
8	5	-1	-2	1	1	12	1	1	2
21	12	-4	-5	1	3	26	0	3	4
38	21	-1	-10	0	5	37	-3	5	9
57	57	-1	-16	-2	8	91	-5	8	13
69	58	-1	-19	-3	10	90	-6	9	16
80	51	0	-23	-4	11	72	-7	10	19
89	35	2	-26	-6	12	41	-9	11	22
98	39	1	-28	-8	14	44	-10	13	25
107	42	-3	-31	-9	15	46	-11	14	29
110	39	-3	-33	-9	15	42	-12	14	29
114	39	-4	-34	-10	16	41	-12	14	30
116	40	-5	-35	-10	16	41	-12	15	32
119	42	-7	-36	-10	15	38	-13	16	35

5.2.2 Service Stress versus Deflection and Permanent Set

Figure 5.10 and 5.11 show the ratio of service stress of the bottom and top flanges at the east and west actuators to the yield strength versus the deflection at these locations. The data reflects the expected linear elastic trend. As stated, the Service II limit state often governs the design by limiting the flange stress for a composite girder to 95 percent of the yield stress and thus the reason for experimental evaluation. The resulting data in both of these figures does not reach this level of stress and therefore makes any further evaluation or application of this experimental data irrelevant for this purpose. Again, the three outlying data points in Figure 5.10 of the east actuator and in Figure 5.11 at the interior pier that show high stress ratios greater than 95 percent yield are believed to be related to

unexpected torsional behavior of the test specimen during the experiment loading. These stress values were only temporary and are not an accurate reflection of the desired beam behavior near the yield stress of the test specimen.

Figure 5.12 shows the permanent set for the highest level of load that the test specimen experienced. At the conclusion of the experimental testing, all applied load was removed and a final data record was collected for the residual stresses and permanent deformations of the test specimen. A resulting permanent set of 0.23 inches at the east and west actuator was recorded, which again is insignificant and irrelevant for the application to the objectives of this research. This small amount of permanent set indicates that a minimal level of yielding (e.g., at the isolated points discussed above) occurred, but based on the data analysis above it is clear that gross yielding did not occur in any region of the girder. Figure 5.13 shows the application of the permanent set data to the AASHO Road Test data for Service II stress limits, but because of the low stresses induced in the experiment, no significant conclusion can be gained from this comparison.

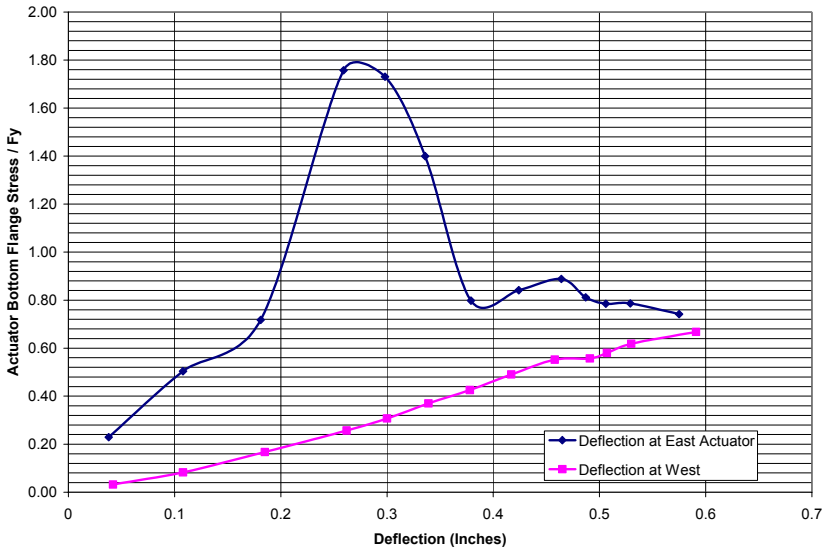

Figure 5.10 Service Stress of the Bottom Flange versus Deflection at the East and West Actuators

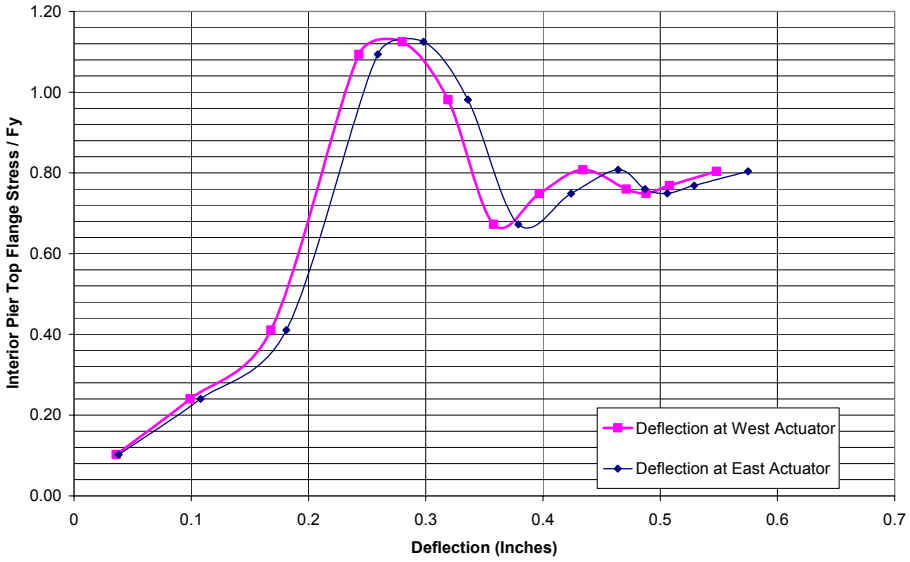

Figure 5.11 Service Stress of the Top Flange versus Deflection at the East and West Actuators

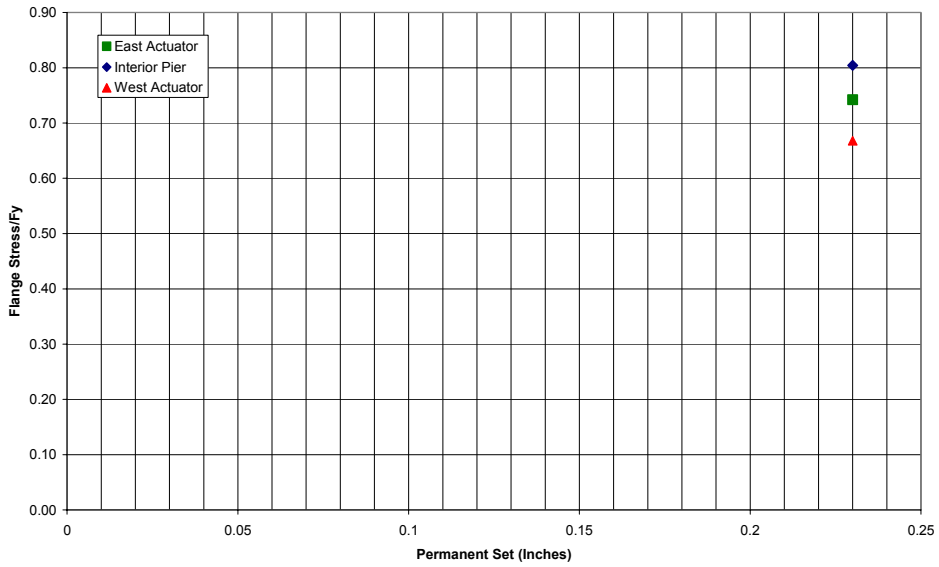

Figure 5.12 Ratio of the Service Stress and Yield Strength versus Permanent Set

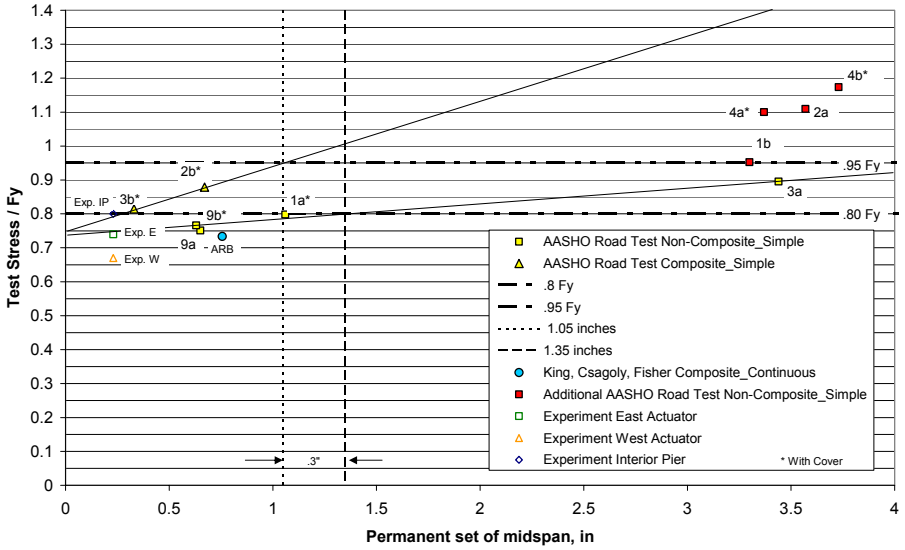

Figure 5.13 Addition of Experimental Test Permanent Set Data to the Updated AASHO Road Test Data for Service II Stress Limits

5.2.3 Applied Load versus Moment

As previously mention, in the absence of stress-strain data, the strains recorded from the experimental testing were converted to stress via the modulus of elasticity using Hooke's Law, see Equation 5-1. For example, the experimental elasticity of modulus, 26,450 ksi, as determined by the tensile coupon test was multiplied by the recorded strain values to get corresponding stress values. The experimental moment was then calculated using these stress values, theoretical moment of inertia, and distance from the neutral-axis to the location of strain instrumentation, see Equation 5-2.

$$\sigma = E\varepsilon \qquad (5\text{-}1)$$

$$M = \frac{\sigma\ I_x}{y_{bar}} \qquad (5\text{-}2)$$

By using the data presented in Figures 5.5, 5.6, and 5.7, the distance from the neutral-axis to the location of strain instrumentation, y_{bar}, in Equation 5-2 were determined. The moment of inertia, I_x, used in Equation 5-2 for calculation of experimental moment at the interior pier and east/west actuator locations was 274 in^4 and 127 in^4 respectively. Moment of inertia value 274 in^4 represents the W8X35 steel beam including the reinforcement bar, while the moment of inertia value 127 in^4 represents the W8X35 steel beam alone. The test specimen included the design for full composite action, however after viewing the resultant experimental data it was clear that slipping occurred. This is the reason for the exclusion of the slab from the moment of inertia values for the calculation of experimental moment.

Figures 5.14, 5.15, and 5.16 graphically display the applied load versus moment data. The moments shown in these figures include the actual experimental moments at the top flange, center-line of the web, and bottom flange for the interior pier, east actuator, and west actuator cross-sectional locations. Additionally, the average moment of these three locations is displayed along with

the calculated theoretical moment. The data reflects the linear elastic trend as expected by the calculation of stresses in the test specimen, with the exception of the three increments were torsional behavior was recorded. If these three increments are taken out it is clear that all locations of instrumentation correspond relatively well to the theoretical trend line. If the experimental testing would have continued loading of the test specimen past the yield stress and into the plastic region, moment redistribution would have occurred and Figures 5.14, 5.15, and 5.16 would have reflected that behavior. Figures 5.17 and 5.18 are examples of what the load versus moment figures would look like for moment redistribution at the interior pier and at the actuators. As the load increases the test specimen begins to redistribute moment to the actuators (spans), therefore the moments start to become less than theoretical at the interior pier and greater than theoretical at the actuators.

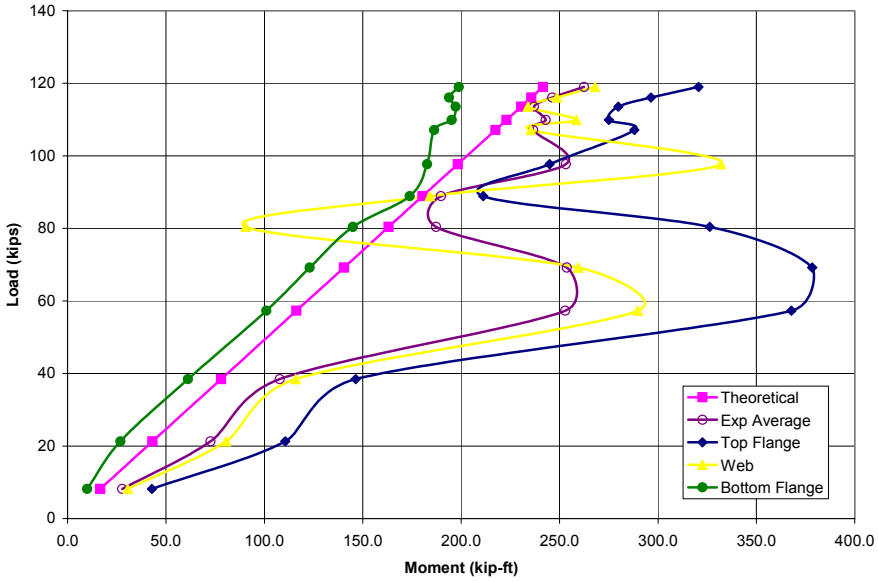

Figure 5.14 Applied Load versus Moment at the Interior Pier

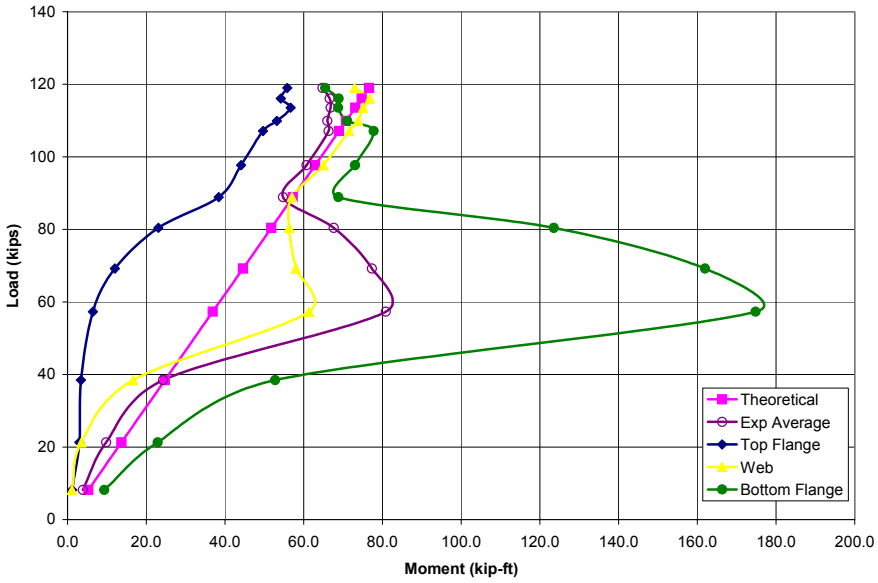

Figure 5.15 Applied Load versus Moment at the East Actuator

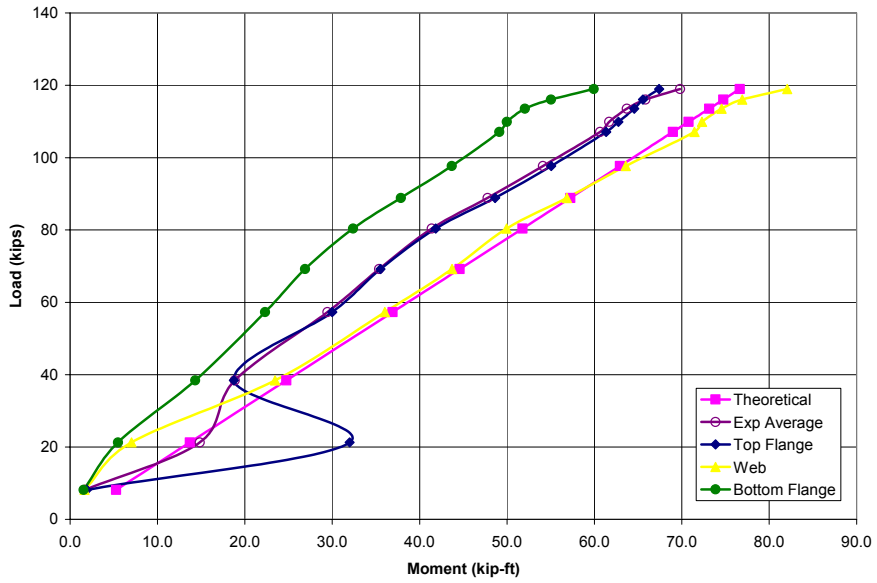

Figure 5.16 Applied Load versus Moment at the West Actuator

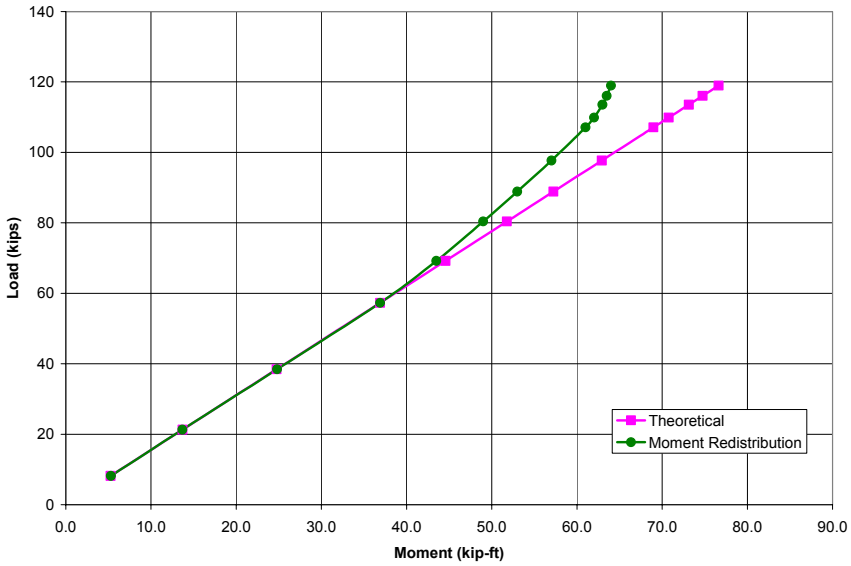

Figure 5.17 Example Moment Redistribution at the Interior Pier

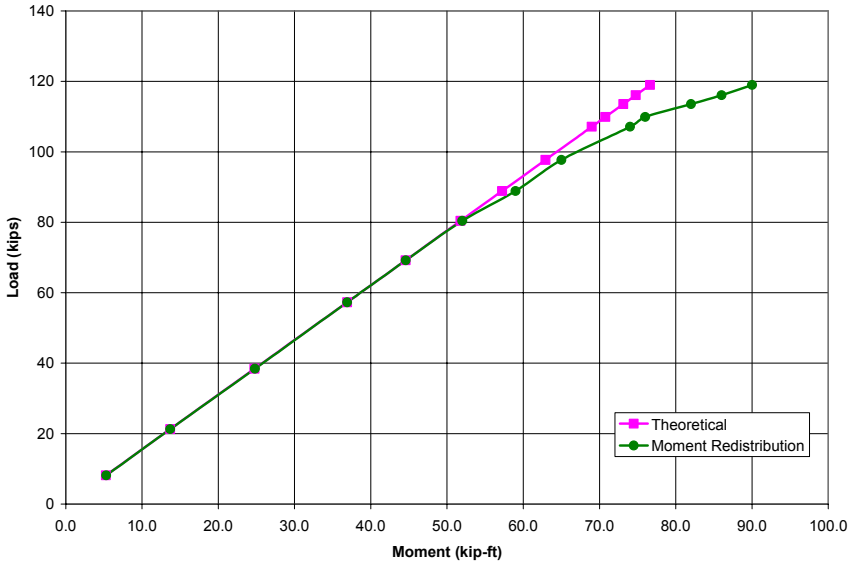

Figure 5.18 Example Moment Redistribution at the Actuators

In general, the experimental moments match the theoretical moments within a reasonable tolerance. Tables 5.2, 5.3, and 5.4 show the values of

experimental moment for corresponding applied loads and include the relative percent error from the theoretical moments. As previously mentioned, the moment of inertia values for the interior pier and actuator locations were 274 in^4 and 127 in^4 respectively. Both of these values exclude the concrete and therefore any composite action. The reason for the inclusion of the reinforcement steel in the I_x calculation at the interior pier is because the concrete at that location cracked almost immediately. Once the concrete cracked at this location, the reinforcement steel began experiencing tensile stresses and became effective. The reinforcement steel in the spans at the east and west actuators were not effective because the concrete was not cracked.

The large relative percent error in the tables at the low levels of applied load indicates that a higher moment of inertia value should have been used. The relative percent error decreases as the applied load increases, therefore it was determined that there was initially partial composite action and then a progressive loss of the composite action as the loads increased.

Further investigation into the lack of composite action for the test specimen and the calculated I_x values was done with a back calculation. This was performed to determine the I_x values that would give perfect correlation between the experimental moments and the theoretical moments at each steel strain gage. After these I_x values were determined and an average was calculated it became apparent that there was partial composite action initially, which dissipated as the applied loads increased to very minimal composite action during the final load application. Table 5.5 shows an example at the west actuator of this progression of composite loss in the test specimen by means of these I_x values. The reason that the relative percent errors in Table 5.5 are not zero is because the experimental moment used is taken as an average at the top flange, web, and bottom flange. It

is uncertain why such a significant amount of slipping and composite loss between the steel connectors and the concrete occurred.

Table 5.2 Relative % Error of the Experimental Moment at the Interior Pier

	Experimental Moment @ Interior Pier (kip-ft)								Theoretical
Load (kips)	Top Flange	% Error	Web	% Error	Bottom Flange	% Error	Avg.	% Error	Moment (kip-ft)
8	43	158%	31	84%	10	40%	28	67%	17
21	111	156%	81	87%	27	38%	73	68%	43
38	146	88%	116	48%	61	22%	108	38%	78
57	368	216%	290	149%	101	13%	253	117%	116
69	378	169%	260	85%	123	12%	254	81%	140
80	326	100%	91	45%	145	11%	187	15%	163
89	211	17%	184	2%	174	4%	190	5%	180
98	245	23%	332	67%	183	8%	253	28%	198
107	288	32%	235	8%	186	14%	237	9%	217
110	275	23%	259	16%	195	12%	243	9%	223
114	280	21%	234	1%	197	14%	237	3%	231
116	296	26%	249	6%	194	18%	246	5%	236
119	321	33%	268	11%	199	18%	262	9%	242

Table 5.3 Relative % Error of the Experimental Moment at the East Actuator

	Experimental Moment @ East Actuator (kip-ft)								Theoretical
Load (kips)	Top Flange	% Error	Web	% Error	Bottom Flange	% Error	Avg.	% Error	Moment (kip-ft)
8	1	78%	1	79%	9	77%	4	27%	5
21	3	78%	4	74%	23	67%	10	28%	14
38	3	86%	17	33%	53	113%	24	2%	25
57	6	83%	61	66%	175	374%	81	119%	37
69	12	73%	58	30%	162	263%	77	73%	45
80	23	55%	56	9%	124	139%	68	31%	52
89	38	33%	57	0%	69	20%	55	4%	57
98	44	30%	65	3%	73	16%	61	4%	63
107	50	28%	72	4%	78	13%	66	4%	69
110	53	25%	74	4%	71	0%	66	7%	71
114	57	23%	75	3%	69	6%	67	9%	73
116	54	28%	77	3%	69	8%	67	11%	75
119	56	27%	73	5%	65	15%	65	16%	77

Table 5.4 Relative % Error of the Experimental Moment at the West Actuator

	Experimental Moment @ West Actuator 4 (kip-ft)								Theoretical
Load (kips)	Top Flange	% Error	Web	% Error	Bottom Flange	% Error	Avg.	% Error	Moment (kip-ft)

8	2	64%	2	69%	2	71%	2	68%	5
21	32	133%	7	49%	5	60%	15	8%	14
38	19	24%	23	5%	14	42%	19	24%	25
57	30	19%	36	2%	22	40%	29	20%	37
69	36	20%	44	2%	27	40%	35	21%	45
80	42	19%	50	4%	32	37%	41	20%	52
89	49	15%	57	1%	38	34%	48	17%	57
98	55	13%	64	1%	44	31%	54	14%	63
107	61	11%	71	4%	49	29%	61	12%	69
110	63	11%	72	2%	50	29%	62	13%	71
114	65	12%	75	2%	52	29%	64	13%	73
116	66	12%	77	3%	55	26%	66	12%	75
119	67	12%	82	7%	60	22%	70	9%	77

Table 5.5 Progression of Composite Loss

Load (kips)	Experimental Moment @ West Actuator (kip-ft)			Theoretical Moment (kip-ft)
	Average I_x (in^3)	Average Moment	% Error	
8	**395.5**	5	1%	5
21	**206.27**	24	76%	14
38	**173.74**	26	4%	25
57	**165.45**	38	4%	37
69	**166.51**	46	4%	45
80	**163.95**	53	3%	52
89	**156.44**	59	3%	57
98	**151.27**	64	2%	63
107	**147.91**	71	2%	69
110	**149.12**	72	2%	71
114	**148.97**	75	2%	73
116	**146.91**	76	2%	75

Finally, the fact that the steel did not yield makes the analysis for the second objective of providing service stresses at various levels of moment redistribution impossible. Moment redistribution takes place once the steel has yielded and is in the plastic state, therefore there could not have been any moment redistribution in the test specimen. Unfortunately, the test specimen could not be further loaded and as a result reaching the objectives of this research within the scope of this thesis was not possible. The test specimen could not be further loaded

because it was destroyed by circumstances beyond the control of the research team.

Chapter 6

6. Summary and Conclusions

6.1 Summary

The work for this research has resulted in the development of a systematic approach to study the effects of Service II Limit State and moment redistribution procedures on steel girders through the experimental testing and analysis of a composite continuous-span test specimen. The research framework has provided guidance on experimental design considerations, construction methods, testing procedures, numeric data analysis, and the graphical display of data/results. The scope of the research included the collection of the strain and deflection data needed for the evaluation of the research objectives. Analysis of this strain and deflection data provides the stress and moment data needed to further evaluate the Service II Limit State and moment redistribution procedures. Furthermore, the developments of this research thesis will be valuable in future experimental testing of continuous-span specimens.

The introductory information, including brief background information on the AASHTO Limit States, the Service II Limit State, and moment redistribution was presented in Chapter 1. Additionally, Chapter 1 discussed the need for the research, objectives of the research, scope of the research, and the organization of this thesis. The objectives of this research were to provide experimental data on service stresses versus deflection and to provide experimental data on service stresses at various levels of moment redistribution.

Chapter 2 provided a detailed background review of topics critical to this research. Topics included the AASHTO Limit States, the Service II Limit State, and moment redistribution. The AASHO Road Test was found to be the origin of the Service II Limit State flange stress limits and a detailed discussion of this study is also included in Chapter 2. Finally, criteria for the basis of the flange stress limits of the Service II Limit State was investigated and discussed to provide guidance on future rational design criteria. Existing research in this area was presented and future recommendations for research were provided.

Details for the design of the experimental test set-up and test specimen were discussed in Chapter 3, including the scope of the design, test specimen characteristics, lateral bracing, and instrumentation for the experimental testing. Here the decision process used to determine the test set-up geometry and specific test specimen characteristics was detailed. Aspects regarding the experimental testing of the research were presented in Chapter 4 through a discussion of the construction process and testing procedures. The construction process provided an overall sense for the steps needed to build the test set-up and test specimen, while the testing procedure discussion provided the details of load application during the experimental testing.

The experimental strain and deflection data was graphically displayed and discussed in Chapter 5 through load versus deflection and load versus strain graphs. Analysis of the experimental data resulted in determining the experimental stresses and moments, which were was also graphically displayed and discussed in Chapter5. Figures of applied load versus service stress, service stress versus deflection, and applied load versus moment provided a detailed method for the evaluation of experimental testing results and formulation of conclusions. In short, the objectives of the thesis were not met due to loading circumstances beyond the control of the research team.

6.2 Conclusions

As mentioned throughout this thesis, the intention of the design criteria for the Service II Limit State is ambiguous and not well founded. The limit state places restrictions on the flange stresses in an effort to avoid unacceptable deformations and corresponds to the overload check in the 1992 AASHTO Standard Specifications. The background research for this thesis established the AASHO Road Test of the 1950's as the foundation for the flange stress limits according to Hansell & Viest (1971). This basis for the flange stress limits of the Service II Limit State confirmed the weak justification for their application to modern bridge design methodology and raises several concerns.

The concerns for the establishment of the Service II flange stress limits are as follows. First, the limit state is based on limited experimental data obtained from a single study that included variation of relatively few parameters. Second, the alternative flange stress limits for composite girders and non-composite girders are intended to result in the same permanent set. However, this intent is not achieved based on the experimental data from the AASHO Road Test. Third, deflection data recorded for the experiment was the result of all test bridges having the equivalent span length. The deflection and permanent set of a girder is directly related to span length, therefore experimental data must include varying span lengths. Fourth, the majority of modern bridges are continuous-span structures, however all test bridges used for the Road Test were simple-span structures. Continuous-span structures will result in lower levels of deflection and permanent set compared to a simple-span structure. Therefore, the basis of the flange stress limits needs to include experimental data on continuous-span structures. Lastly, according to Hansell & Viest (1971) the test bridges experienced the equivalent of 20 overload crossing everyday for more than 50 years. Because the test bridges

experienced such extreme loading in forming the eventual basis of a limit state, concerns that the loading is unnecessarily conservative are raised.

Evaluation of the criteria for the Service II Limit State was discussed in Chapter 2. The classification "objectionable" deformation must be quantified in terms relative to span length and/or accelerations in the bridge, because it is these perceptions by the public that define a bridge as unacceptable in terms of rideability. Further research is needed in this area to determine how the deflection/permanent set of a bridge is affected by variations in the span length. Additional research is needed to determine what magnitude and direction of acceleration is deemed unacceptable by the public.

The first objective of the research was to provide experimental stress versus deflection/permanent set data to evaluate what live load deflections and permanent set deformations can be expected at high levels of stress. The experimental testing for this research provided experimental stress versus deflection/permanent set, but not at high levels of stress. The locations of strain gage instrumentation showed no local yielding of the 51.8 ksi yield strength steel and further evaluation showed no reason to believe gross yielding of the test specimen occurred. In short, the data recorded for this objective did not attain high levels of stress; therefore it is irrelevant and provides no further application for the purposes of this research.

The second objective of the research was to provide service stresses at various levels of moment redistribution for comparison to the existing service stress limits included in the service limit state for moment redistribution design. Moment redistribution procedures require the steel to yield and behave in a plastic state. This objective was not achieved because the steel in the test specimen did not yield.

The reason the test specimen was not loaded past yield, into the plastic range, and finally to ultimate capacity was due to complications with the actuators

beyond the control of the research team. The actuators failed to apply additional load beyond approximately 119 kips, therefore loading the test specimen below the yielding threshold. This was confirmed through the collection of strain and deflection data and analysis of that data determining stress and moment. Strain versus deflection plots showed a linear elastic behavior and calculation of the stress in the steel revealed values less than the yield stress of 51.8 ksi. Before the problem with the actuators could be corrected, the specimen was inadvertently destroyed, terminating any potential for additional loading.

Further analysis of the experimental data revealed minor torsional effects through a portion of the experimental loading. Additionally, by satisfying the equilibrium requirements of the system in terms of experimental moment data, it was determined that the test specimen experienced a progression of composite action loss. The test specimen was designed for full composite action; however the analysis revealed that the composite action ranged from partial to none.

6.3 Recommendations

Although the final outcome of the experimental results did not satisfy the objectives for this research, the methods and procedures presented will prove useful. As mentioned, the failure to meet the research objectives was not the result of decisions made by the research team regarding the experimental design and/or testing. The construction methods, testing procedures, numeric data analysis, and the graphical display of data/results presented in this research thesis are an adequate and efficient method for achieving the research objectives.

Additional experimental research and data regarding the Service II Limit State and moment redistribution procedures must be attained for further investigation into the efficiency of these design criteria. This thesis has provided a

systematic approach to acquire the experimental data necessary; therefore this research thesis should be utilized as a guide for future testing.

It is recommended that future testing of continuous-span specimens include High Performance Steel (HPS), grade 50 steel, non-composite girders, composite girders, plate girders, and variations in span length. Future experimental testing must apply enough incremental loading to reach the eventual ultimate capacity of the test specimen, thus achieving both objectives regarding high levels of stress and moment redistribution. The data analysis files and methods for graphical display used for this research thesis may be used for rapid experimental interpretation and conclusion. One potential minor area of experimental improvement is the application of strain gages at all locations of recorded deflection. This would be beneficial because this would have provided more locations for further analysis of stress versus deflection data at the locations of theoretical maximum deflection in the spans.

Appendix A: Geometric Trends for Bridge Design Study

A.1 Grade 50 / 20 Percent Moment Redistribution

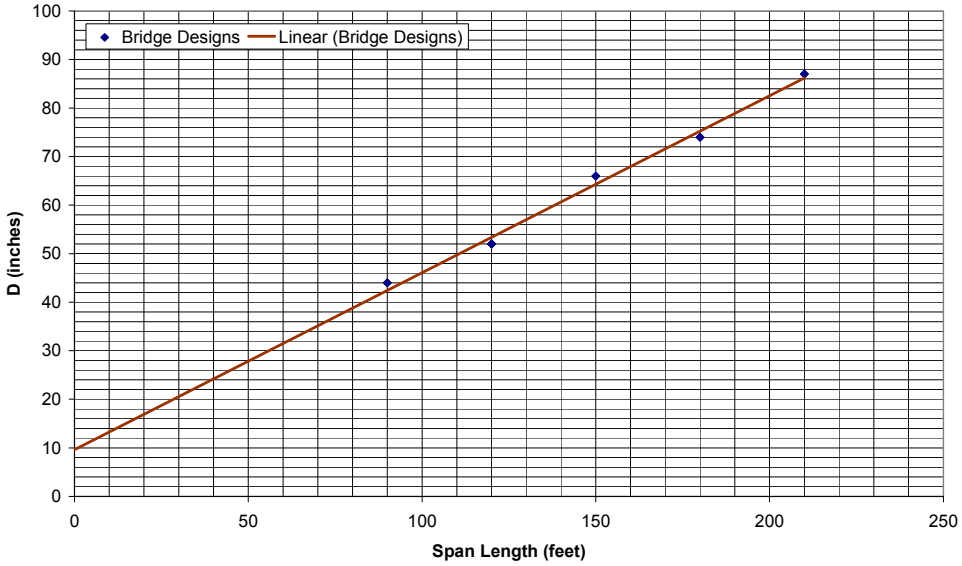

Figure A.1 Trend of Girder Depth Based on Bridge Design Study

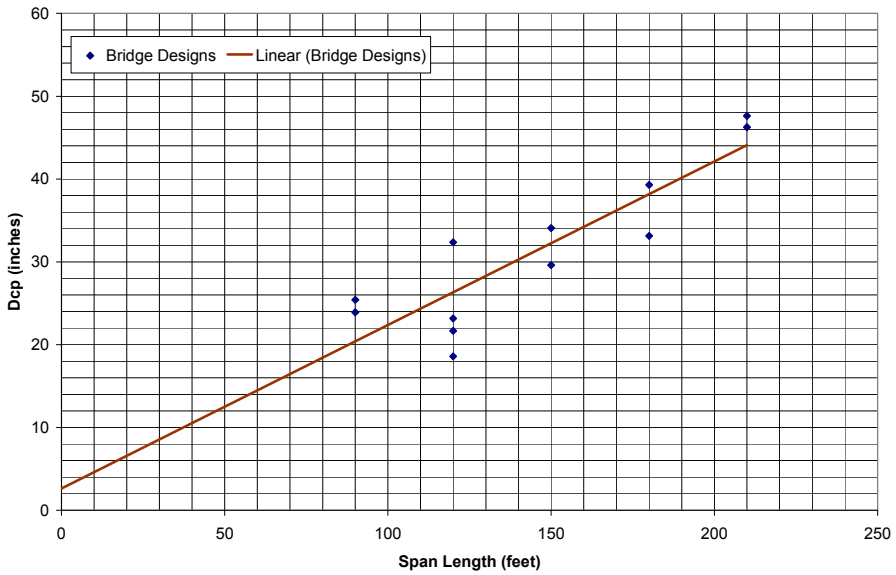

Figure A.2 Trend of Girder Depth in Compression Based on Bridge Design Study

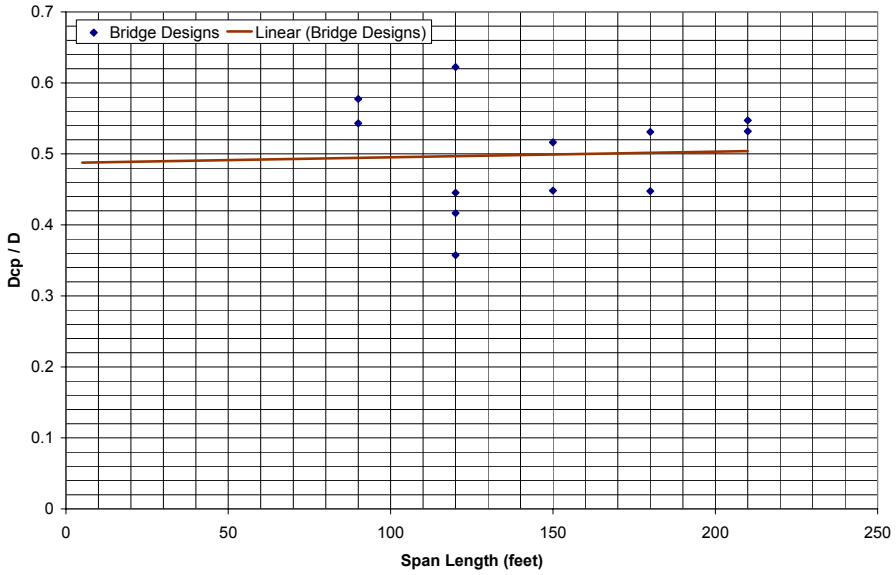

Figure A.3 Trend of D_{cp}/D Ratio Based on Bridge Design Study

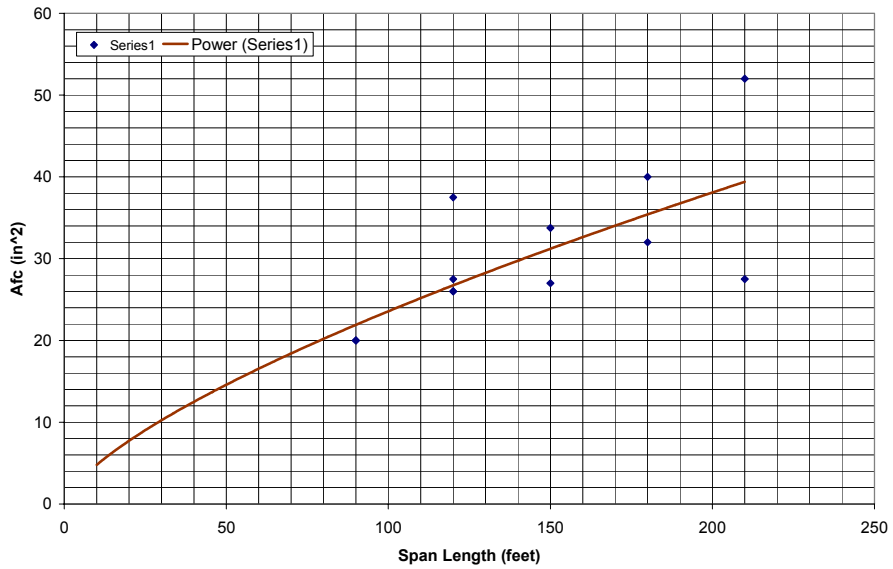

Figure A.4 Trend of Area of Flange in Compression Based on Bridge Design Study

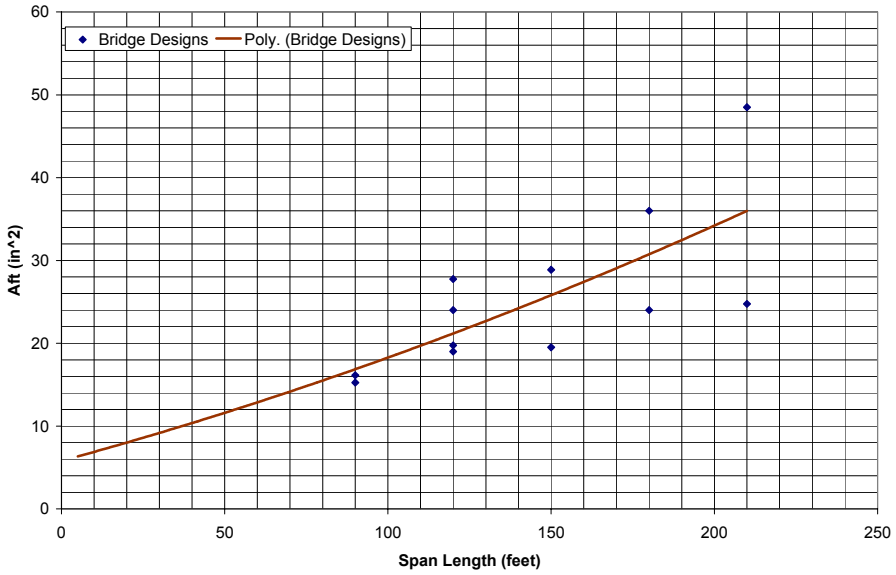

Figure A.5 Trend of Area of Flange in Tension Based on Bridge Design Study

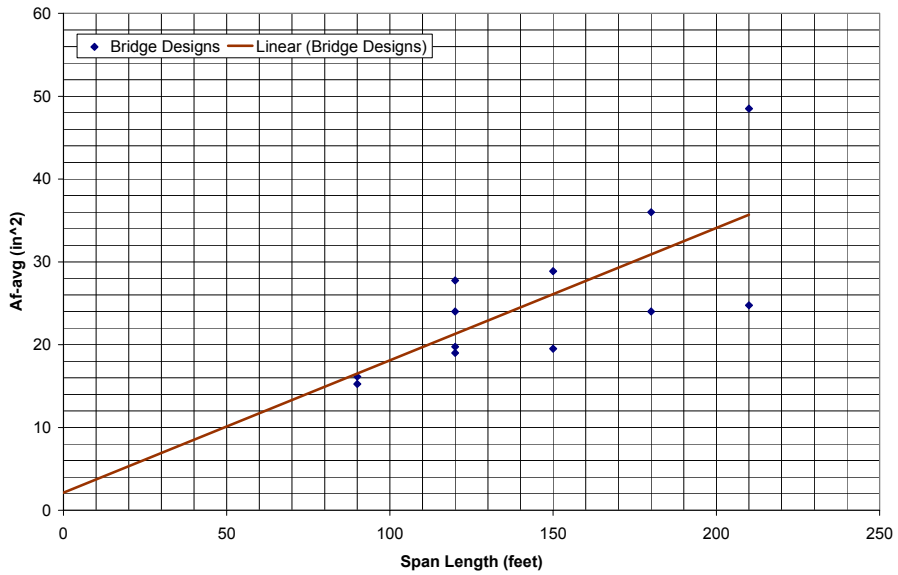

Figure A.6 Trend of Average Area of Flange Based on Bridge Design Study

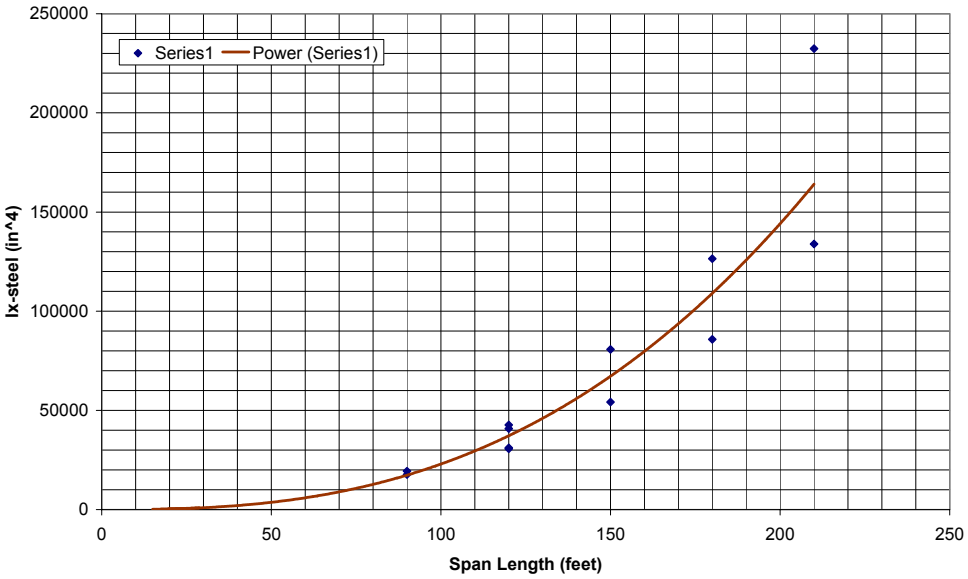

Figure A.7 Trend of Steel Moment of Inertia Based on Bridge Design Study

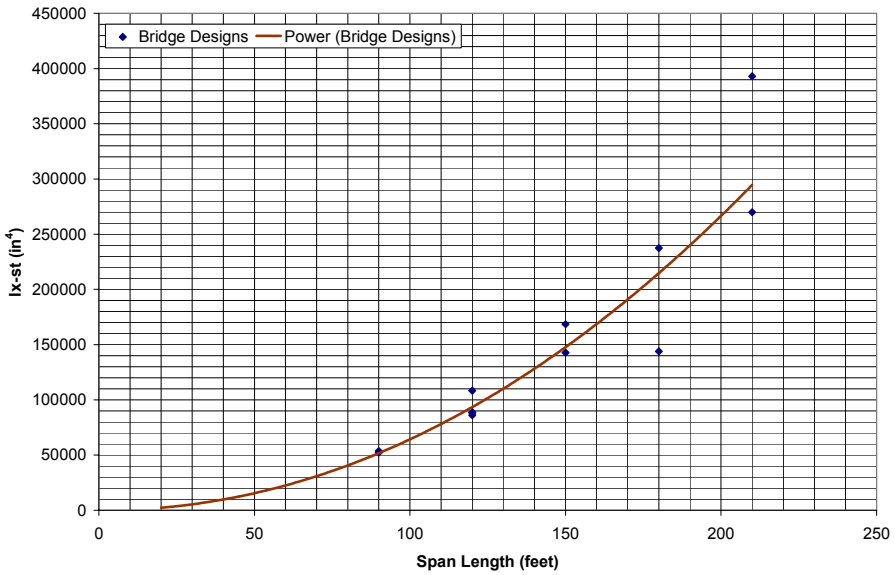

Figure A.8 Trend of Short-Term Steel Moment of Inertia Based on Bridge Design Study

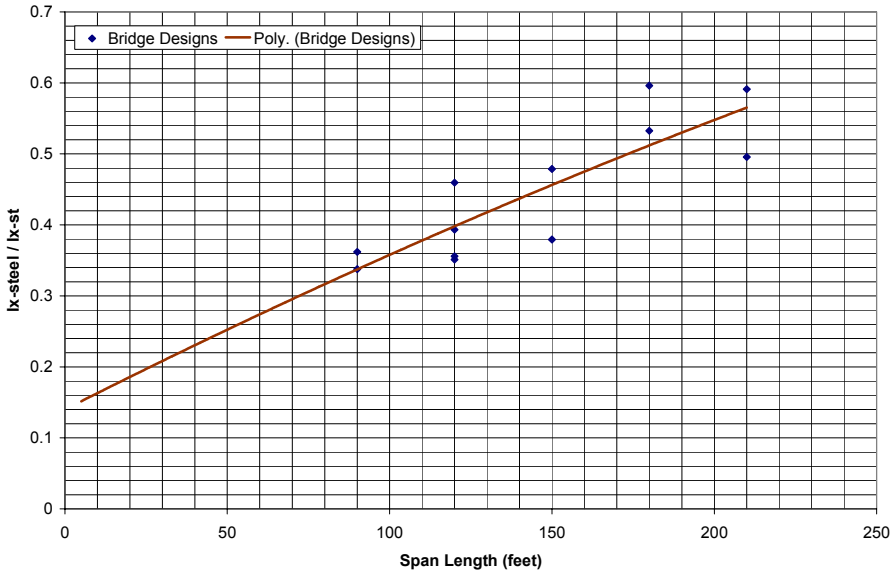

Figure A.9 Trend of Short-Term and Steel Moment of Inertia Ratio Based on Bridge Design Study

A.2 Grade 50 / 30 Percent Moment Redistribution

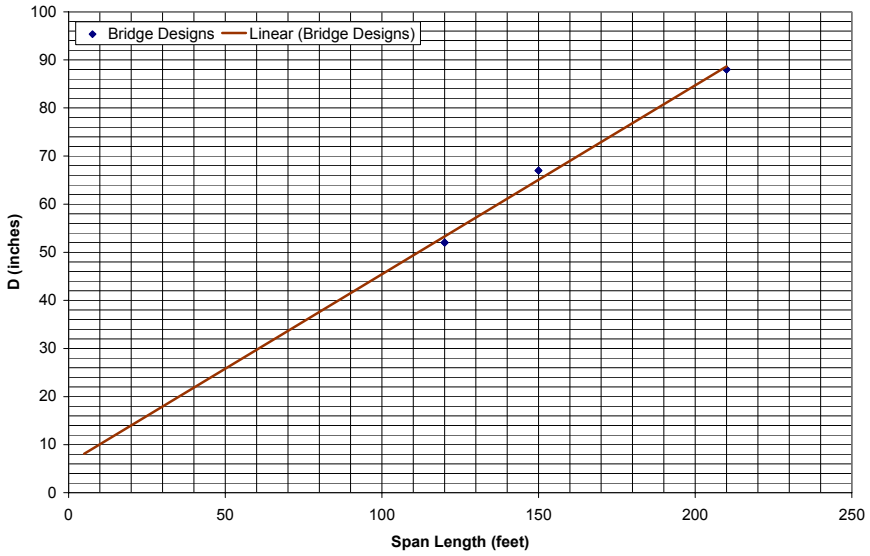

Figure A.10 Trend of Girder Depth Based on Bridge Design Study

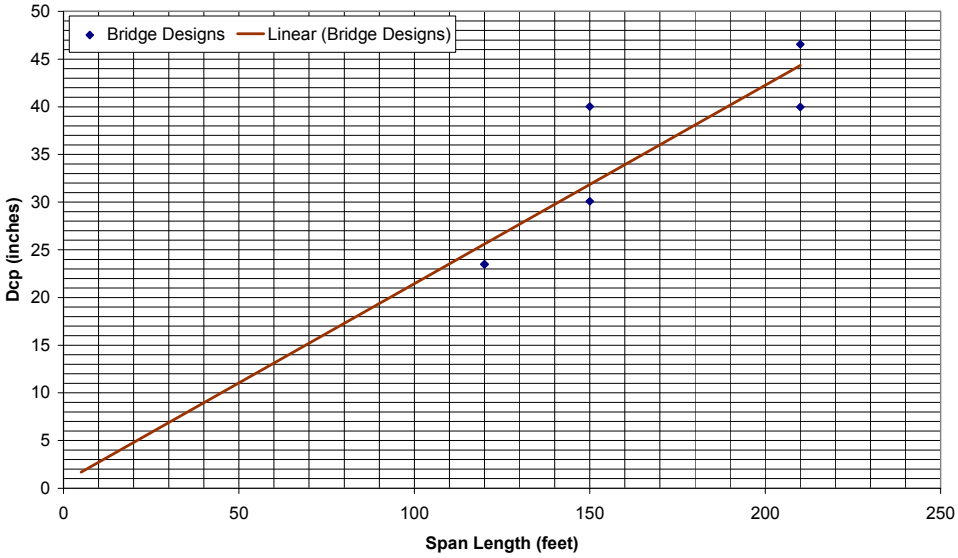

Figure A.11 Trend of Girder Depth in Compression Based on Bridge Design Study

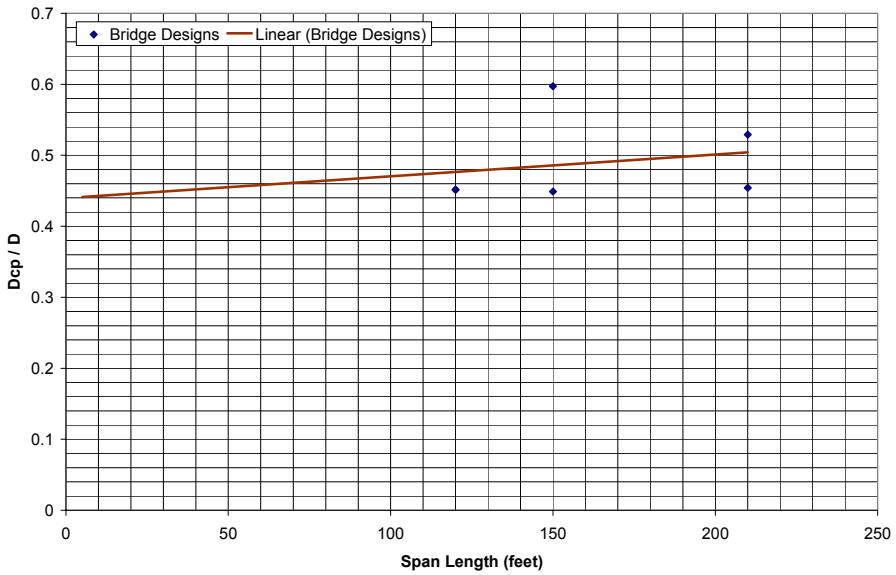

Figure A.12 Trend of D_{cp}/D Ratio Based on Bridge Design Study

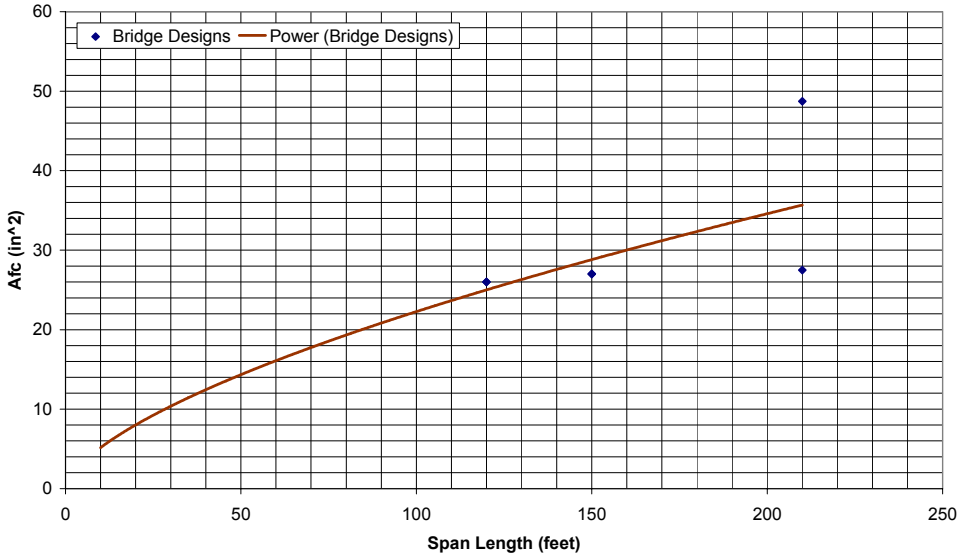

Figure A.13 Trend of Area of Flange in Compression Based on Bridge Design Study

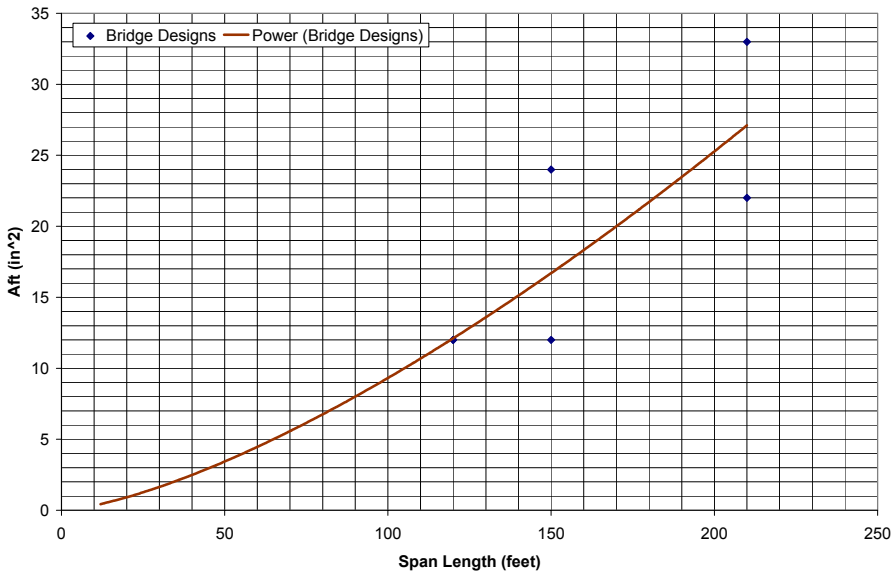

Figure A.14 Trend of Area of Flange in Tension Based on Bridge Design Study

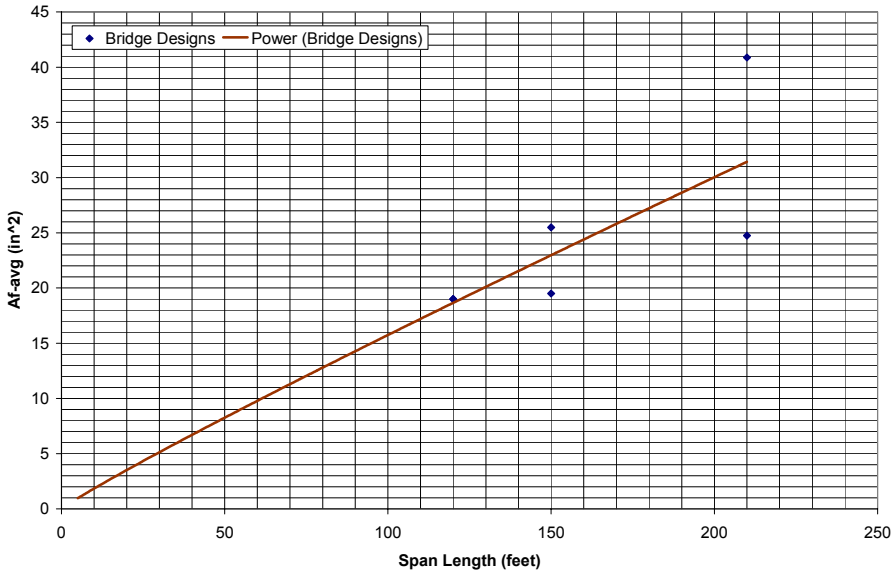

Figure A.15 Trend of Average Area of Flange Based on Bridge Design Study

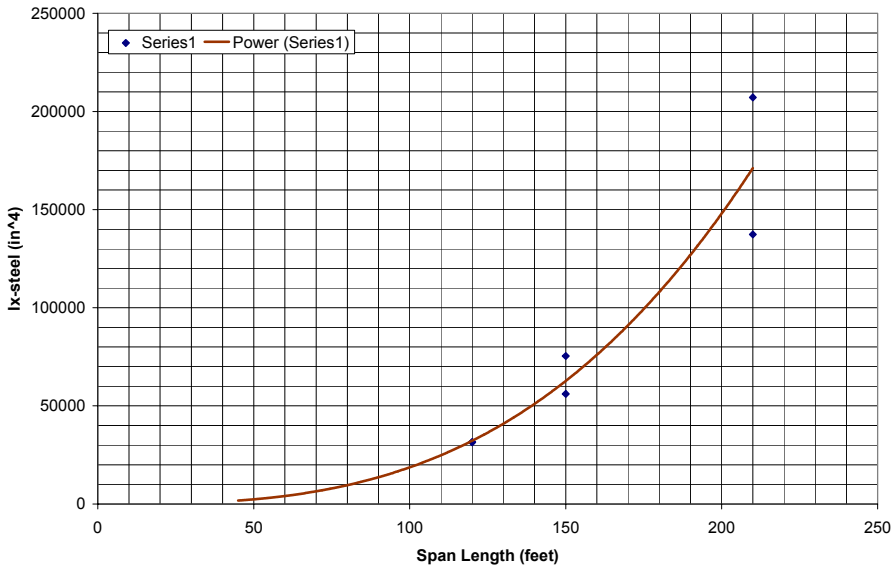

Figure A.16 Trend of Steel Moment of Inertia Based on Bridge Design Study

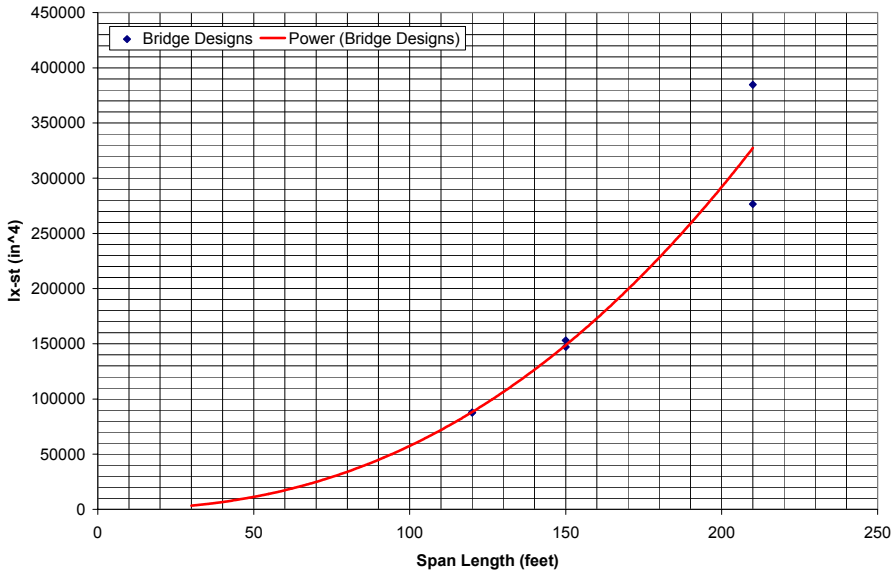

Figure A.17 Trend of Short-Term Steel Moment of Inertia Based on Bridge Design Study

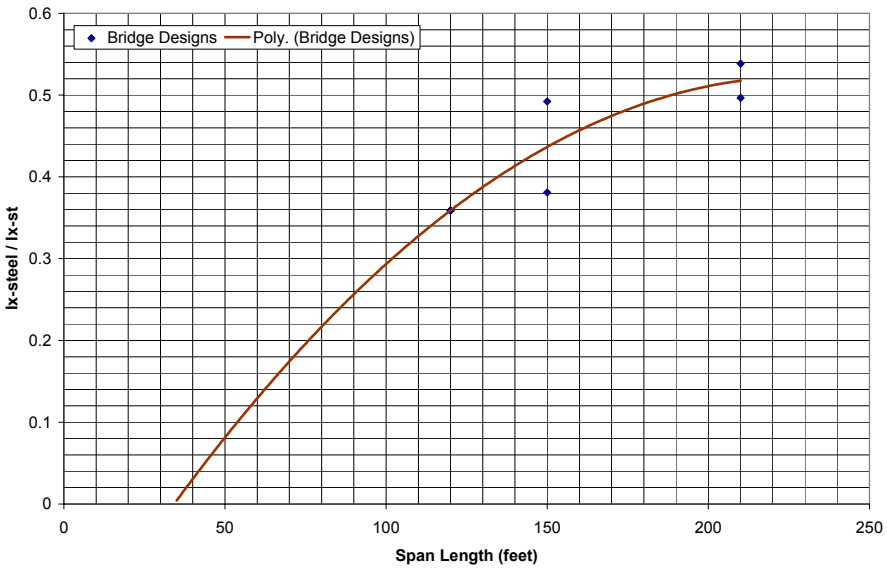

Figure A.18 Trend of Short-Term and Steel Moment of Inertia Ratio Based on Bridge Design Study

A.3 HPS70 / 20 Percent Moment Redistribution

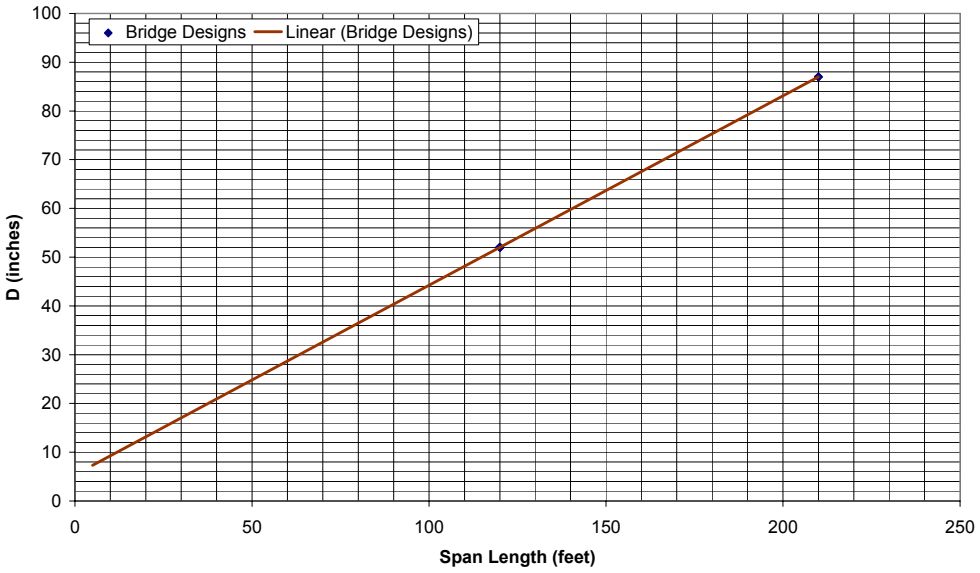

Figure A.19 Trend of Girder Depth Based on Bridge Design Study

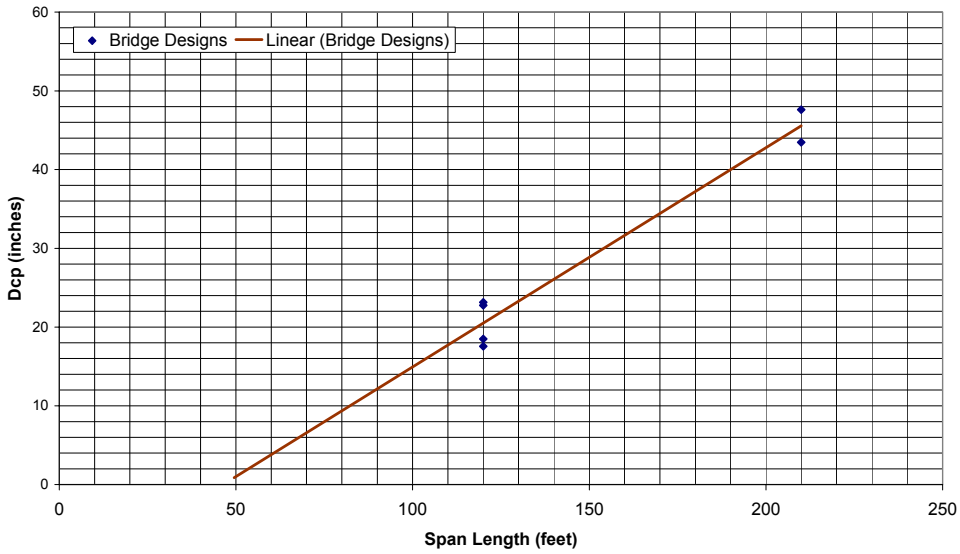

Figure A.20 Trend of Girder Depth in Compression Based on Bridge Design Study

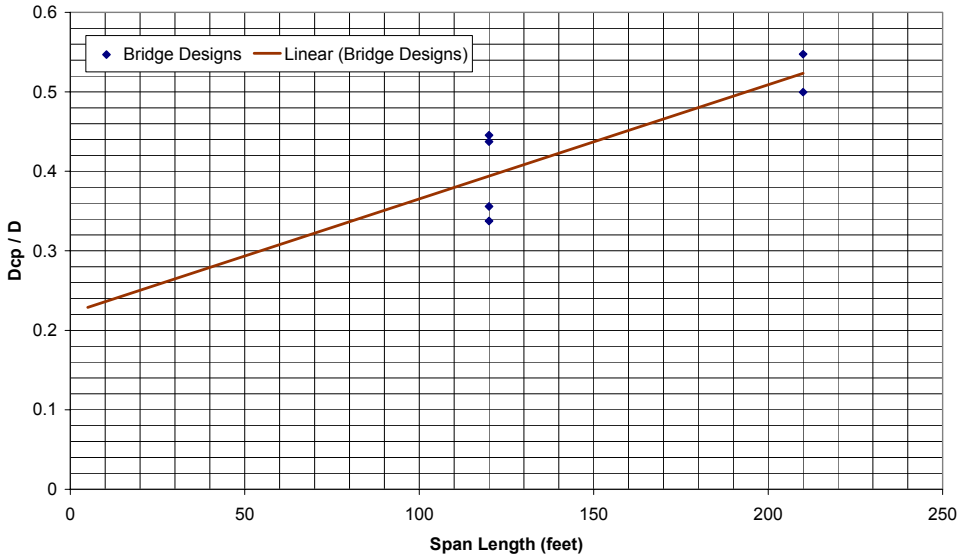

Figure A.21 Trend of D_{cp}/D Ratio Based on Bridge Design Study

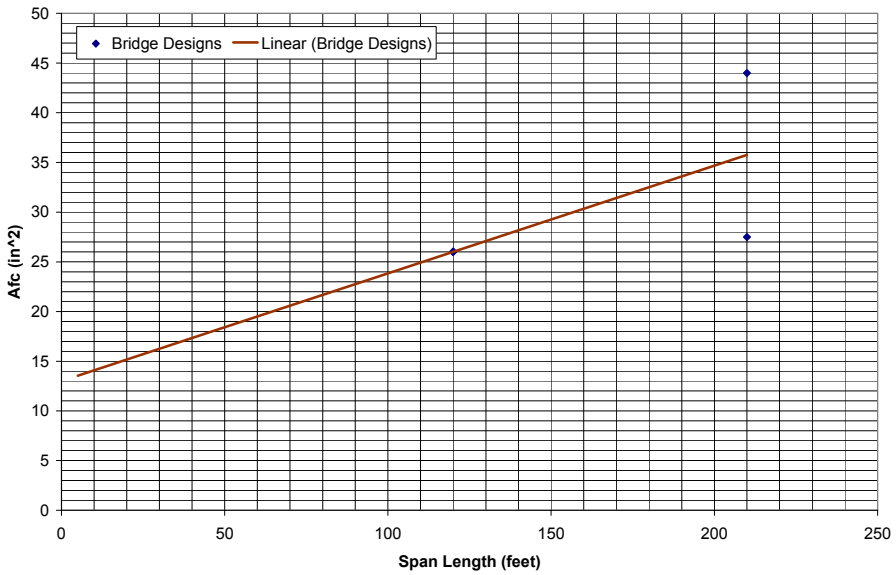

Figure A.22 Trend of Area of Flange in Compression Based on Bridge Design Study

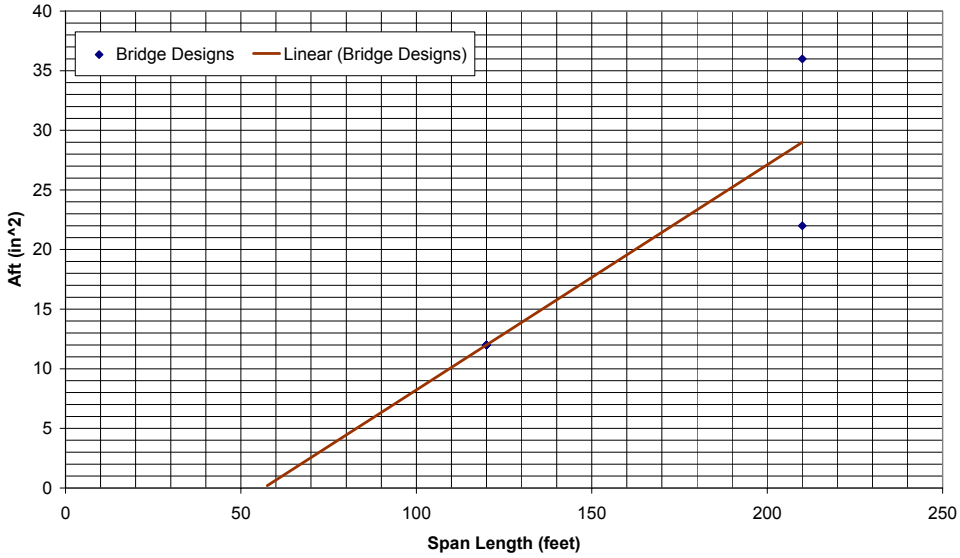

Figure A.23 Trend of Area of Flange in Tension Based on Bridge Design Study

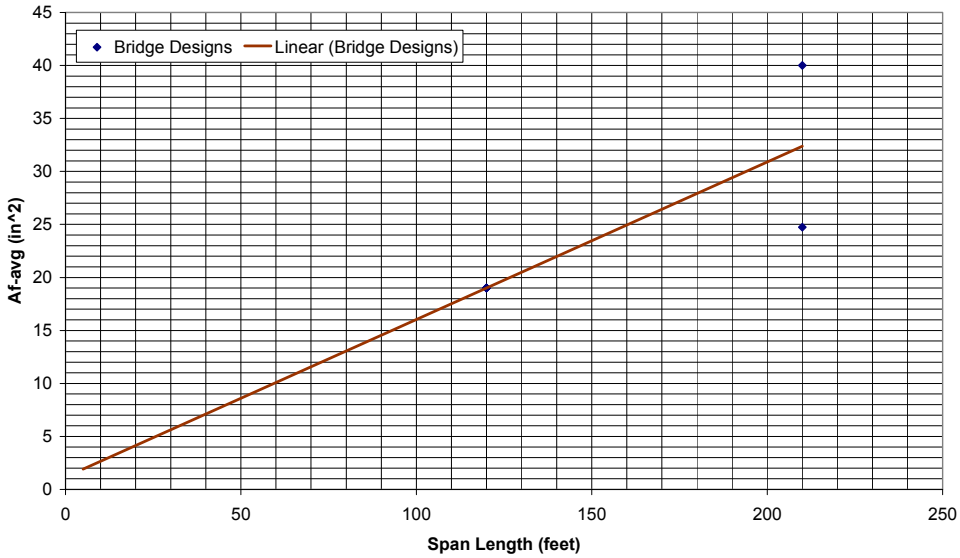

Figure A.24 Trend of Average Area of Flange Based on Bridge Design Study

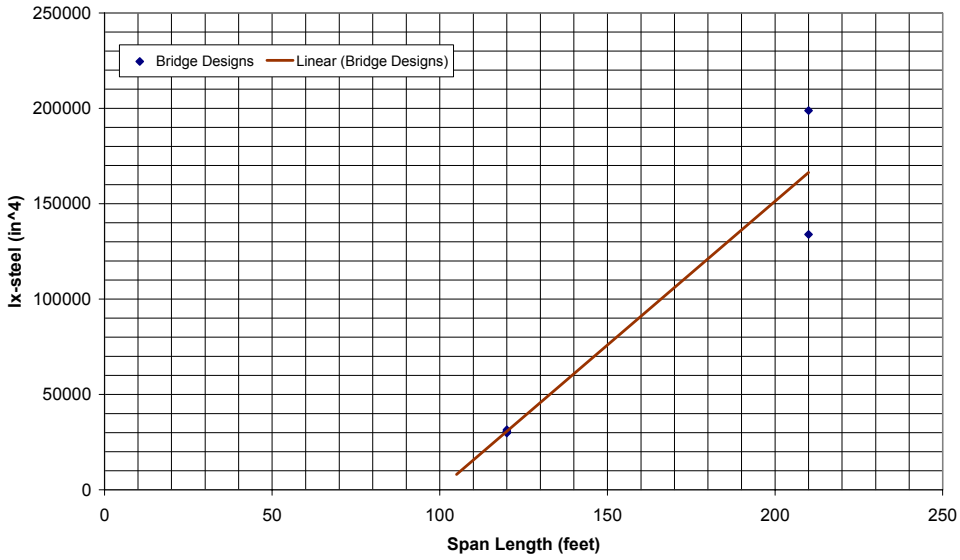

Figure A.25 Trend of Steel Moment of Inertia Based on Bridge Design Study

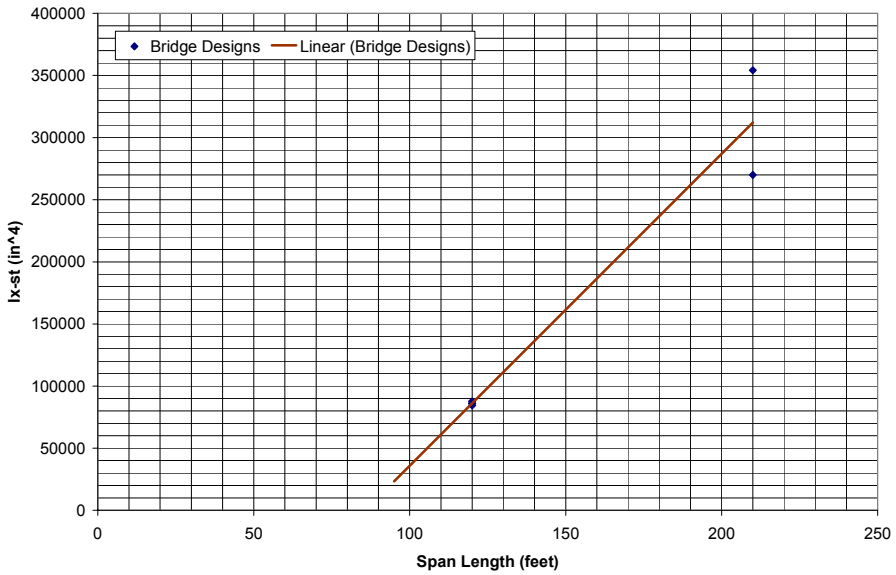

Figure A.26 Trend of Short-Term Steel Moment of Inertia Based on Bridge Design Study

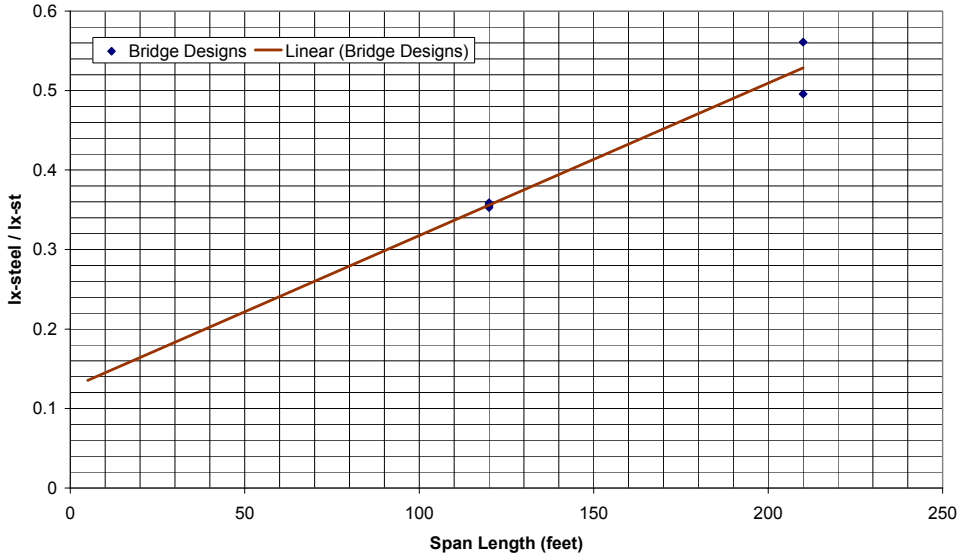

Figure A.27 Trend of Short-Term and Steel Moment of Inertia Ratio Based on Bridge Design Study

Delaware Center for Transportation
University of Delaware
Newark, Delaware 19716